1-2-2013

Low Energy Positron Interactions With Biological Molecules

Indika Lasantha Wanniarachchi
Wayne State University,

LOW ENERGY POSITRON INTERACTIONS WITH BIOLOGICAL MOLECULES

by

INDIKA L WANNIARACHCHI

DISSERTATION

Submitted to the Graduate School

of Wayne State University,

Detroit, Michigan

in partial fulfillment of the requirements

for the degree of

DOCTOR OF PHILOSOPHY

2013

MAJOR: PHYSICS

Approved by:

_____

Adviser Date

_____

_____

_____

_____

DEDICATION

To my parents, the most important people in my life.

ACKNOWLEDGMENTS

I am happy to express my heartfelt thanks to all the people who helped me to complete my Ph.D. Their advice and help have come in various situations. My special words of thanks goes to these people here.

Foremost, I would like to express my sincere gratitude to my advisor Prof. Caroline Morgan, for her valuable guidance given to me throughout the period of this project. She is an outstanding mentor and an excellent teacher. She always gave me the instruction to improve my professional writing and presentation skills.

Besides my advisor, I would like to thank the rest of my thesis committee: Prof. Gavin Lawes, Prof. ZhiFeng Huang, Prof. Bernhard Schlegel (Department of Chemistry), and Prof. Marry Rodgers (Department of Chemistry), for their encouragement, insightful comments, and hard questions.

Also I would like to thank Dr. Gary Kedziora and Dr. Xiaofeng Duan (AFRL High Performance Computing Center), Prof. Larry Burggraf and Dr.Eugene Sheely (Air Force Institute of Technology), Dr. Mike Pak and Prof.S. Hammes-Schiffer (University Illinois) for valuable discussions and computational assistance.

My sincere thanks also go to Dr. Alan Sebastian and Dr. Panagiotis Papoulias for valuable discussions. In addition, I would like to thank Dr. Scott Payson for his valuable time and suggestions given to me for shape up the thesis.

Many thanks go to department chair, Prof. Ratna Naik & graduate adviser, Prof. Jogindra Wadehra and Dr.Punya Thalagala for their support and advice in countless ways throughout my graduate studies.

Also I would like to thank the people who implemented the Sri Lankan free education system, which made the bridge to get my higher education in United States.

I would like to thank my parents, Dhamma and Chithra Wanniarachchchi and my brother, Sanath Wanniarachchi for whom I can always count on. Also, I would like to appreciate the encouragements and support given by my parents-in-laws Chandrasiri de Silva and Shanthi Gunawardana.

Finally, very special thank goes to my loving wife Dakshika and my son Vidas for their love and kindness that they have given to me not only during my studies but also throughout my life.

TABLE OF CONTENTS

LIST OF FIGURES

LIST OF TABLES

CHAPTER 1

INTRODUCTION

The existence of the positron, which is the antiparticle of the electron, was first predicted by Dirac in 1928 [1]. Dirac also predicted that an electron and an anti-electron could annihilate by converting their mass into the energy of photons. He theoretically calculated the e^-e^+ annihilation rate by explaining the possible two-photon and three-photon decays with respect to the electron-positron spin orientation [2, 3]. In 1933, C.D. Anderson observed the anti-electron predicted by Dirac in the cloud-chamber tracks of cosmic radiation and named it the positron [4, 5]. The existence of a bound state of an electron and a positron was also suggested in 1934 [6], and it was named positronium (Ps) by R. E. Ruark in 1945 [7]. In 1940, annihilation of positrons with the electrons in matter was studied, leading to the understanding that energy and momentum conservation during the annihilation process can be utilized to study properties of solids [6].

Currently, there are many applications that make use of positron annihilation spectroscopy in the areas of medical imaging and material science. Positron emission tomography (PET), a 3D medical imaging technique, uses an unstable radionuclide that emits positrons as a source of positrons to investigate metabolic activity in the human body. In this technique, the radionuclide atoms are introduced into the body as part of a biologically active molecule, and the three dimensional concentration of this molecule in the body is computationally constructed by capturing the emitted gamma rays as positrons annihilate with the surrounding media. The PET medical imaging technique is very effective for investigating metabolic activity in the human brain in order to diagnose tumors.

In industries based on material science, mono-energetic positron beams are used to investigate semiconductor defects and porosity [8,9]. Positron lifetime measurements are frequently used in electronic manufacturing industries to investigate defective electronics, and the mechanical integrity and operational criteria of semiconductor devices.

The applications mentioned above are but a few of the techniques where positron spectroscopy is applied. More applications are anticipated in the future, including using positrons as a source for gamma ray laser production, [10] and possibly positron-induced mass spectrometry for identification of large biological molecules [11]. The main focus of this research is to contribute to the scientific understanding of the interaction of low energy positrons with organic and biological molecules, information that is essential to the possible future development of tandem positron-induced mass spectrometry techniques for biological and organic molecule analysis.

1.1 Experimental Studies of Positron Interaction with Atoms and Molecules

In the 1940s, positron lifetime spectroscopy and Doppler broadening annihilation radiation (DBAR) techniques were developed by studying two gamma and three gamma annihilation experiments [6]. After the existence of the electron-positron bound state (Ps),was theoretically proved by J. A. Wheeler in 1946, experimentalists began to study positron-atom and positron-molecule interactions in the gas phase [6, 12]. Positron annihilation rates for oxygen, helium and nitrogen were measured in the 1950s [6,13,14] and the existence of Ps, which was experimentally confirmed by a study of the three photon e^+-e^- annihilation process [15]. The experimental result for the three-photon annihilation rate is in good agreement with

the theoretical calculation done by A. Ore *et. al*. in 1949, and based on positron annihilation with a free electron gas of the same density [16].

The e^-e^+ annihilation rates for low energy e^+ incident on small alkane molecular gases at room temperature were further studied by Paul and Saint-Pierre [17]. They found that the annihilation rates increased more rapidly (by factors of 3-700) with respect to the molecular size than the theoretically predicted values, as calculated by Dirac [17,3]. This enhancement of the annihilation rates was proposed to be due to the polarization effect when introducing the positrons. The higher annihilation rate observed than the predicted values in Smith and Paul's experiment on positron-methane interaction is due to positron trapping in a positron-molecule bound state [18].

Another series of experiments on total cross-section measurement for positrons colliding with inert gases [19], di-atomic gases, [20] alkali metals, [21] and some molecular gases [20,22] was carried out by W.E. Kauppila *et. al*. at Wayne State University. They introduced new techniques of producing and interacting positrons with molecules [23]. A comparison of the positronic total cross-sectional data to the electronic cross-sectional data in the energy range 1-500eV showed that at energies >70 eV both curves merge, and at lower energies, the positronic cross-section was lower compared to the electronic measurements, for most of these gases. However, collisions with alkali metals the opposite behavior was found. Further, they observed that when the incident positron energy is < 5 eV, the total cross-section is increased in the case of diatomic [20].

Significant experimental efforts have also been expended to develop efficient positron accumulators to trap and cool positron plasmas to desired energies in the range of energy 0.05-100 eV; because the positrons from radioisotopes and from electron accelerators are

generally produced at higher energies [24-29]. In this energy range, positron-molecule interactions are significantly different from electron-molecule interactions due to the repulsive force between nuclei and the positron and the attractive force between electrons and positrons. It was suggested that as these interactions are opposite in sign for positrons, such that the overall interaction between the positron and the target molecule is likely to be weaker than the interaction between the electron and the target [6]. However, there is vast experimental evidence in the literature that indicate that the total cross-section of the target is considerably enhanced for low energy positrons, due to vibrational resonance modes [30, 34]. These experimental results were explained as a result of low-energy positrons becoming temporarily bound to the molecule via a vibrational Feshbach resonance, thus increasing the overlap time with the molecular electrons, and probability of annihilation [35].

1.2 Vibrational Feshbach-Resonance (VFR) and Positron-Molecule Binding Energy

The rate for two gamma positron-electron annihilation ($\lambda_{2\gamma}$) and the cross-section ($\sigma_{2\gamma}$) for a free gas was theoretically calculated by Dirac in 1930 for low positron energies ($v<<c$), as shown below [3].

$$\lambda_{2\gamma} = 4\pi r_0^2 c n_e \tag{1.1}$$

$$\sigma_{2\gamma} = \frac{4\pi r_0^2 c}{v} \tag{1.2}$$

Here $r_0=e^2/4\pi\varepsilon_0 mc^2$ is the classical electron radius *(r_0~$10^{-4}a_0$; a_0-Bohr radius)* and n_e is the electron density of the annihilation site. Equation 1.1 represents the annihilation rate due to a positron-electron pair in the spin singlet state. Because the positron-electron triplet spin state contributes <1% to the total annihilation rate of the singlet spin state, [6] it can be approximated that the total free gas positron-electron annihilation rate (λ) is given by $\lambda_{2\gamma}$ in

equation 1.2. For a system with a number density of n atoms/molecules where each atom/molecule has Z electrons, then the electron density n_e can be replaced by nZ (n_e=nZ) such that equation 1.1 can be expressed as below (1.3)

$$\lambda = 4\pi r_0^2 cnZ \tag{1.3}$$

The charge distribution of the parent atom/molecule changes due to the influence of electron-positron attraction when a positron is introduced to the system. To take this into account, the dimensionless parameter Z_{eff} (the effective number of electrons) needs to be included in the above equation.

$$Z_{eff} = \frac{\lambda}{\pi r_0^2 cn} = \frac{v\,\sigma_{2\gamma}}{\pi r_0^2 c} \tag{1.4}$$

If there are weak correlations between positrons and molecular electrons, Z_{eff} is expected to be close to Z, the actual number of electrons per molecule [6].

Many experimental studies have determined Z_{eff}, which is proportional to the annihilation rate, by measuring the total cross section of positron-atom/molecule interactions directly for a range of positron energies as explained in Section1.1.

According to the experimental data, at low incident energies there is a higher annihilation rate than theoretically predicted, even for small molecules [17], and the annihilation rate increases even more strongly with decreasing energy for larger molecules [32-34]. These Z_{eff} values differ from the theoretically predicted values, which are on the order of 10-10^6, and increase with molecular size. These, higher annihilation rates are too large to be explained only taking into account the attractive polarizing potential between the positron and the molecule [35].

The vibrational Feshbach-resonance (VFR) mechanism was proposed by G. F. Gribakin to explain the higher annihilation rates observed at low positronic energies. His

calculations of the annihilation rate in terms of the same well-defined parameters are in generally good agreement with the experimental results [35]. The VFR mechanism is a resonant annihilation mechanism in which the positron is temporarily captured into a bound state on a molecule. During capture, the positron transfers its excess energy (kinetic + binding) into the vibrational motion of the molecule. For the most effective capture, the incident positron energy must not be too large on the scale of the characteristic energies (hν) of the molecular vibrational modes [35]. The capture of the positron into a bound state on the molecule greatly extends the time that the positron spends near the molecule, increasing its annihilation rate with the electrons of the molecule.

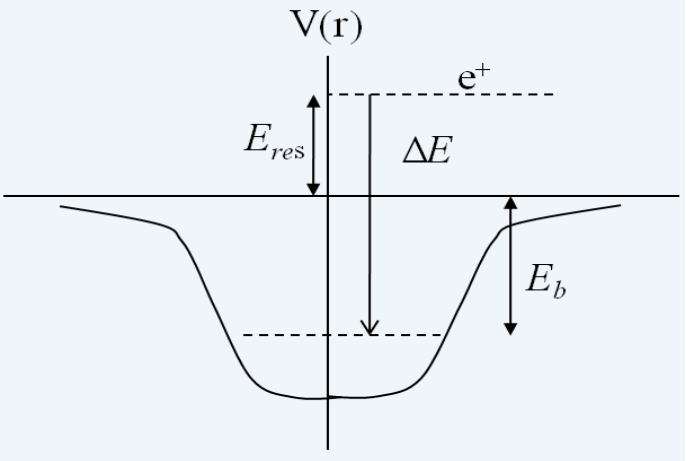

Figure 1.1 e^+-Molecule Bound State-VFR Mechanism

A schematic picture of a positron approaching a molecule with kinetic energy E_{res} *(incident positron energy)* falls into a bound state with binding energy, E_b, while transferring energy, ΔE, into the vibrational modes of the molecule as shown in Figure 1.1. In the case of a resonance involving the excitation of a single vibrational quantum of energy, $\Delta E = E_\upsilon = h\nu$. For this resonant capture to occur, the incident positron must have the energy given by equation 1.5:

$$E_{res} = E_v - E_b \quad (1.5)$$

The experimental entanglement of this VFR mechanism was further confirmed by L. D. Barnes *et. al.*[36] in their work on a series of experimental measurements of Z_{eff} with low energy positrons interacting with alkenes, C_nH_{2n+2} (n=2-12) of different configurations. As an example, a rapid increment of Z_{eff} for the $e^+C_5H_{12}$ system can be seen when the positron incident energy (E_{res}) is 300meV. The resonance energy for C-H stretching lies just above E_{res} at 380meV. According to VFR theory, the positron and molecule make a temporary bound state by exciting one of the vibrational modes of the molecule. In the case of C_5H_{12}, the C-H stretching gets excited, allowing the positron to become bound, and spend more time interacting with the target molecule. According to equation 1.5, the positron binding energy is 80 meV for $e^+C_5H_{12}$ system. The resonance will increase the interaction of the positron with the electrons in the molecule thus leading to higher Z_{eff}. When the positron becomes trapped in a temporary bound state, the ionization mechanism is given by in equation 1.6 below.

$$AB + \text{slow } e^+ \longrightarrow e^+AB \longrightarrow \text{photons} + AB^+ \quad (1.6)$$

This mechanism has been used to determine the positron-molecule binding energy experimentally for many molecules [36]. More than 30 molecules, including alkanes, alkane-related molecules, aromatics, alcohols and partially halogenated hydrocarbons, where all of the molecules have ionization energies that exceed the positronium formation energy (6.8 eV), were studied using the VFR mechanism to calculate positron-molecule binding energies [37]. The measured binding energies fitted well to a linear combination of the molecular dipole polarizability (α *in* $Å^3$) and the permanent dipole moment (μ *in D*) of the molecule, and the number of π bonds (N_π) in aromatic molecules according to equation 1.7.

$$\varepsilon_b = 12.4(\alpha + 1.6\mu + 2.4N_\pi - 5.6) \quad (meV) \quad (1.7)$$

In addition to the higher annihilation rates observed for low energy positrons interacting with molecules, there is also evidence that low energy positrons are capable of enhancing molecular ionization and fragmentation [11,38-42]. Because the positron is the anti-particle of the electron, even with negligible kinetic energy, it can annihilates with one of the electrons in the molecule, forming a molecular ion. Mass-spectrometry studies on low energy positron interaction with molecules [11,39-42] show that the positron can produce molecular fragmentation both above and below the positronium formation threshold. Further, the fragmentation rate can be varied by varying the incident positron energy. The importance of positron-induced fragmentation will be discussed in the next section. Theoretical investigation of low energy positron-induced fragmentation is the main objective of this research.

1.3 Positron-Induced Dissociation: Possibilities for a New Complementary Technique for Identifying Large Biological Molecules and Comparison with Existing Techniques

Positron ionization mass spectrometry was studied over a wide range of positron incident energies [38-42], where it was found that positrons can lead to molecular fragmentation. The fragmentation patterns observed for positrons-molecular gas collisions at high incident kinetic energy are similar to those for collisions with fast electrons [38]. This suggests that both fast positrons and fast electrons produce similar excitation in the parent molecule even though the Coulomb forces are opposite in sign for positron-electron and electron-electron interactions. The mechanism of such positron-induced fragmentation is shown in equation 1.8 below.

$$AB + \text{fast } e^+ \longrightarrow AB^+ + \text{fast } e^+ + \text{slow } e^-$$

$$AB^+ \longrightarrow A^+ + B^* \qquad (1.8)$$

Hydrocarbons interacting with low energy positrons above and below the Ps-formation threshold energies, (IE– 6.8 eV, where the IE is the ionization energy of the parent molecule and the e^+-e^- (Ps) binding energy is 6.8 eV), were carried out [39-42]. As an example, mass spectra were compared for decane ($C_{10}H_{22}$, IE=9.65 eV) for an incident positron energy of 4.3 eV (above the Ps-threshold) and 0.5eV (below the Ps-threshold) [40]. In the first case, the parent ion was observed as the base peak, whereas the other smaller peaks observed were produced by C- C bond cleavage along the backbone of the molecule. When the positron impact energy was 0.5 eV, which is below the Ps-formation threshold, the prominent species observed are $C_3H_7^+$ and $C_4H_9^+$, whereas species resulting from C-C bond cleavage at other points in the chain were observed as minor products. Above the Ps-formation threshold, ionization and fragmentation occurs as follows.

$$AB + e^+ \longrightarrow Ps + AB^+ \longrightarrow A^+ + B^* + \text{photons} \qquad (1.9)$$

Below the Ps- formation threshold, the positron binds to the molecule and annihilates with an electron, forming an ion molecule and then the fragmentation occurs as follows.

$$AB + e^+ \longrightarrow e^+AB \longrightarrow AB^+ + \text{photons}$$

$$AB^+ \longrightarrow A^+ + B^* \qquad (1.10)$$

A mechanism involving positron annihilation with an electron in an orbital below the highest occupied molecular orbital (HOMO) was proposed for molecular fragmentation induced by positrons at incident energies below the Ps-threshold [43]. If the positron annihilates with one of the electrons in a lower-energy molecular orbital, an excited molecular ion will be formed, with a missing electron in the lower energy molecular orbital. The energy

dissipated when one of the electrons in the HOMO jumps into the vacancy may be sufficient to break the bond and form the fragments ions. This mechanism is supported by semiempirical Hartree-Fock calculations for alkanes, and by comparison to experimental data for these molecules [43].

Experiments by Jun Xu *et al.* [39-42] on low energy positron (0.5-3 eV) collisions with hydrocarbons and phenyl hydrocarbons showed preferred cleavages along the backbone of the hydrocarbon chain, similar to the results obtained by Passner *et al.* [11]. The fragmentation rate was found to depend on the energy of the incident positrons. They also found that the fragmentation occurs by breaking σ bonds C—C, rather than double and triple bonds with π bonding.

There are several potential advantages of introducing positrons to induce fragmentation, allowing identification of long-chain biological molecules such as proteins, DNA, RNA, etc. Experiments on positron scattering with hydrocarbons show preferred fragmentation of linear chains rather than cyclic structures [39-42]. This is the preferred behavior for proteomics applications, where it is desirable to fragment the peptide backbone to determine the sequence of amino acids. Further, due to the polarity of peptides, (where the polarity occurs by connecting adjacent amino acids in peptides via an amide bond) a positron should attract strongly with the negatively charged sites. The annihilation of a positron with an electron at this site would result in rearrangement and possible cleavage of this bond. If cleavage can be stimulated by introducing a positron, it may potentially give useful complementary information for extracting sequence information for peptides. Therefore, positron ionization fragment analysis using mass spectrometry may find use in proteomics applications.

Collision induced dissociation (CID) [44], surface induced dissociation (SID) [45], electron capture dissociation (ECD) [46], and electron transfer dissociation (ETD) [47] are currently the most commonly used fragmentation methods for peptide and protein sequence analysis. The peptides (which have been protonated and transmitted into the gas phase using electrospray ionization (ESI) or matrix-assisted laser desorption/Ionization (MALDI) are accelerated in a vacuum using an electric field and directed to collide with an inert gas (He, N_2, Ar) in the CID method. In the SID method, accelerated ions collide with an organic surface. When the collisions occur, a certain percentage of the kinetic energy of the ions is converted to internal energy, and distributed over the ion leading to dissociation at the weaker bonds in the backbone, or more accurately along the low-energy fragmentation pathways.

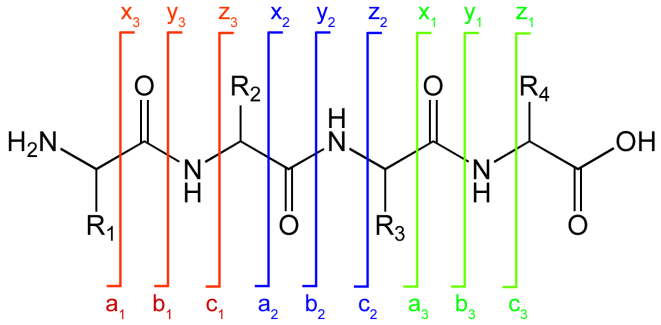

Figure 1.2 Peptide Fragmentation Scheme

The three possible cleavage patterns along a peptide backbone are shown in Figure 1.2, namely a_n-x_n, b_n-y_n and c_n-z_n. Preferential cleavage at the CO-NH amide bonds is observed for CID and SID methods producing b_n-y_n sequence ions. The fragmentation pathways observed for CID and SID of protonated peptides has been explained using the mobile proton model [48]. The protons in the collisionally activated protonated peptide can move throughout the peptide and become more populated in the backbone amino group, side chains, and amide oxygen and nitrogen sites. Protonation at the amide nitrogen forms CO-

NH_2^+, which weakens the amide bond and if there is sufficient internal energy gained via the collision, dissociation will occur by forming the preferred b_n-y_n fragments.

In contrast, the ECD and ETD methods result in preferential cleavage at the bond next to the peptide bond resulting in c_n-z_n sequence ions. In ECD, protonated peptides are directly introduced to low energy electrons.

$$[\ M + nH\ ]^{n+} + e^- \longrightarrow [\ [M + nH]^{(n-1)+}\ ]^* \longrightarrow \text{fragments} \qquad (1.11)$$

The capture of an electron by the peptide ion forms an excited radical species, which undergoes rapid cleavage along the backbone. In ETD radical anions are used as electron donors to the protonated peptides, and produce fragments in a fashion similar to the ECD mechanism.

$$[\ M + nH\ ]^{n+} + A^- \longrightarrow [\ [M + nH]^{(n-1)+}\ ]^* + A \longrightarrow \text{fragments} + A \qquad (1.12)$$

Activated dissociation of peptides via CID, SID, ECD and ETD requires that the peptides converted to gas phase ions, typically using ESI [49] or MALDI [50].

In positron-induced mass spectrometry (PIMS) /electron ionization (EI), protonation of the peptide prior to fragmentation is not needed. Therefore, for both of these methods, it would be possible for the analyte to be directly introduced to the positron without undergoing ionization. In PIMS, low energy positrons many act as the ionization source. In the EI method, molecules are ionized by a 70 eV electron beam, which leads to production of a number of fragmentation ions, and the molecular ion is often not observable. However lower electron energies generally do not produce efficient fragmentation resulting in poor sensitivity [51]. In contrast, low energy positrons in the range of 0-10 eV have shown capacity to produce considerable fragmentation without loss of the information of the parent molecular ion. Further, the fragmentation yield can be fine tuned by varying the incident positron energy

[11, 39-42]. Neutral and negatively charged ions can also be analyzed using PIMS due to the Coulomb attraction between the positron and the electronegative sites in the molecule.

In PIMS, further information about the annihilation site within the molecule can be determined by analyzing the γ ray spectrum emitted during the positron – electron annihilation process [33]. For example, it would be possible to statistically differentiate between a positron annihilating with electrons in a C-H bond and the C-C bonds in alkane chains via the γ ray spectrum. This additional chemical information regarding the specific sites where the annihilation occurred may be useful in proteomics. Post translational modifications (PTM's) of peptides may be difficult to observe if an insufficient number of fragments containing the PTM become charged. If the PTM's contain regions of high electron density, as in the case of phosphorylation and sulfation, then positrons may be strongly attracted to these sites. Evidence of annihilation of positrons with electrons belonging to PO bonds in the gamma ray photon spectrum, for example, may then indicate the presence of phosphorylation in a straightforward way.

Experimental evidence suggests that there are several potential advantages of PIMS over current methods used in proteomics as explained above. There are several experimental groups working on developing the experimental knowledge necessary to determine the long-term usefulness of PIMS including the Department of Physics, at Wayne State University, First Point Scientific, Inc., CA, and the Department of Engineering Physics at the Air Force Institute of Technology (AFIT).

Molecular fragmentation due to the annihilation of low energy positrons with electrons in organic molecules has been investigated experimentally and theoretically for possible applications and form the desire to understand how e^+ irradiation can damage DNA and

RNA. However, quantitative agreement between theory and experiment, based on first-principles calculations, has yet to be achieved. This research work has focused on a theoretical investigation of the interactions of low energy positrons with organic and biological molecules, and the development and testing of theoretical methods capable of obtaining a qualitatively correct picture of where annihilation occurs, and the amount of energy that is available for fragmentation as a result of e^+e^- annihilation for positrons bound to organic and biological molecules.

1.4 Dissertation Outline

Chapter 2 presents the theoretical calculations reported in the literature for positron-atom/molecule systems. The positronic wavefunction and the charge density distribution of positronic systems in different theoretical models are compared. In the latter part of Chapter 2, the qualitative reliability of the e^+e^- contact density at the Hartree-Fock level of theory will be discussed.

Chapter 3 explains the mathematical expressions used in the calculations and the methodology followed to obtain the atom-centered positronic basis sets (both contracted and uncontracted) with different sizes based on s, p, and d Gaussian functions. These atom-centered basis sets were developed for the first time in this field during this research. Further, the fundamental concepts that explain the observed fragmentation mechanisms and calculation methods are discussed.

In Chapter 4, the basis sets developed in Chapter 3 are tested against a range of molecules. In the case of diatomic molecules interacting with positrons, possible annihilation sites, and the variation of positronic and contact densities with respect to electrostatic

potential are discussed and compared to results available in the literature. Then with moderately sized molecules, the variation of contact densities with respect to basis centers, identification of criteria necessary for low cost calculation methods, population analysis of molecular orbitals, molecular orbital annihilation rates, and possible fragmentation pathways are discussed. The next set of molecules was selected because of biological interest or the availability of experimental positron-induced mass spectra or electron impact mass spectra. In this case all of the above mentioned parameters for moderately sized molecules were evaluated for interaction with a positron.

Chapter 5 discusses the conclusions, advantages and limitations of this theoretical model and future directions.

CHAPTER 2

THEORETICAL INVESTIGATION OF LOW ENERGY POSITRON INTERACTIONS WITH MOLECULES

Low-energy positron scattering experiments have shown that there are unexpectedly large annihilation cross sections for many organic molecules [17], which have been attributed to positron trapping in a positron-molecule bound state [18,30]. Low-energy positrons interacting with moderately sized and larger organic molecules can have annihilation cross sections enhanced by factors of 100-1000 or more [30-34], compared with cross sections in the absence of positron trapping, which was theoretically proved by Dirac in 1930 [2]. These experimental results have been explained as a result of the ability of low-energy positrons to become temporarily bound to the molecule via a vibrational Feshbach resonance, thus increasing their interaction time with the molecular electrons, and the probability of annihilation [35]. This simple explanation has been used to experimentally determine the positron-molecule binding energy for many molecules [37].

It has also been observed that the annihilation of low-energy positrons incident on organic molecules often leads to considerable molecular fragmentation with preferred cleavages along linear chains rather than in cyclic structures [11,39,41]. This suggests that analysis of the molecular fragments produced by positron annihilation may ultimately be able to provide useful complementary information for sequencing biological polymers such as proteins, DNA, and RNA. In order to predict fragmentation pathways of low-energy collisions of positrons with organic and biological molecules, it would be useful to know all possible e^+-e^-annihilation sites of the positron-molecule system. Calculation of the relative annihilation probabilities for a captured positron in different regions of the molecule can be used to

determine the possible e^+-e^- annihilation sites. Even a qualitatively correct picture of the relative probabilities for the positron to annihilate an electron in different regions of the molecule may provide a useful starting point for investigation of the possible fragmentation pathways for the molecule that may result from annihilation. Thus, a qualitatively correct calculation of the e^+-e^- contact density in the e^+-molecule system is needed.

However, obtaining even a qualitatively correct calculation of the e^+-e^- contact density is a challenging problem for large molecules. A few theoretical studies to determine the positron binding energies of e^+-monatomic, e^+-diatomic and e^+-triatomic systems were performed in the explicit correlated Gaussian (ECG) [52-54], quantum Monte Carlo (QMC) [55-58] and nuclear electronic orbital- explicit correlated Hartree Fock (NEO-XCHF) [59] methods of high accuracy. The most accurate calculations reported to date are for the e^+LiH based on ECG method [54]. The above methods cannot be expanded to the bigger e^+-molecule systems due to the higher computational demand [60]. The methods based on single particle-orbital calculations such as Configuration Interaction method (CI), cannot represents the Ps cluster well and require orbitals of very high angular momentum to properly describe the correlation between an electron-positron pair [60-62]. It has been reported [60] that to achieve a qualitatively acceptable energy for a small system such as e^+Li, where the electron-positron cluster formation is required because of the dramatic electron density changes due to the positron attraction, higher angular momentum $l=29$ are needed to form the total wave-function at the CI level. The ultimate accuracy that can be achieved for calculations of contact density at every level of theory depends on the ability of the basis set to capture the essentials of the wave-function at that level of theory. Basis sets are severely limited and must be carefully chosen due to computer limitations, especially for large molecules. More

accurate calculations require large basis sets to achieve high accuracy and truly converge the e^+e^- correlation.

Early work on positron interactions with moderately-size molecules (including acetone and urea) has often used a single center for the positron basis placed at the center of mass of the molecule [63,64]. Recent work by the same group, studied moderately size positron-molecule systems, placing the positron basis set at the most electronegative atom of the parent molecule [65,66]. In both studies they considered single- and double-excitation configuration interaction (MRI-CI) for the positron-electron correlation and used a bigger-diffused positronic basis set, including s, p and d functions in the early work and s, p, d, f, and g type Gaussian orbitals for the latest work. In order to guarantee accurate descriptions of positron-molecule bound states, other calculations [59,60] based on NEO-XCHF and CI have used a set of "ghost atom" positron basis centers with optimizable locations.

Present results indicate that, using a single-center positron basis does not provide the flexibility necessary to describe the contact density qualitatively correctly at the Hatree-Fock (HF) level, and more positron basis centers are needed to achieve qualitatively acceptable e^+e^- contact densities. On the other hand, optimizable positron basis centers are not feasible for investigating the interactions of positrons with large molecules, particularly those with no obvious axis of symmetry on which to place the "ghost atoms".

Determination of the e^+e^- annihilation sites requires calculation of the e^+ density and the e^+e^- contact density distribution for the e^+-molecule system. The e^+ density was calculated at the MRI-CI level for e^+ binding to alkali hydrides [67]. In all cases, the positron density contracted near (behind) the H atom, which is the most electronegative atom of the system. Recent work on positron binding to amino acids [66] and carbonyl containing species [65]

were performed at the same level of theory, and show higher positron density at the O atom where the most electronegative site of the system. Positron density and the contact density of the e^+LiH system were calculated at the ECG [53,54] and the NEO-XCHF [59] levels, and are the most accurate results done up to date. The higher positron density is located around the H atom, opposite the Li atom, in these methods. ECG and NEO-XCHF methods are much more sophisticated than the MRI-CI method. The relative positron density is also higher in ECG and NEO-XCHF methods as expected, but they are in qualitative agreement. Even though Li provides greater electron density than H, the e^+e^- contact density is almost four times smaller than that of the H site, and both methods find very similar e^+ density and e^+e^- contact density distribution along the range. Based on the relative probability of the contact density distribution of e^+LiH, it is obvious that the most probable annihilation site is at the H atom.

Theoretical investigations of the properties of positron bound states with atoms and molecules have included both computationally expensive calculations with state-of-the-art accuracy for positron bound states with atoms and diatomic molecules, and less expensive calculations with more qualitative than quantitative accuracy for positron bound states with moderate sized molecules.

2.1 Criteria for Qualitative Reliability of Hartree-Fock-Based Calculations of Contact Density and Application to Positrons Bound to Peptides, DNA and RNA Fragments, and Similar Organic Molecules

Peptides and proteins, DNA and RNA fragments, and similar organic molecules have regions containing significant excess negative charge, and should therefore be able to bind a positron in HF calculations, which is the first requirement for getting a qualitatively reliable description of the properties of a positron bound to a molecule at the Hartree-Fock level, MP2, or other low-level perturbative calculations based on Hartree-Fock. Both the amino acids of which peptides and proteins are composed and the nucleotides of which DNA and RNA are composed are made up of primarily C and H atoms, and containing a small number of more electronegative atoms (O, N and S). In Chapter 4, we show plots of the electrostatic potential for small organic molecules of similar composition considered in this work, and demonstrate that there is a deep well of negative electrostatic potential near the most electronegative atom in these molecules that is capable of binding a positron.

Proper inclusion of electron-positron correlation is necessary to obtain an accurate description of the formation of the positronium cluster that occurs when the most loosely bound electron is bound more strongly to the positron than to the remainder of the system. This occurs for a positron bound to a neutral atom or molecule with ionization energy (IE) << the formation energy of the positronium, 6.8 eV, or for a positron bound to a negatively charged atom or molecule with an electron affinity (EA) << 6.8 eV. In such systems, the electron-positron correlations are so strong that the most loosely bound electron and the positron are best described as a positronium cluster loosely bound to the remaining system, as has been discussed for positron-atomic systems in the review by Mitroy *et al.* [61]. For

example, the stochastic variational method (SVM) and the fixed-core stochastic variational method (FCSVM) calculations, using explicitly correlated Gaussian (ECG) basis functions, show that e^+Li [68], e^+Na [69], HPs [68] and the alkali positrides LiPs, NaPs and KPs [70] are well described as a positronium cluster bound to a core consisting of the remainder of the system.

Because HF calculations cannot properly represent the formation of the Ps cluster within such systems, significant differences are seen between HF results and the results of more accurate calculations of the positron, electron, and contact densities in these systems. Results for the electron and positron radial densities for LiPs obtained from NEO-XCHF calculations [59], which include only electron-positron correlation and not the smaller electron-electron correlation effects, agree well with the SVM results [68], and both show that the positron and valence electron densities for LiPs coalesce at large distances from the nucleus. However, HF positron and valence electron densities [59] for LiPs do not coalesce at large distances from the nucleus to the same extent as is seen in the NEO-XCHF [59] and SVM [68] calculations, where the valence electron density falls off faster with increasing distance from the nucleus and the positron density extends further out from the nucleus than in the calculations that include electron-positron correlations [59]. In addition, significant differences are found between the qualitative features of the contact density distribution for LiPs obtained using HF and those obtained using NEO-XCHF calculations [59]. The HF contact density is shifted significantly towards the nucleus relative to the NEO-XCHF contact density, and the HF contact density has a much more prominent secondary peak in the core region, indicating that the positron can annihilate with core as well as valence electrons at the HF level. In the NEO-XCHF calculations, which can properly represent the formation of the

Ps cluster in LiPs, the positron will mainly annihilate with valence electrons [59]. Preferential annihilation of valence electrons is in agreement with the suggestion [61] that because the annihilation rate for LiPs is only slightly higher than 2 x 10^9/s, annihilation of the positron with electrons that are not part of the Ps cluster makes a relatively small contribution to the total LiPs annihilation rate.

Electron-positron correlations are weaker when the most loosely bound electron is bound less strongly to the positron than to the rest of the system. Such weaker binding occurs for a positron bound to a neutral atom or molecule with an IE >> 6.8 eV, or for positronium bound to a negatively charged atom or molecule with an EA >> 6.8 eV. Because the positron and the nucleus (or nuclei) repel each other and cannot simultaneously be closely bound to the most weakly bound electron, such systems can be well described as a weakly bound positron orbiting at some distance from the remainder of the system, as has been discussed for positron-atomic systems by Mitroy *et al.* [61]. In these systems, the effect of the positron on the electronic wavefunctions is small. For example, FCSVM calculations with ECG basis functions show that the mean positron distance from the nucleus in e^+Be is 3.7 times the mean distance for the valence electrons from the nucleus, and the mean distance of the valence electrons from the nucleus is only increased 3% by the presence of the positron [61].

Hartree-Fock calculations have been found to give qualitatively reliable results for the relative contributions of different atoms to the contact density for a positron bound to a molecule with an IE >> 6.8 eV. For e^+LiH, the qualitative features of the contact density distributions from two HF calculations [71,59] using different electron and positron basis sets agree well with the contact density distribution computed from explicitly correlated Gaussian

(ECG) calculations [53]. Both find a larger peak in the contact density on the H atom, demonstrating that for molecules with an IE >> 6.8 eV, HF calculations can predict on which atom in a molecule the contact density will be the greatest. The larger molecules of interest, including biological molecules such as amino acids, peptides, DNA and RNA bases were found to have IE's greater than 6.8 eV (9-11 eV). As those molecules have few electronegative sites such as O and N, the positron should bind to them even at the HF level. Due to the weak e^+e^- correlation (IE >> 6.8 eV) this bound state should be correctly described as positron-molecule (not as the positronium-molecule) bound state and therefore qualitatively correct positron density as well as the contact density can be expected for these biological molecules (and other molecules with IE >> 6.8 eV and regions of different electronegativity) at the HF level of theory.

However, obtaining qualitatively accurate results for the contact density at the HF level requires careful convergence with respect to the positron basis set. Although the scaled contact densities from two well-converged HF calculations using different positron basis sets [71,59] both agree very well with the ECG contact density [53], the relative magnitudes of the contact density peaks are found to be more sensitive to the basis set in the HF calculations than in the NEO-XCHF calculations: use of a less complete basis set produces a larger peak in the HF contact density on the Li atom than on the H atom in e^+LiH, which is qualitatively incorrect [59].

To date, positron basis sets for HF calculations have generally included basis functions centered on "ghost atoms" [see *eg.* Refs.59 and 71] whose optimal placement in the molecule is not easily determined [60]. For large molecules, which may have considerably lower symmetry than diatomic molecules, optimizing the placement of such "ghost atoms" is not

feasible. Even the optimization of positron basis sets at fixed centers becomes difficult for very large molecules.

2.2 Research Goal

The goal of this work is to develop a way of doing reliable and computationally less expensive calculations of properties such as the distribution of positron density for positrons bound to large biological molecules, ultimately allowing investigation of the most likely e^+e^- annihilation sites and the resulting fragmentation pathways for the molecule.

CHAPTER 3

ATOM-CENTERED POSITRONIC BASIS SETS AND THE e^+-e^- CONTACT DENSITY

The purpose of this work is to investigate whether positron basis sets composed solely of a practical set of atom-centered functions are able to produce qualitatively correct HF contact densities for organic molecules similar in composition to larger molecules of biological interest, such as peptides and DNA fragments. Therefore, atom-centered basis sets of different sizes were developed that can be used without further optimization to study interactions of positrons with organic and biological molecules containing C, H, O and N.

3.1 Computational Expressions

It is necessary to treat electrons and positrons quantum mechanically as they are quantum particles. The system that we are interested in consists of one positron and many electrons (N_e) with a N_c classical nuclei. The Born-Oppenheimer Hamiltonian of such a particle system (in atomic units) can be written as follows:

$$\hat{H} = -\frac{1}{2}\sum_{i}^{N_e}\nabla_i^2 - \frac{1}{2}\nabla_p^2 - \sum_{i}^{N_e}\sum_{A}^{N_c}\frac{Z_A}{|r_i^e - r_i^c|} + \frac{1}{2}\sum_{i\neq j}^{N_e}\frac{1}{|r_i^e - r_j^e|} + \sum_{A}^{N_c}\frac{Z_A}{|r^p - r_A^c|} - \sum_{i}^{N_e}\frac{1}{|r_i^e - r^p|} \quad (3.1)$$

where coordinates of the electrons, positron and classical nuclei are given as r_i^e , $r^p$and r_A^c respectively. The charge on classical nuclei is denoted by Z_A. Indices *i*, and *j* refer to electrons, whereas index *A* refers to the classical nuclei.

The multi-particle Hartree-Fock wavefunction, Ψ_{tot} is taken as a single product of electronic and nuclear determinants of spin orbitals [72,73] as follows:

$$\Psi_{tot} = \Psi^e(r^e)\Psi^p(r^p) \quad (3.2)$$

where $\Psi^e(r^e)$ and $\Psi^p(r^p)$ are antisymmetrized electronic and positronic wavefunctions (single Slater determinant of single particle spin-orbitals), and r^e and r^p represent the spatial coordinates of the electrons and the positron, respectively. The variational method with respect to the mixed positronic-electronic wavefunction is used to minimize the energy of a given system [74,75]. The positron single-particle wavefunction is expressed in terms of a linear combination of Gaussian-type orbitals, centered at the nuclei of the atoms in the molecule. For a positron at (r^p, θ, φ):

$$\phi(r^p,\theta,\varphi) = \sum_{\substack{\mu=O_1,O_2\ldots \\ \mu=N_1,N_2\ldots \\ \mu=C_1,C_2\ldots \\ \mu=H_1,H_2\ldots}} \sum_{l,m} Y_l^m(\theta_{\mu p},\varphi_{\mu p}) \sum_i^N C_{\mu lmi} r_{\mu p}^l e^{-\alpha_{\mu li} r_{\mu p}^2} \qquad (3.3)$$

where $r_{\mu p}$ is the distance between the atomic nucleus and the positron. Optimization of the Gaussian functions $\{C_{\mu lmi},\ \alpha_{\mu li}\}$ becomes increasingly difficult as the number of Gaussian primitives N increases, due to very strong coupling between nonlinear variational parameters. Therefore, alternative methods are developed to optimize Gaussian exponents using a limited number of parameters. George A. Petersson *et al.* [76] have proposed a new methodology to optimize the basis sets from even-tempered to a fully optimized. They have expanded the logarithm of the exponents in the orthonormal Legendre polynomials, P_k, as follows:

$$ln(\alpha_{\mu li}) = \sum_{k=0}^{k_{max}} A_k P_k \left(\frac{2i-2}{N-1} - 1\right) \qquad (3.4)$$

where A_k is the variational parameter, $k_{max} = 1$ corresponds to an even tempered basis set, and $k_{max} = N-1$ corresponds to a fully optimized basis set. Hence, variational collapse of $\{\alpha_{\mu li}\}$ can be eliminated in this approach, $k_{max} = 1$ was used in this research work. A computer algorithm was developed by Dr. Gary Kedziora at Air Force Institute of Technology in Dayton, 2008, using the proposed procedure described in Ref. [76], with help of the nonlinear optimization

algorithm developed by Powell [77]. The program is named as “BasOpt” and is capable of optimizing electronic and positronic basis sets using GAMESS and GAMESS NEO. Fundamental steps involved in constructing the algorithm are summarized as follows.

The BasOpt program algorithm

1. Guess $\alpha_{\mu li}$
2. Calculate non-linear parameter A_k using the Legendre mapping
3. Generate GAMESS -NEO basis functions using the $\alpha_{\mu li}$
4. Run GAMESS-NEO
5. Filter energy from GAMESS-NEO output
6. Call optimization routine with energy and A_k and receive new A_k
7. If not converged, use returned A_k and repeat steps (2) through(6)

Initially, the BasOpt algorithm could handle only un-contracted positronic basis sets, but now we have added the capability to handle contracted positronic basis sets as well. We have optimized different sizes of contracted and uncontracted positron basis sets that are appropriate to use for C, H, N, O, Li, Na, and Be atoms centers. The procedure for the optimization of these basis sets is discussed in the Section 3.2.

In order to understand and predict fragmentation mechanisms when a low energy positron interacts with a molecule, it is necessary to identify which electrons in the molecular orbitals overlap heavily with the positron wavefunction. If the positron annihilates with one of the electrons in the highest occupied molecular orbital (HOMO), it leads to the formation of the molecular ion. But if the positron annihilates with an inner electron, energy is liberated when one of the electrons in the HOMO falls to the vacant state and leads to fragmentation of the molecule if the liberated energy exceeds the relavant activation energy. Because the

annihilation rate is directly promotional to the probability of finding an electron and a positron in a same place, the probability of overlap between the positron wavefunction and each of the molecular electronic orbitals can be found by calculating the annihilation rate. The spin averaged annihilation rate for an electronically closed-shell system with *N* doubly-occupied electron orbitals and a single positron is given by equation 3.5.

$$\lambda = 2\pi r_0^2 c \sum_{i=1}^{N} \int_{R^{3(N+1)}} \Psi^*(r^e, r^p)\delta(r_i^e - r^p)\Psi(r^e, r^p) dr^e dr^p \qquad (3.5)$$

where r_0 is the classical electron radius ($r_0=e^2/m_e c^2$ *in cgs units*) and *c* is the speed of light. It has been shown that the annihilation rate can be simplified to the summation of individual contributions to the annihilation rate of each molecular orbital at the HF level of theory [73] as implemented in to the GAMEES-NEO package.

$$\lambda = 2\pi r_0^2 c \sum_{i=1}^{N} S_{i\,i}^{1\,1}\,;\ \ where\ S_{i\,j}^{k\,l} = \int \phi_i^e \phi_j^e \phi_k^p \phi_l^p dr \qquad (3.6)$$

By knowing the individual molecular orbital annihilation rates, the most probable molecular orbital at which positron annihilation takes place can be found. Further, energy liberated when an electron in the HOMO jumps to the vacant molecular orbital can also be calculated.

3.2 Development of Positronic Basis Sets

Atom-centered basis sets of different sizes can be used to study the interaction of positrons with large organic and biological molecules (containing C, H, O and N) without further optimization. Tests were conducted to determine which basis sets are sufficient to give a qualitatively correct picture of the electron-positron contact density both in comparison to ECG results for e^+LiH, and moderately-sized molecules having compositions similar to peptides and other biological molecules.

First, diatomic positron-molecule systems such as e^+LiH, e^+BeO, PsCH, PsOH, and PsCN were used to optimize the positron basis sets considering positron basis centers on both atoms. In order to obtain the exponents of the optimized basis set, energies of a representative set of molecules were minimized by varying one exponent at a time (using the BasOpt code as explained in previous section and using the NEO-HF level theory with the 6-31+G(d,p) electronic basis set). The optimization of a positronic basis set for a particular atom center can be expressed as follows.

Development of un-contracted positronic basis set

1. Geometry optimization for parent molecule at the DFT B3LYP/6-31+G(d,p) level of theory

   Here we performed a freq-opt calculation to make sure that the molecule possessed no imaginary modes, i.e no negative frequencies. Then a stable=opt calculation is performed to ensure that the wavefunction optimized to the ground state conformation with the proper frequency modes. This process is repeated until the structure is optimized to the desired convergence.

2. Call the BasOpt algorithm ($k_{max}=1$) to optimize the even-tempered positronic exponent of the one basis center (while freezing the other centers) for the optimized structure.

   Here the same starting even-tempered ($\alpha_{\mu,l,i+1} = c\alpha_{\mu,l,i}$; *c-constant*) positronic basis set was used for both centers. (The procedure associated with the BasOpt algorithm was discussed in the previous section.)

3. The second basis center was optimized while freezing the previously optimized basis set at the first center.

4. Iteratively optimize the positronic exponents one center at a time until the energy of e^+-molecule system converges.
5. Repeat the steps1 though 4 with different starting even-tempered positronic basis sets.
6. Each of the starting basis sets can be determined by investigating the Eigenvectors of the NEO-HF output file. The range of the different types of (different *l* values) exponents was determined according to the coefficient corresponding to each exponent. Exponents that are heavily used (higher coefficient value) were included in the next starting basis set. This step is essential to avoid the selection of a wrong basis set that yields energy of a local minimum.

We have also added the capability to handle the contracted positronic basis set to the BasOpt program. The process of development of a contracted basis set follows same steps as described above except for the step 3.

Development of Contracted positronic basis set

3.1. Heavily used exponents with similar *l* values were contracted and the un-contracted positronic exponents at the second basis center were optimized.

3.2. Heavily used positronic exponents with similar *l* values at the second basis center were contracted and the un-contracted positronic exponents at the first basis center were re-optimized while freezing the contracted exponents.

We have developed 13s9p, 13s9p3d larger un-contracted positronic basis sets, and contracted positronic basis sets consisting of s, p and d functions for the five di-atomic systems mentioned above. Also smaller contracted positronic basis sets for C atom centers (3s6p, 2s), N atom centers (3s5p, 2s), and H atom centers (1s) were developed for the lager

e^+-molecule systems (See Appendix A). In all of these cases we found diffused positronic basis sets were used heavily.

In order to evaluate the ability of the positronic basis set developed using five di-atomic systems mentioned above to properly describe larger molecule systems, we have conducted the following series of tests.

1. First, energy, positron density and the contact density changes were tested for optimized positronic basis sets obtained from various molecule systems. As an example, we shuffled the optimized positronic basis sets for the H centers obtained from the e^+LiH, e^+NaH, PsOH and PsCH systems and changes in the energy, positron density and the contact density were observed. Similar tests were conducted for all other systems in this study. Results indicate energy changes less than a micro-Hartree and the effect on positron density and the contact density were negligible. The minimum energy value was observed for the molecule to which the basis set was originally used.
2. Next, similar calculations were carried out for the $e^+CH_3COCH_3$, $e^+CH_3CONH_2$, $e^+NH_2CONH_2$, e^+HCOCH_3, e^+HCONH_2 and e^+H_2CO systems. Tests were also conducted to decide whether the exponents should be scaled to account for different charges on the atoms in these molecules. Scaling resulted in changes in the minimum in the micro-Hartree range, and no significant impact on the positron density and the contact density were observed.

According to the calculations, different sizes of un-contracted and contracted positronic basis sets for the e^+(H), e^+(C), e^+(N) and e^+(O) basis centers were selected for larger e^+-molecule systems in a way that the basis set indicates minimal impact on the energy

change. A detailed discussion of the results on the positron density distribution and the contact density distribution of different sized of e^+-molecule systems are presented in Chapter 4.

3.3 Visualization of e^+e^- Contact Density Distribution

The contact density distribution of e^+e^- is the probability of finding a positron and an electron at the same place. This allows identification of the possible e^+e^- annihilation site in a given e^+-molecule system. In equation 3.2. a mixed electronic-positronic wavefunction was defined as the product of an antisymmetrized electronic wavefunction and the positronic wavefunction at HF the level of theory. Individual electronic and positronic densities can be calculated by multiplying each wavefunction with its own complex conjugate ($\rho = \Psi^* \Psi$). Because, individual the electronic and positronic distribution is already available, the contact density can be calculated as the product of the electron and positron density distribution ($\rho_e \rho_{e+}$) at the HF level of theory.

It is important to visualize the positron density and the contact density of a given e^+molecular system in 1D, 2D and 3D spaces. This lead to a clear understanding of how these properties vary with the electronic properties such as molecular electrostatic potential of the molecule with respect to the positronic basis sets. Therefore, a Mathematica code was developed to visualize electron density, positron density, contact density, molecular electrostatic potential and molecular orbitals in 1D, 2D and 3D spaces.

CHAPTER 4

RESULTS AND DISCUSSION

The positronic basis sets developed here were tested with moderately size molecules as well as larger molecules consisting of H, C, N and O atoms. The positron and positron-electron contact density variation is calculated as function of the size of positronic basis sets. Because our main focus is to develop an efficient theoretical method that is reliable and computationally tractable which will allow us to study the interactions of positrons with large biological molecules, a series of calculations were carried out to determine which basis centers are necessary to form positronic basis sets, and then discuss the limitations. The possible e^+e^- annihilation sites and the possible fragmentation pathways were also determined for larger e^+-molecule systems. The positronic basis sets developed can be found in Appendix A. In this chapter, we discuss the results of the positron density, contact density, and possible fragmentation patterns of e^+-molecule systems.

We first studied the interaction of positrons the diatomic systems LiH, BeO, $(C\text{-}H)^-$, $(C\text{-}N)^-$, and $(O\text{-}H)^-$. This study will allow us to determine the relationship between the most probable sites a positron will associate with and the relative electronegativity of the associated atoms.

4.1 Positron Affinity of e^+-Diatomic Systems

The optimized large atom-centered positron basis sets (13s9p, 13s9p3d and contracted) were tested with the five above-mentioned e^+-diatomic systems. Table 4.1.1 shows the positron affinity of e^+-diatomic systems at the NEO-HF/NEO-MP2 levels of theory, and is compared to the best calculated values available in literature. The 6-31+G(d,p) electronic basis set was used for all of the calculations.

Table 4.1.1 Computed Positron Affinity (PA) for the e^+-Diatomic Systems

Method HF/MP2 E(au)	Positronic basis set (both centers) NEO-HF/NEO-MP2			Best in Literature
	13s9p E(au) PA(mH/meV)	139p3d E(au) PA(mH/meV)	Contracted (s,p,d) E(au) PA(mH/meV)	PA (mH)
LiH -7.981450 -8.001797	-7.986791 5.34/145.32 -8.010173 8.34/227.93	-7.986793 5.34/145.39 -8.010231 8.43/229.43	-7.986793 5.34/145.38 -8.010226 8.43/229.36	34 (0.9 eV) ECG (Ref.54)
BeO -89.414914 -89.656420	-89.426602 11.69/318.05 -89.666948 10.53/286.49	-89.426609 11.70/318.23 -89.667363 10.94/297.78	-89.426607 11.69/318.18 -89.667213 10.79/293.69	28 (0.8 eV) QMC (Ref.55)
PsCH -38.219308 -38.336499	-38.369219 149.91/4.079 eV -38.498855 162.35/4.417eV	-38.371229 151.92/4.133eV -38.502654 166.15/4.521eV	-38.371227 151.92/4.133eV -38.502603 166.10/4.519eV	153 (4.2 eV) QMC (Ref56)
PsCN -92.313779 -92.602801	-92.452180 138.40/3.766eV -92.738481 135.68/3.692eV	-92.452202 138.42/3.766eV -92.762014 159.12/4.332eV	-92.452201 138.42/3.766eV -92.761981 159.18/4.331eV	140 (3.8 eV) HF(Ref.78)
PsOH -75.383956 -75.601605	-75.562886 178.93/4.868eV -75.792992 191.38/5.207eV	-75.562897 178.94/4.869eV -75.793854 192.25/5.231eV	-75.562897 178.94/4.869eV -75.793860 192.25/5.231eV	194 (5.3 eV) QMC (Ref.56)

All five e^+-diatomic systems were studied at many levels of theory. The most accurate positron affinities were obtained using the ECG method for e^+LiH [54], the QMC method for the e^+BeO, PsCH and the PsOH systems [55,56], and the HF method for the PsCN system [78]. Electron-electron and electron-positron correlations were taken into account in the ECG and QMC methods. Therefore, the calculated positron affinity of each system at the NEO-HF level exhibits a significant difference as the NEO-HF method does not consider any of the correlations between the particles. The positron affinity was considerably improved for the NEO-MP2 method as it contains the electron-positron correlation, even though the positron affinity is well below that calculated in the ECG and QMC methods for binding to neutral

molecules, such as e^+LiH and e^+BeO. When the positron binds to negatively charged molecules, such as PsCH, and PsOH, the agreement in the positron affinity is considerably improved for all the methods.

Based on results determined in this work, adding d functions to the positronic basis sets did not improve the positron affinity at the NEO-HF level of theory, but slightly improved it at the NEO-MP2 level of theory. The e^+ density and the e^+-e^- density distributions for the five diatomic systems examined exhibit insignificant changes with these three types of positronic basis sets. Therefore, the 13s9p atom-centered positronic basis sets were (at the NEO-HF level of theory) used for further comparisons.

4.2 Molecular Electrostatic Potential and the e^+e^- Contact Density Distribution of e^+-Diatomic Systems

The relation between the molecular electrostatic potential and the positron density distribution of the e^+-diatomic molecules were determined. Most important, the e^+-e^- annihilation site, using the electronic-positronic contact density, was identified for each system. In all cases, the 13s9p atom-centered positronic basis sets and 6-31+G(d,p) electronic basis sets were used within the NEO-HF model.

The molecular electrostatic potential, positron, and contact density variation along the bond axis of the e^+LiH system are illustrated in Figure 4.2.1. The highest positive potential can be seen at the Li nucleus, whereas the positive potential at the H nucleus is significantly smaller. The negative potential is located on the opposite side of the H atom. The positron density is also greater in this region of negative potential. The positron density at the Li atom vanishes due to the positron nucleus repulsion and, at the H nucleus, a dip can be seen. Even

though, a higher electron density occurs at the Li site, the most probable e^+e^- annihilation site is at the H site where the contact density is also large.

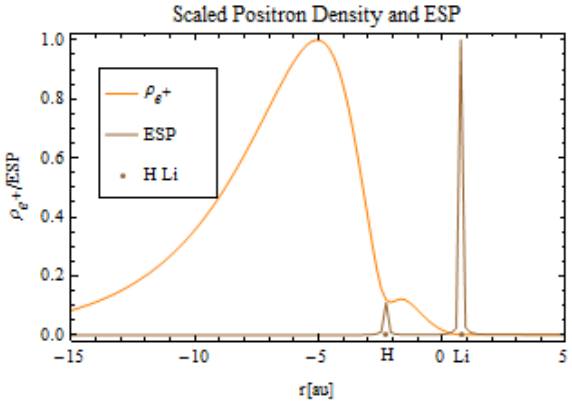

(a)

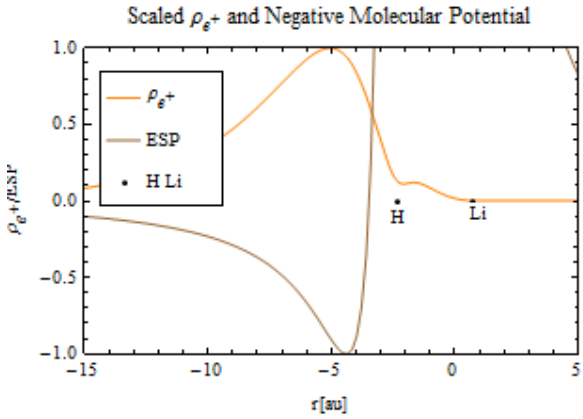

(b)

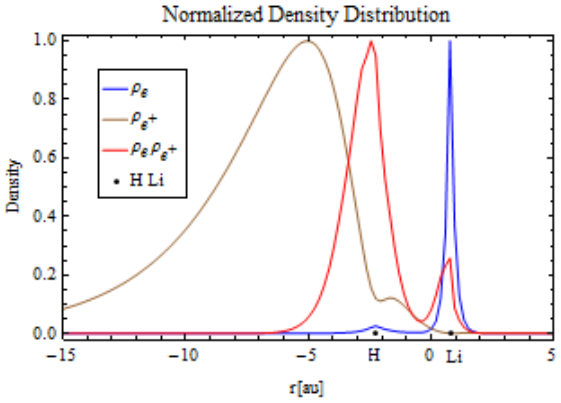

(c)

Figure 4.2.1 e^+LiH Molecular Electrostatic Potential and Electronic, Positronic and Contact Density distributions (a) Scaled ESP and the ρ_{e+}, (b) Scaled Negative ESP and the ρ_{e+} and (c)Normalized ρ_e, ρ_{e+} and ρ_{ee+}

The next system studied was e^+BeO. Figure 4.2.2 shows the molecular electrostatic potential and the individual electronic, positronic and contact density variation along the bond axis of the e^+BeO system. The positive potential peaks can be seen at each of the nuclei while at the Be nucleus there is a respectively higher positive potential than that at the O nucleus. A very low positive potential distribution can be seen in between the two atoms and in the region close to the Be atom opposite to the O atom. The negative potential well can be seen close to the O atom opposite to the Be atom. The positron density is higher in the region

where the potential is most negative. The positron density is minimum at the nuclei sites. The calculated electron density is higher at the O atom and the electron density at the Be atom is respectively very low. The calculated contact density is highest at the O site where the most negative potential is located. The highest peak represents the core region of the O atom and the region above the O atom represents the valance region.

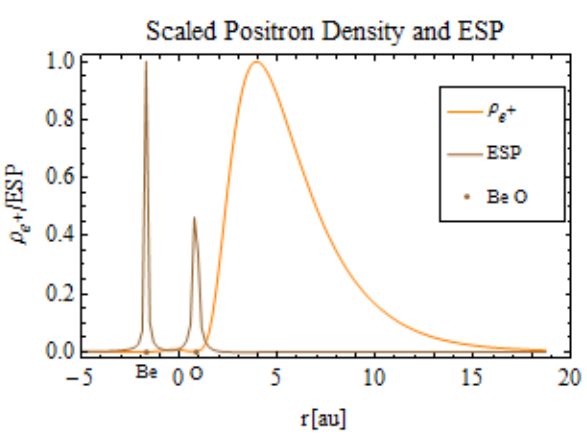

(a)

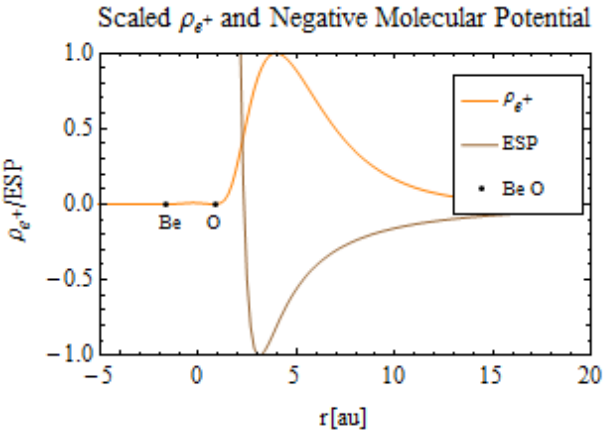

(b)

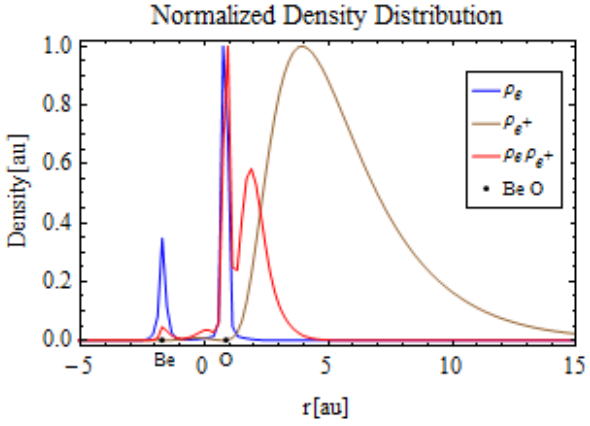

(c)

Figure 4.2.2 e^+BeO Molecular Electrostatic Potential and Electronic, Positronic and Contact Density Distributions (a) Scaled ESP and the ρ_{e+}, (b) Scaled Negative ESP and the ρ_{e+} and (c)Normalized ρ_e, ρ_{e+} and ρ_{ee+}

Prior to extending the study towards biomolecules, it is important to study the positron interactions with C-H bonds. As shown in Figure 4.2.3, a positive potential is seen between the atoms and negative potential elsewhere. On the top of each nucleus a positive potential

peak can be seen with the smaller peak associated with the H atom. Even though, there are considerable negative potential regions on both sides, the deepest negative potential well can be seen near the C atom end (opposite to the H atom). Therefore, a higher positron density is seen at the C atom site, where the deepest negative potential region exists. Due to the repulsive potential between the positron and each nucleus, the positron density is minimized at each nucleus; however, it is not zero in between the nuclei, albeit, it is small.

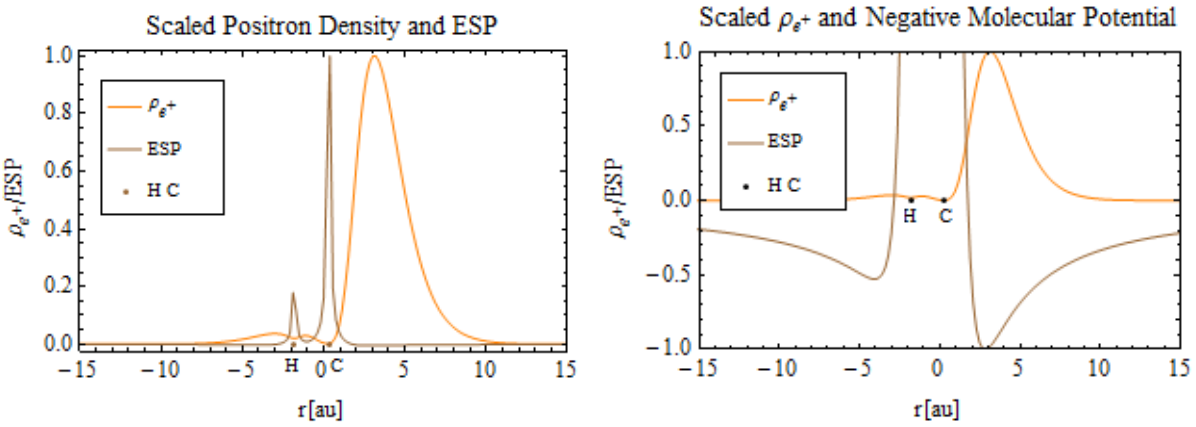

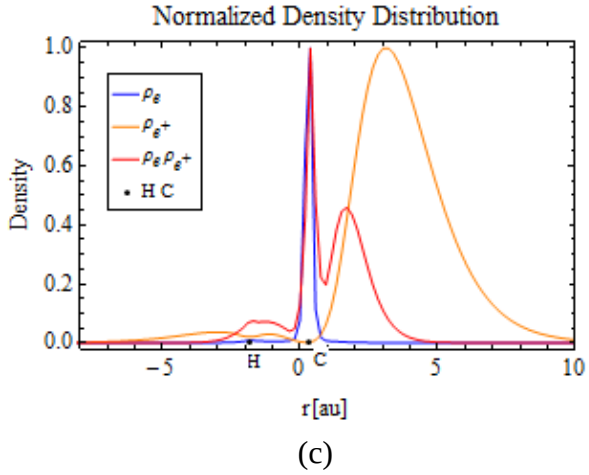

Figure 4.2.3 PsCH Molecular Electrostatic Potential and Electronic, Positronic and Contact Density Distributions (a) Scaled ESP and the ρ_{e+}, (b) Scaled Negative ESP and the ρ_{e+} and (c)Normalized ρ_e, ρ_{e+} and ρ_{ee+}

According to the calculated contact density, the positron wavefunction overlaps heavily with the electronic wavefunction near the C atom end, and due to the higher electron density on the C atom, a larger contact density peak is found on the C atom.

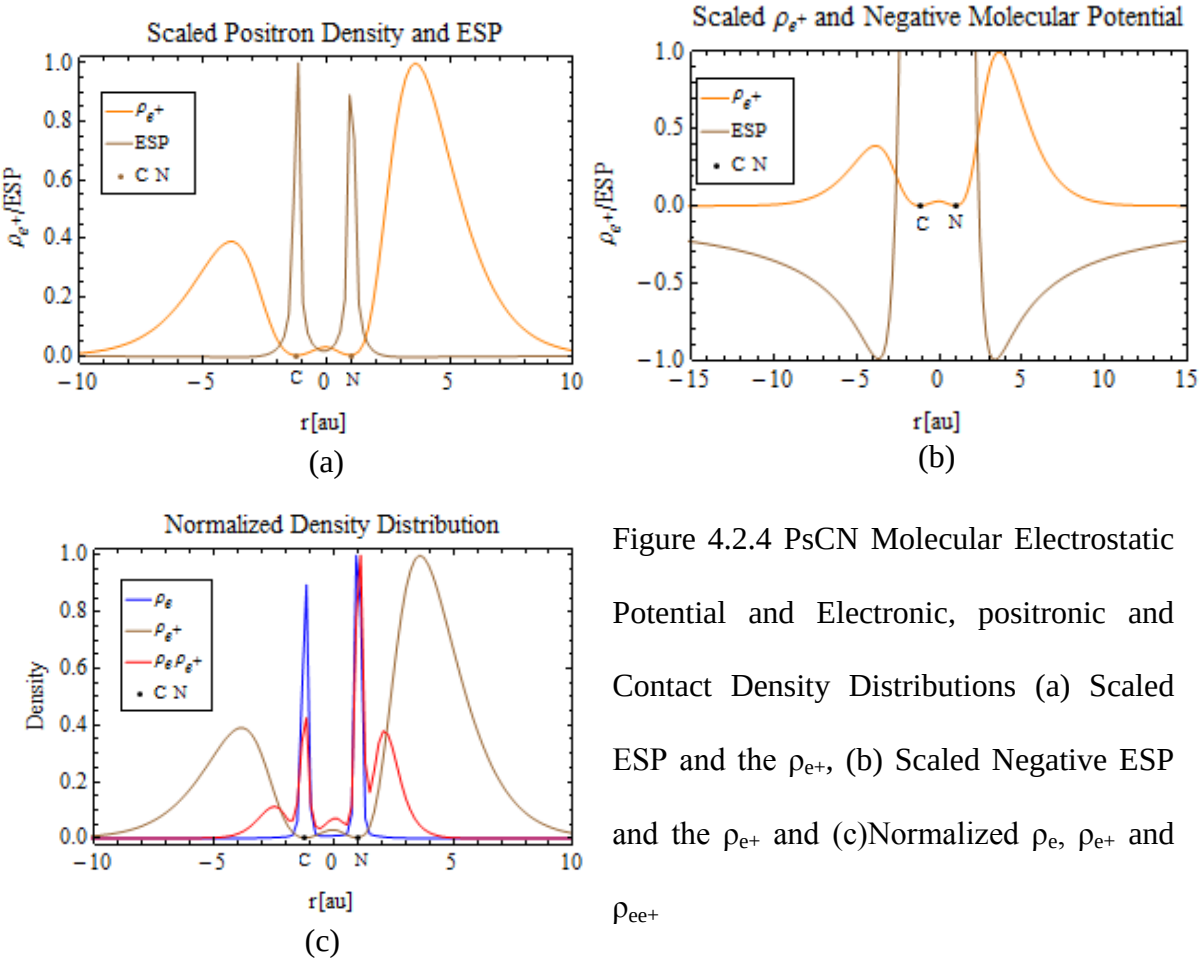

Figure 4.2.4 PsCN Molecular Electrostatic Potential and Electronic, positronic and Contact Density Distributions (a) Scaled ESP and the ρ_{e+}, (b) Scaled Negative ESP and the ρ_{e+} and (c)Normalized ρ_e, ρ_{e+} and ρ_{ee+}

Similar to the other cases, the positive potential peaks can be seen centered on each nucleus of the PsCN system, whereas the minimum positive potential is observed between the two atoms, as illustrated in Figure 4.2.4. On both ends of the molecule (N atom and C atom), the negative potential wells exhibits of similar depth. The positron density is highest in the regions where the negative potential sites are located. Further, higher positron density is observed at the N atom site (opposite to the C atom) due to the higher repulsion potential at the C atom site with respect to that of N site. The electron density is slightly greater on the N atom and, as a result, a higher a peak is found in the contact density at this same site. In both

negative potential regions, the contact density is large with the N atom site having the highest contact density.

The next system focuses on how a positron interacts with an OH^- moiety. According to Figure 4.2.5 the PsOH system has positive potential located between the atoms and negative potential above the O and below the H atom while the deeper negative potential well is located at the O atom end (opposite to the H atom). The positive potential peak at the H atom is much smaller than that found at the O atom, while minimum positive potential is seen between the atoms.

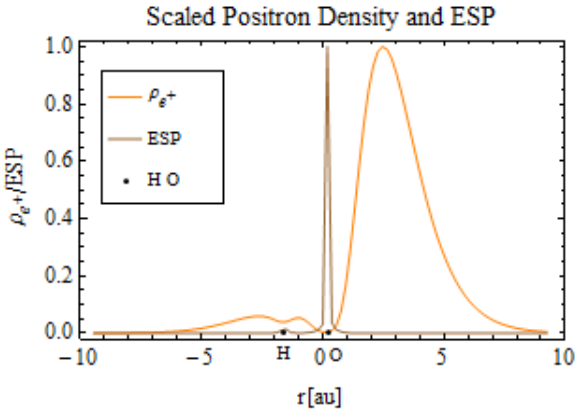

(a)

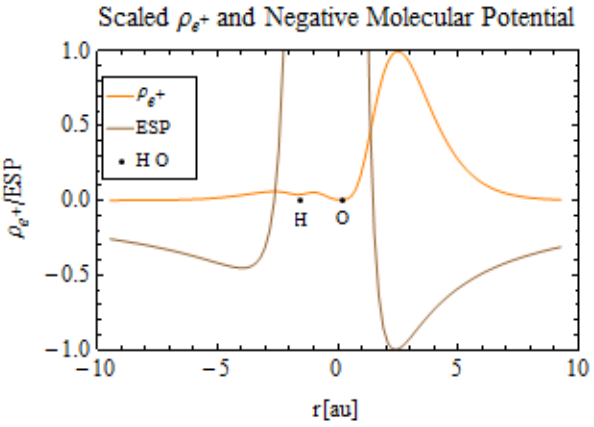

(b)

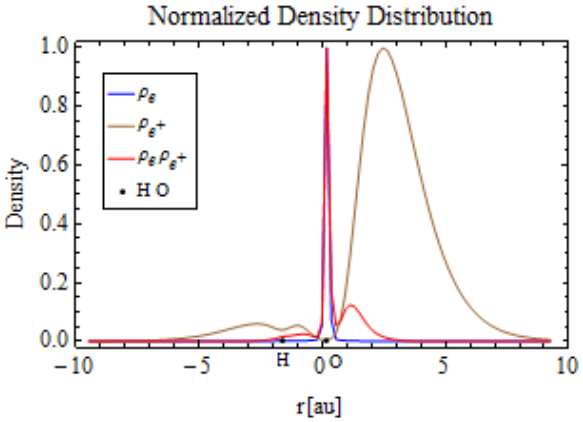

(c)

Figure 4.2.5 PsOH Molecular Electrostatic Potential and Electronic, Positronic and Contact Density Distributions (a) Scaled ESP and the ρ_{e+}, (b) Scaled Negative ESP and the ρ_{e+} and (c)Normalized ρ_e, ρ_{e+} and ρ_{ee+}

The positron density is higher at the O site where the deeper negative potential region exists. According to the calculated contact density, the core electronic region of the O atom overlaps heavily with the positron wavefunction with a considerable valance contribution.

In what follows, we present the trends observed when a positron interacts with a diatomic system. As shown in Figures 4.2.1-4.2.5, (i) higher positron density can be found at the most negative potential sites, (ii) the positron wavefunction becomes minimum near the nucleus (Coulombic repulsion) (iii) the potential is much lower between the atoms than on the nuclei; therefore, the positron density appeares to be non-zero in between the atoms with respect to the positron density on each nucleus. If the positron density and the electron density are high at the same site, then the core contribution of the contact density appears to be high at that site and the valence region also makes a significant contribution to the contact density. If the region of high electron density and high positron density occur in opposite regions as in the case of e^+LiH, the greatest contact density is found at the most electronegative site (higher positron density region) without involvement of the core. Based on the contact density results, the most probable e^+e^- annihilation site will be the most electronegative site of the molecule.

4.3 e^+LiH System (our work vs NEO-XCHF vs ECG)

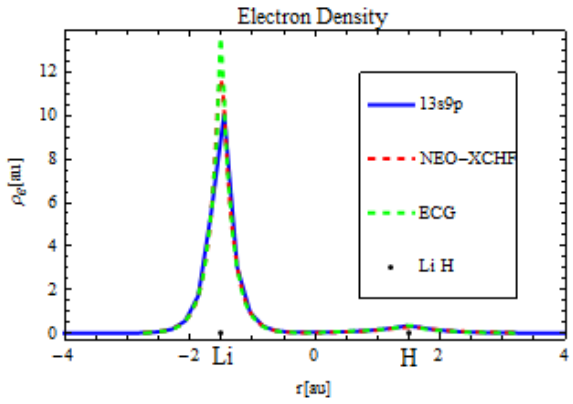

(a)

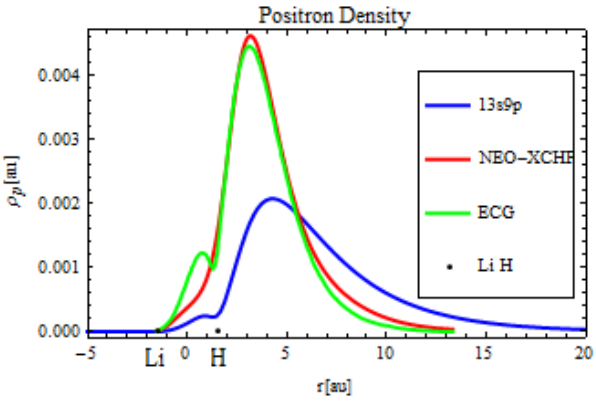

(b)

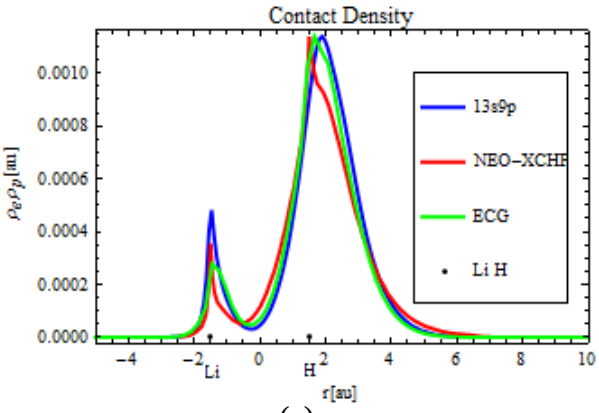

(c)

Figure 4.3.1 e^+LiH System (a)Electron Density (b) Positron Density and (c) Contact Density

In order to check for qualitative accuracy, the results (electron density, positron density and contact density) were compared for e^+LiH (blue) using the ECG (green) and NEO-XCHF (red) methods, which are the most accurate calculations available in the literature [54,59]. The comparison is done by taking in to account the geometrical equilibrium of the LiH molecule ($R_{Li–H}$=3.015 bohr). The results for the contact density were scaled to the same maximum value; and show good qualitative agreement as seen in Figure 4.3.1C.

In the ECG [54] method, 1024 ECGs were utilized to construct five particle wavefunctions with optimized position for one basis center. The correlation between electron-

electron and electron-positron was considered in the ECG method. The ground-state energy of the system was determined as -8.104850 Hartrees (PA=34mHartrees) using the ECG method. Using the NEO-XCHF [59] method, Gaussian basis sets were utilized to represent electron and positron molecular orbitals and explicitly correlated Gaussian-type geminal functions were used to describe the electron-positron correlation, and used one basis center at the optimized position with eight geminal functions. The electron-electron correlation was not implemented in this calculation. In our results we used 13s9p atom-centered uncontracted gaussian type orbitals to construct the positron wavefunction with the 6-31+G(d,p) electronic basis set for the NEO-HF level of theory. The ground state energy is -7.986563 Hartrees and the calculated positron affinity (5mHartrees) was six times less than found with the ECG method.

For all three methods, the greatest electron density is found at the Li nucleus, whereas the positron density is largest at the H atom site (opposite to the Li). Both the NEO-XCHF and ECG methods quantitatively agree with the positions of the peaks and the magnitudes of the positron density. In our work, we did not take into account the correlation between the particles, particularlythe electron-positron correlation. Therefore, the positron wavefunction is more diffuse and the density peak not as localized on the H atom, as found with the other two methods. But there can is found a second maxima in the calculated positron density between the Li and H atom using the ECG method. According to the characteristics of the positron density in our calculations, it is clear that there is qualitative agreement with the positron density distribution along in the surrounding space found using highly accurate methods such as ECG and NEO-XCHF. The calculated contact density shows similar behavior in each of the other methods, while our results were much less localized in comparison. For all methods,

smaller peak occurs at the Li atom, whereas a bigger peak occurs at the H atom. According to the contact density distribution, a higher overlap between the electron and positron wavefunctions can be seen at the H site. Thus, we can conclude that the positron is more likely to annihilate with one of the electrons at the H site.

Even though the ECG method produces more accurate positronic and contact density distributions for the e^+-molecule systems, the computational cost of the ECG method precludes extending this work to bigger molecules [61]. Our results for the positron density and the contact density are in qualitative agreement with the most accurate results available in the literature. The ionization energy of the LiH molecule (~ 8 eV) is greater than the positronium formation energy (6.8 eV). Therefore electrons are more likely to remain near the nuclei, while the positron and the nuclei repell each other. Such a system can be studied qualitatively using the NEO-HF model and can be expanded to bigger molecules as these calculations are not nearly as demanding as e.g using the ECG model.

4.4 Low-Energy Positron Interactions with Moderate Sized Molecules

The optimized positron basis sets were tested with moderate-size molecules such as formaldehyde (H_2CO), formamide ($HCONH_2$), acetaldehyde ($HCOCH_3$), acetamide (CH_3CONH_2), acetone (CH_3COCH_3) and urea (NH_2CONH_2). All of these molecules have ionization energies greater than the positronium formation energy. The positron was bound to the molecule in all the cases. Table 4.4.1 shows the ground-state energy and the positron affinity of the positron-molecule system in NEO-HF level of theory. The 6-31+G(d,p) electronic basis and 13s9p positron basis centers were used at all heavy atom centers. The 4s3p positron basis was used for the H atom centers.

Table 4.4.1 Positron Affinity of Moderate Sized e^+-Molecule Systems

System	Energy (a.u.) NEO-HF	PA (μH) Our work	PA(μH) Best value
e^+H_2CO	-113.873135	31	684 -CI (Ref. 79)
$e^+(CH_3)_2CO$	-191.975934	244	165 MRD-CI (Ref. 80),Single positronic basis center at CM
$e^+(NH_2)_2CO$	-224.008713	977	492 MRD-CI (Ref. 80), Single positronic basis center at CM
e^+HCOCH_3	-152.926271	152	-
e^+HCONH_2	-168.947144	1041	-
$e^+NH_2COCH_3$	-207.995939	1145	-

Even though the ECG and DMC methods can calculate correlation effects of positron – molecule systems with high accuracy, the computational cost of these methods makes them prohibitive for calculating the positron affinity of larger e^+-molecule systems. There are few studies in the literature that calculate the positron affinity of a few of the above systems for simple models [79,80] The highest positron affinity for the e^+H_2CO system is 684μH which was carried out at the CI level of theory [79] considering the double electron-positron excitations, while core electronic excitations were excluded. Here the 6-311G** electronic basis set was used, and for the positron wavefunction an atom-centered basis sets and off-atom s, p and d type diffused basis sets were used in addition to the 6-311G** basis. In this study, the author found that a greater contribution to the positron affinity was given by the atom-centered positronic basis sets than for the off atom positronic basis sets.

The positron affinity and the positron density distribution of the $e^+(CH_3)_2CO$ and $e^+(NH_2)_2CO$ systems were studied within MRI-CI level model [80] including single

electronic, single positronic, and single positronic–single electronic excitations. To represent the electron wavefunction, aug-cc-pvdz basis and additional diffuse and polarized functions were used. A large positronic basis set, including s, p and d type Gaussian type functions was centered on the center of mass of the molecule. In our study, we used developed atom-centered positronic basis sets consisting of a 4s3p basis on H atom centers.The calculation difficulties due to the linear dependences were occurred when we used the 13s9p large diffuse basis function for all atom centers similar to the study in Ref.79. Therefore the optimized 4s3p positronic basis for the H atom centers was used for the calculations in this work. The calculated positron affinity for the e^+H_2CO system was more than 20 times less in our calculations, with respect to MRI-CI calculations mainly due to the correlation effects considered in Ref.79. Even though correlation effects were considered in Ref. 80 for the $e^+(CH_3)_2CO$ and $e^+(NH_2)_2CO$ systems, our results show higher positron affinity for both systems. According to the calculation done in the Ref.79 the atom-centered positronic basis sets contributed to a lower energy of the e^+molecule system than for the off atom positronic basis sets. In the Ref. 80 the large positronic basis sets was located at the center of mass of the molecular system and it may be the reason for getting a lower positron affinity than for our calculations.

Our main objective here is to obtain the qualitatively correct positron density and the contact density for the above motioned e^+-molecule systems. The following figures show the positron density and the contact density variation with respect the molecular electrostatic potential. In all the figures, molecular electrostatic potential contours and the 3D e^+e^- contact density contours are given in atomic units.

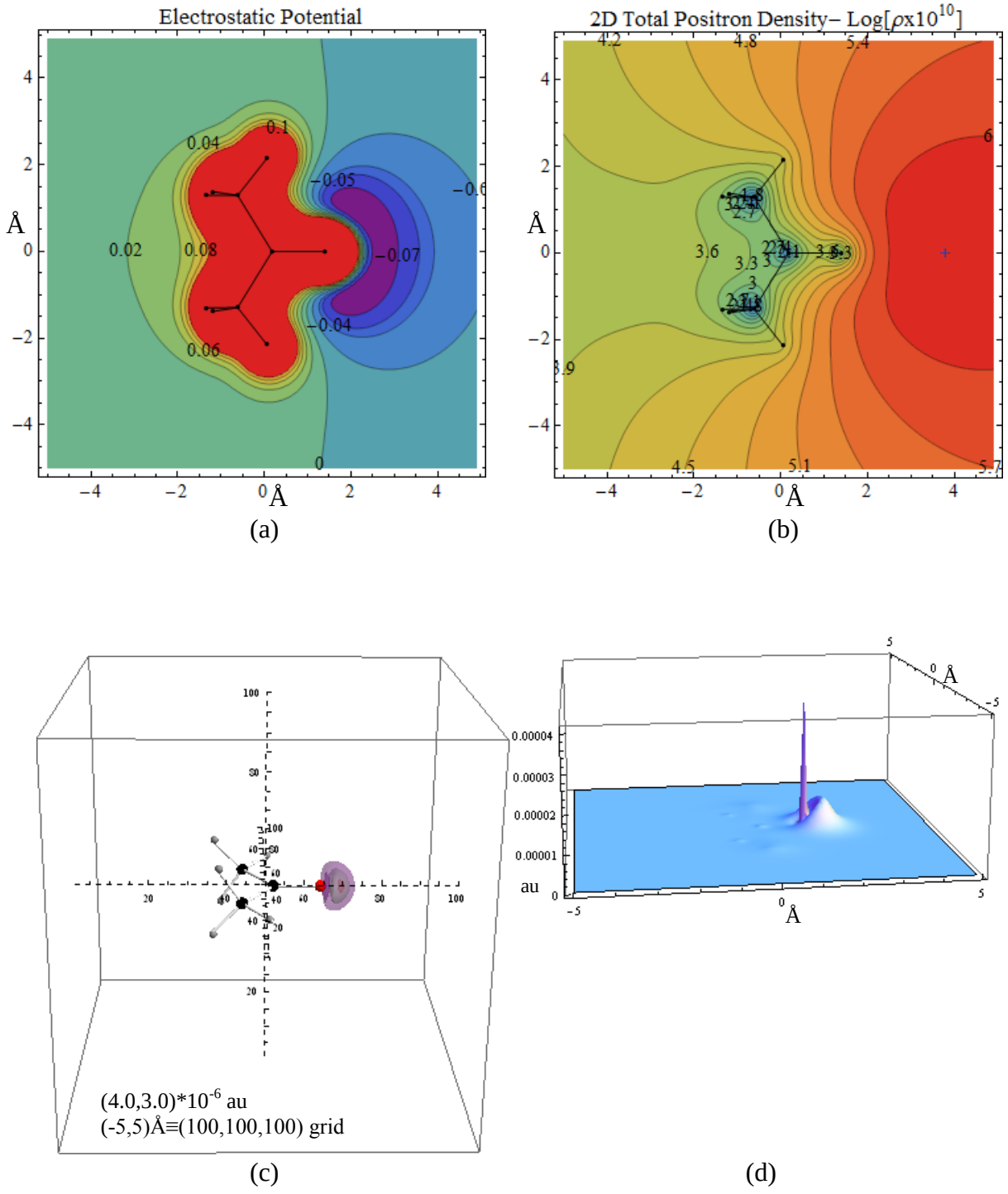

Figure 4.4.1 $e^+CH_3COCH_3$ [e^+(H)4s3p, e^+(C,N,O) 13s9p/ NEO-HF]
(a) Molecular Electrostatic Potential (b) Positron Density Distribution in Log Space
(c) 3-D Contact Density (d) 2D View of the Contact Density of the Center Layer

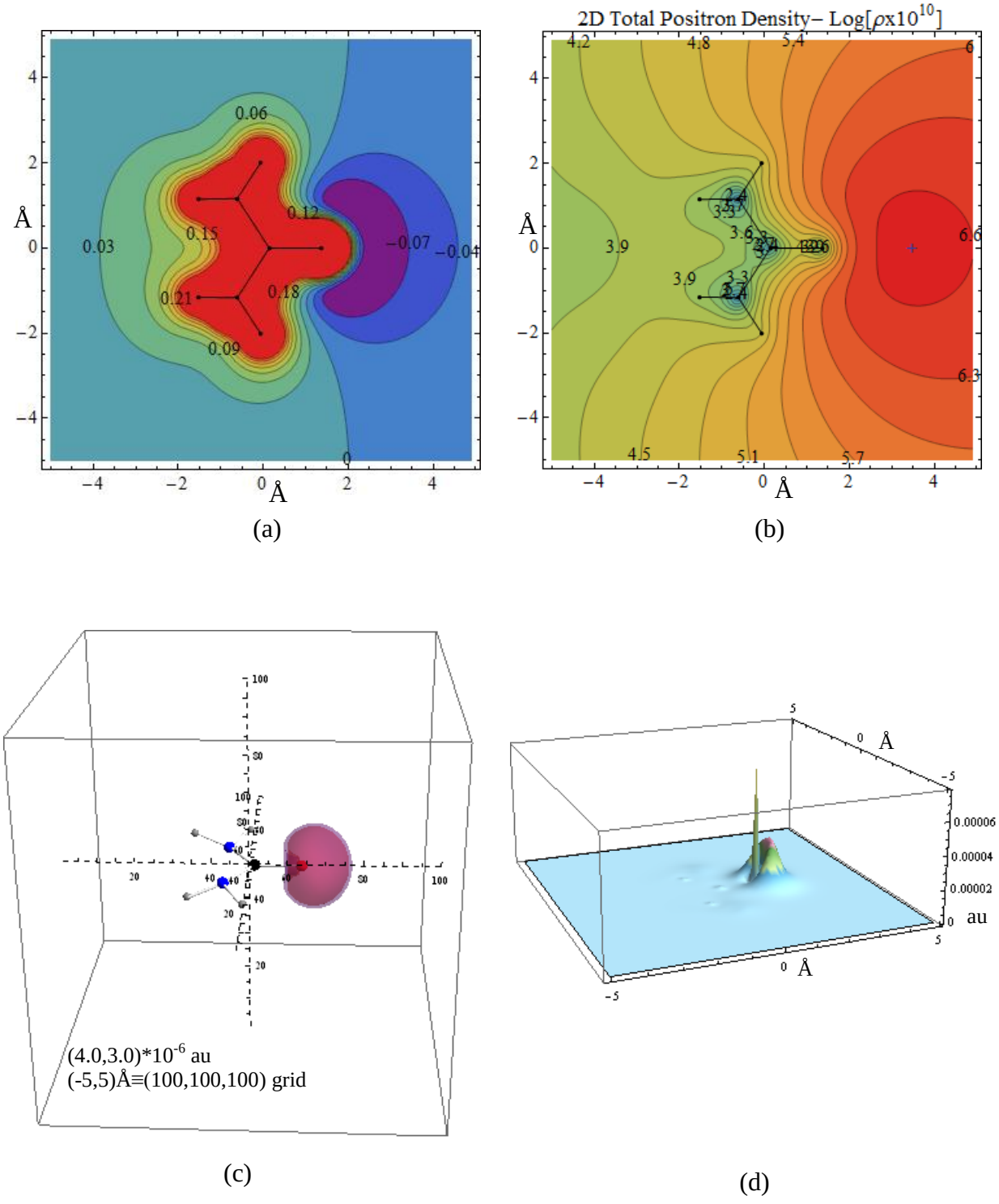

Figure 4.4.2 $e^+NH_2CONH_2$ [e^+(H)4s3p, e^+(C,N,O) 13s9p/ NEO-HF]
(a) Molecular Electrostatic Potential (b) Positron Density Distribution in Log Space
(c) 3-D Contact Density (d) 3D View of the Contact Density of the Center Layer

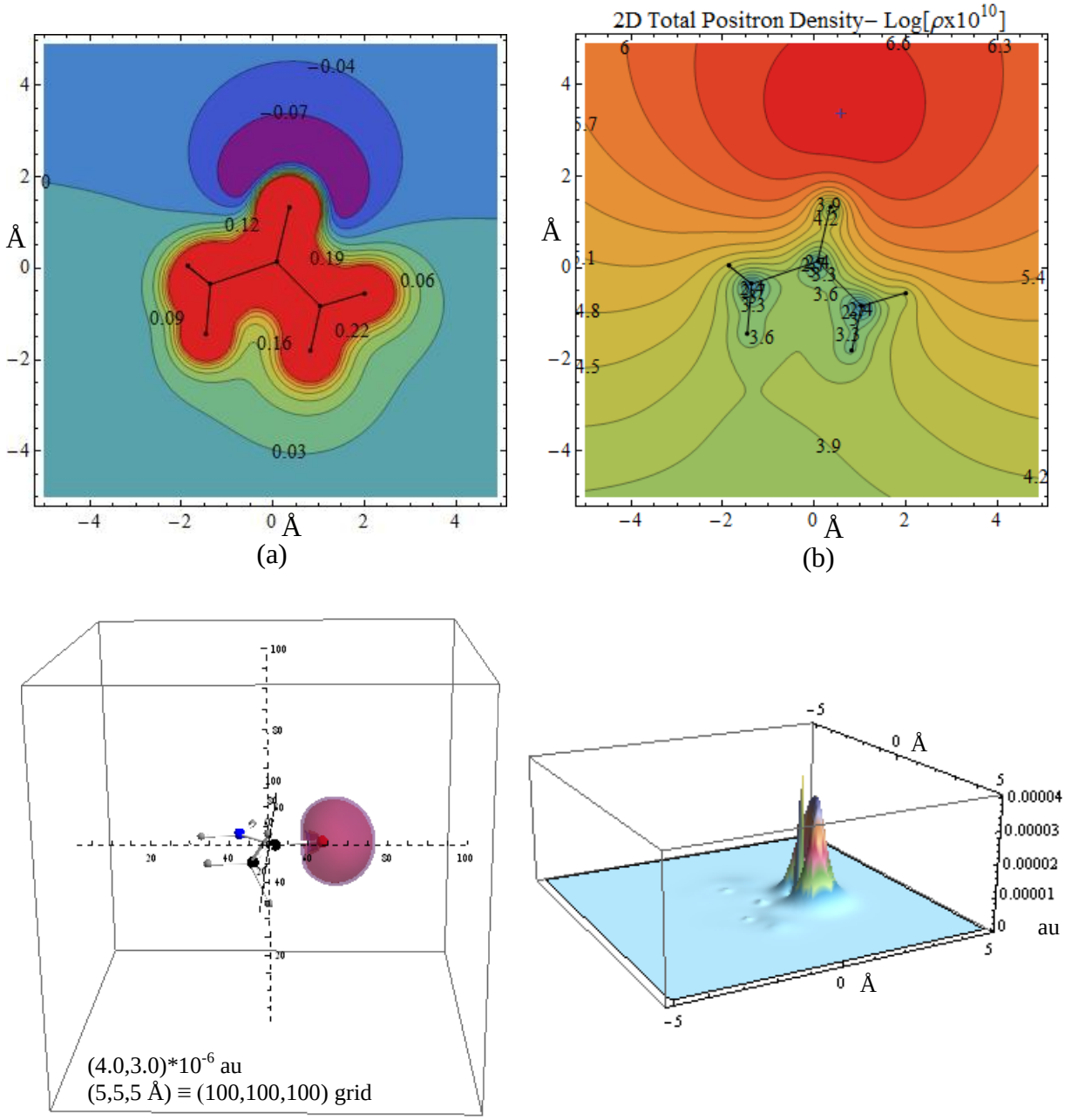

Figure 4.4.3 $e^+CH_3CONH_2$ [e^+(H)4s3p, e^+(C,N,O) 13s9p/ NEO-HF]
(a) Molecular Electrostatic Potential (b) Positron Density Distribution in Log Space
(c) 3-D Contact Density (d) 3D view of the Contact Density of the Center Layer

As shown in above figures the negative potential well can be seen above the O atom and according to that the higher positron density can be seen that same region in all the cases. Also the positron wavefunction clearly avoids the nucleus as we observed in the e^+-diatomic cases. The calculated positron density distribution in this work qualitatively agrees with the calculation done by *Tachikawa et. al.* in Ref.80 for the $e^+CH_3COCH_3$ and $e^+NH_2CONH_2$ systems. The highest electron density is at the O atom of the above systems and the N atom sites have the second highest electron density followed by the C sites and finally the H sites. But as seen in the positron density distribution figures, the positron density almost vanishes below region of Oxygen site. Therefore, the higher contact density peak can be seen above the O site. As shown in the three dimensional view of the 2 dimensional contact density of the center layer in each of the systems, there is a core contribution as well as a valance region of the O atom due to the higher electron density at the O atom. According to the contact density distribution the electron and the positron wavefunctions heavily overlap at the O site and therefore there is a high probability of positron annihilate with one of the electron at that same site.

4.5 Low Cost Calculation for Qualitatively Correct Contact Density

In order to reduce the computational cost the following series of calculations were performed on the above molecules in Table 4.4.1. The calculated energy, positron density and contact density were compared first keeping the positron basis set on all atoms then just on the C, N and O atoms, and then just on N, and O atoms and finally keeping the positron basis set only on the O atom. In all the cases there is no significant difference in contact density

when we omit the positron basis centers at the H atoms. The positron affinity changes by < 1.5% as well.

Table 4.5.1 Ground State Energy (a.u.) and PA with Respect to e^+ Basis Centers e^+(H)-4s3p, e^+(C)-13s9p,e^+(N)-13s9p and e^+(O)-13s9p

System	Basis centers	Energy (a.u)	PA (μH)	PA (meV)
H_2CO	6-31+G(d,p)	-113.873104		
e^+H_2CO	All centers	-113.873135	31.47	0.86
	Omit e^+(H)	-113.873135	31.19	0.85
	Only on O	-113.873122	18.13	0.49
CH_3COCH_3	6-31+G(d,p)	-191.975691		
e^+ CH_3COCH_3	All centers	-191.975934	243.50	6.63
	Omit e^+(H)	-191.975931	240.39	6.54
	Omit e^+(H) and middle e^+(C)	-191.975927	236.86	6.45
	Only on O	-191.975870	179.26	4.88
$HCOCH_3$	6-31+G(d,p)	-152.926118		
e^+ $HCOCH_3$	All centers	-152.926271	152.43	4.15
	Omit e^+(H)	-152.926270	151.31	4.12
	Omit e^+(H) and middle e^+(C)	-152.926266	147.99	4.03
	Only on O	-152.926236	117.33	3.19
NH_2CONH_2	6-31+G(d,p)	-224.007736		
e^+ NH_2CONH_2	All centers	-224.008713	977.27	26.59
	Omit e^+(H)	-224.008703	967.37	26.32
	Omit e^+(C,H)	-224.008669	932.68	25.38
	Only on O	-224.008475	739.16	20.11
$HCONH_2$	6-31+G(d,p)	-168.946102		
e^+ $HCONH_2$	All centers	-168.947144	1041.63	28.34
	Omit e^+(H)	-168.947139	1036.62	28.21
	Omit e^+(C,H)	-168.947116	1013.44	27.58
	Only on O	-168.947005	902.77	24.57
CH_3CONH_2	6-31+G(d,p)	-207.994794		
e^+ CH_3CONH_2	All centers	-207.995939	1145.18	31.16
	Omit e^+(H)	-207.995929	1134.98	30.88
	Omit e^+(H) and middle e^+(C)	-207.995908	1114.08	30.32
	Omit e^+(C,H)	-207.995875	1081.58	29.43
	Only on O	-207.995701	907.08	24.68

The positron density and the PA were significantly changed when the positron basis center was kept on only the O atom in all of the cases (see Table 4.5.1). The e^+(H) basis centers affect the ground state energy, positron density and contact density distribution in e^+-molecules minimally. When we include all positron basis centers, the positron density is more localized near the electro negative site (in these cases, the O site) and when omitting each basis center, as indicated in above table, the positron density distribution tends to be less localized. Therefore, the contact density shows qualitatively correct behavior with all positron centers (see Figure 4.4.1) and omitting the e^+(H) centers (see Figure 4.5.1). But a qualitatively incorrect contact density can be seen when omitting the positron basis centers at heavy atom sites (see Figure 4.5.2-4).

With respect to the electron density at the heavy atoms the H atom is negligible and the higher positron density is localized near the most electronegative site and diffused elsewhere. Therefore, overlap of the electron and positron wavefunction is less at the H sites and qualitatively correct contact densities can be obtained when omitting the positron basis center at the H sites. When omitting the positron basis centers at the heavy atoms the positron basis set at the most electronegative site is not flexible enough to make the small dip at other heavy atom sites, as shown in following positron density figures. Due to the higher electron density at those locations, qualitatively incorrect contact density peaks can be seen. Here the positron density and the contact density variations with respect to the positronic basis centers were shown for the $e^+CH_3COCH_3$ molecule and a similar trend was found for the other e^+-molecule systems, indicated in Table 4.5.1.

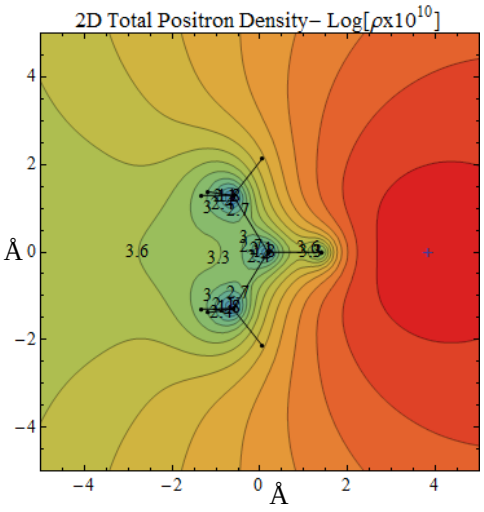

(a)

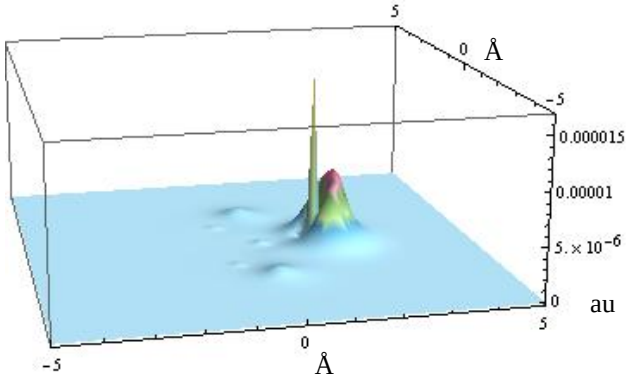

(b)

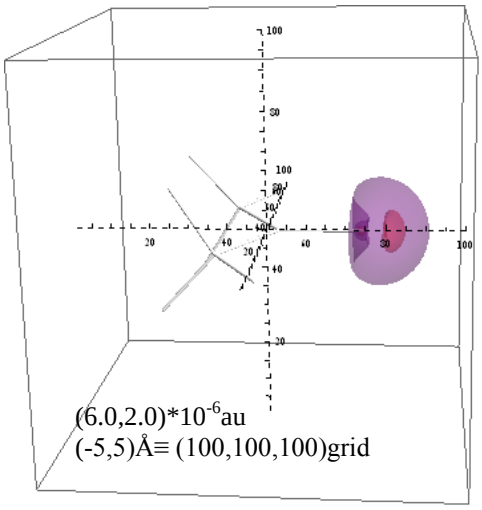

(c)

Figure 4.5.1 $e^+CH_3COCH_3$- Omit e^+(H) Basis Centers

(a) Positron Density

(b) 3D View of the Center Layer Contact Density

(c) 3D Contact Density

Omitting e^+(H) basis centers effects the positron density and the contact density minimally. Figure 4.4.1 shows the most accurate positron density and the contact density for the $e^+CH_3COCH_3$ system. When omitting the positron basis centers at H sites much more diffused smaller peaks can be seen for the contact density as shown in above Figure 4.5.1b. But similar to the most accurate calculation the higher contact density can be seen following the O atom along the C=O bond axis.

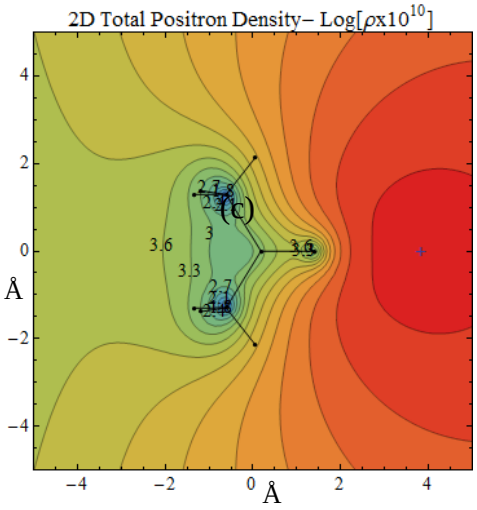

(a)

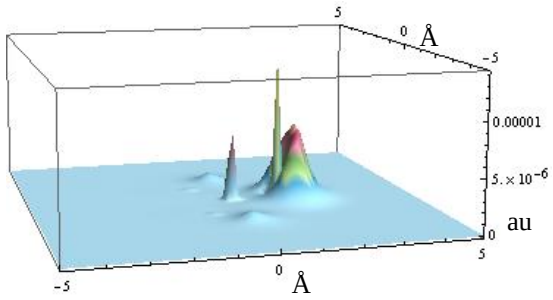

(b)

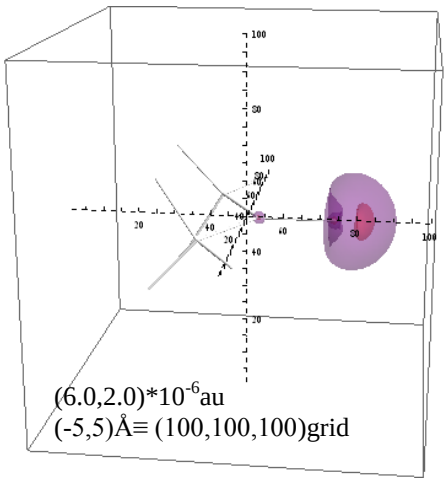

(c)

Figure 4.5.2 $e^+CH_3COCH_3$- Omit e^+(H) Basis Centers and Middle e^+(C) Basis Center

(a) Positron Density

(b) 3D view of the Center Layer Contact Density

(c) 3D Contact Density

As shown in the above figures when omitting the positronic basis center at the middle C atom (C=O) the contact density peak can be seen at that location due to the other positronic basis sets not being flexible enough to make a dip at the middle C atom to reflect the positron nucleus repulsion.

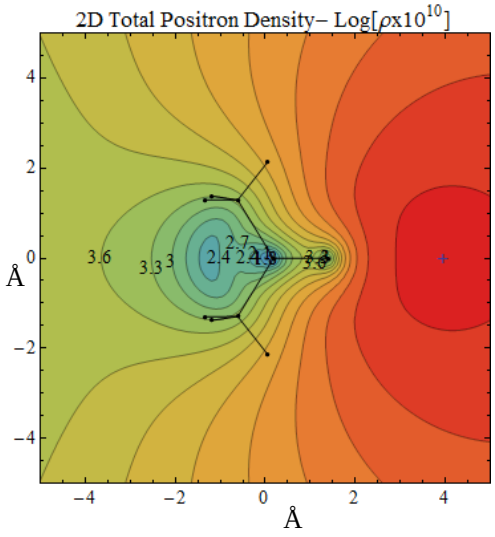

(a)

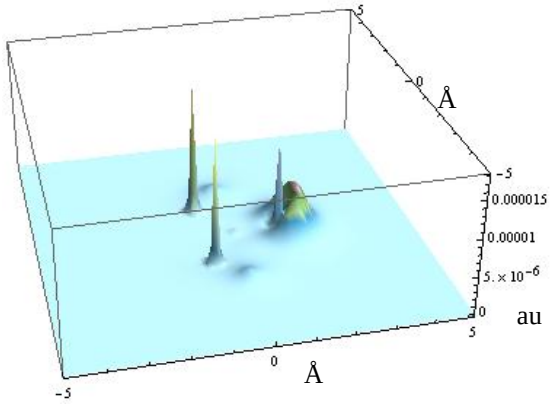

(b)

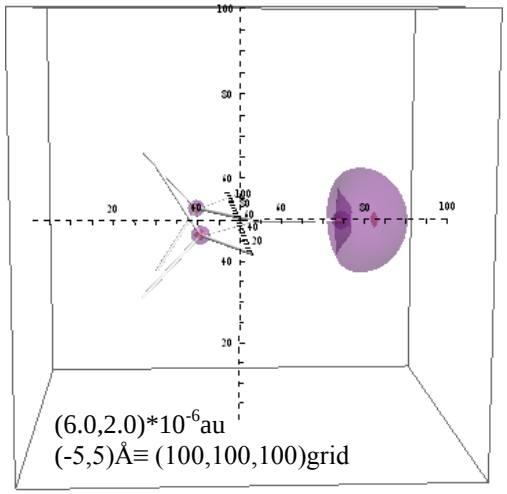

(c)

Figure 4.5.3 $e^+CH_3COCH_3$- Omit e^+(H) Basis Centers and Corner e^+(C) Basis Centers

(a) Positron Density

(b) 3D view of the Center Layer Contact Density

(c) 3D Contact Density

Higher contact density peaks can also be seen when omitting the positron basis centers at the corner C atoms. Also those peaks are greater than when omitting the positron basis center at the middle C, as shown in Figure 4.5.2. The larger positronic basis set with diffused functions on the O atom site effect the positron wavefunction, heavily diffusing it at neighboring atoms, in this case the middle C, to make a smaller contact density peak at the middle C.

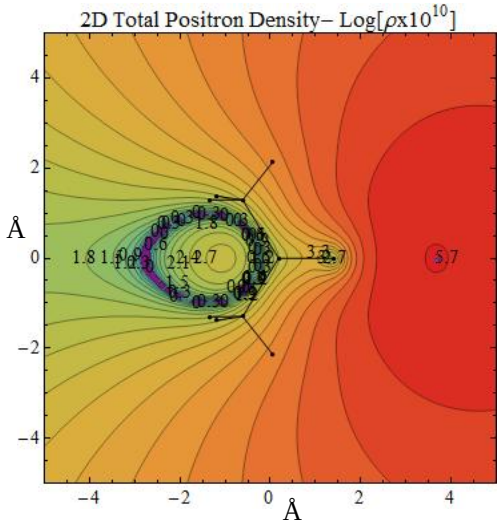

(a)

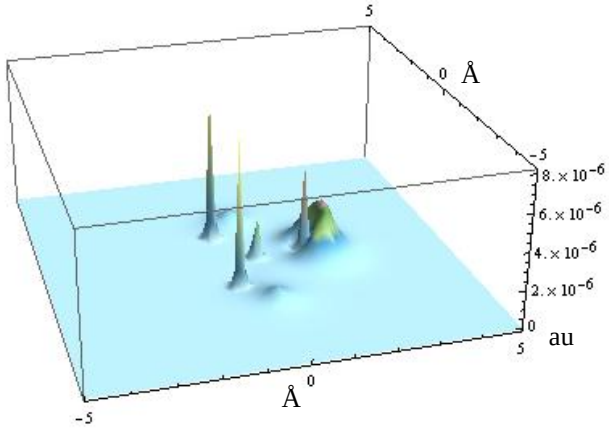

(b)

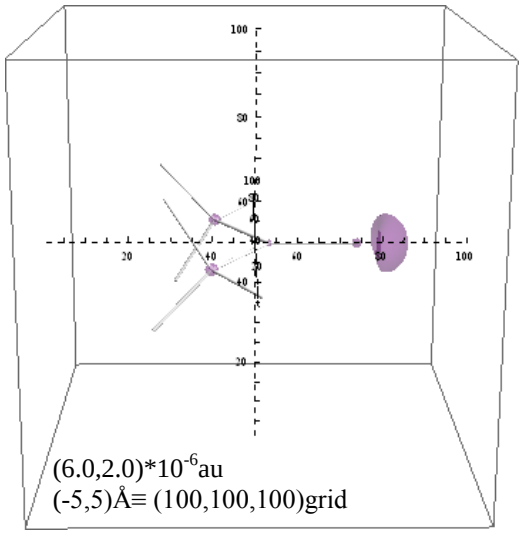

(c)

Figure 4.5.4 $e^+CH_3COCH_3$- Basis Center Only on e^+(O)

(a) Positron Density

(b) 3D View of the Center Layer Contact Density

(c) 3D Contact Density

The large positronic basis set on the O atom site is not flexible enough to get a qualitatively correct contact density using the NEO-HF method as shown in above figure. According to the above results, one can get a qualitatively correct contact density without the positronic basis centers at the H sites while keeping the positronic basis centers at all the heavy atom sites. But when it comes to the bigger e^+-molecule systems there are many C, N

and O atoms. To calculate the qualitatively correct contact density using the above mentioned 13s9p large positronic basis sets for all the heavy atoms requires much more computational time and computational resources and it may also leads to the SCF convergence problem due to the linear dependency. Therefore, it is necessary to have smaller contracted positronic basis sets for C and N sites, that are flexible enough to make the dip on the nucleus of each heavy atom centers. We have developed different sizes of smaller contracted positronic basis sets, which are appropriate to use for C and N atom centers. The following table shows the smallest contracted positronic basis sets for C and N atom centers, which can be used for bigger e^+-molecule systems to calculate qualitatively correct contact densities.

Table 4.5.2 Smaller Contracted Positronic Basis Sets

e^+(C) basis set (exponents	coefficients)
S 2	
1	0.2852285608 0.1915021580
2	0.008278471258 -0.05075701660
S 2	
1	0.06388484782 -0.4787477490
2	0.02333866434 -2.173203710
e^+(N) basis set (exponents	coefficients)
S 2	
1	0.2681755894 0.08640487120
2	0.01725409046 -0.2991832480
S 2	
1	0.05278040745 -0.8069405330
2	0.006629877053 0.2291580040

The following Figure 4.5.5, shows the 2D positron density and the contact density of $e^+CH_3COCH_3$, $e^+CH_3CONH_2$ and $e^+NH_2CONH_2$ which were calculated using the 13s9p positron basis center on the O atom site and smaller contracted positronic basis centers (Table 4.5.2) for C and N atom sites.

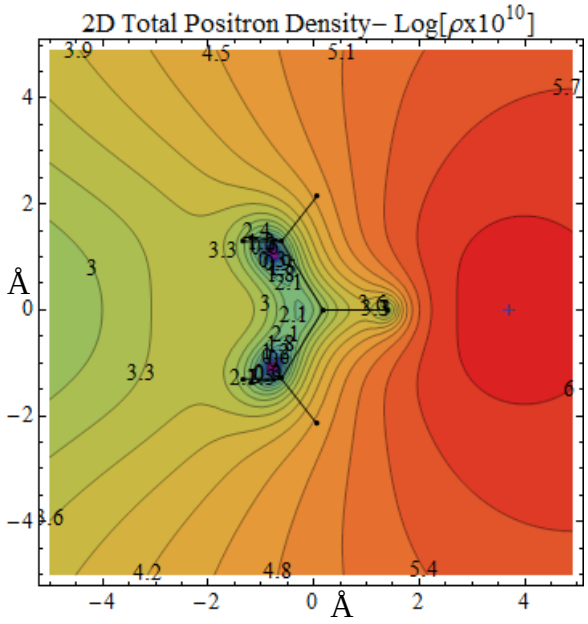

(a1)

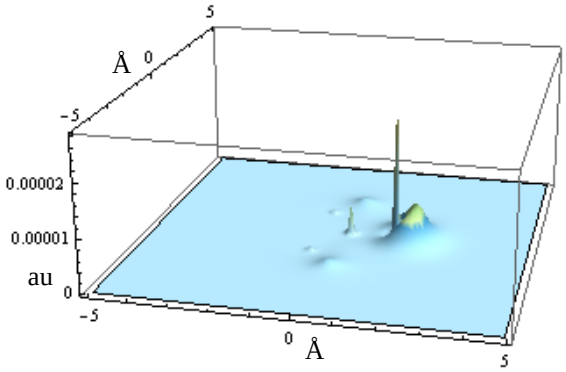

(a2)

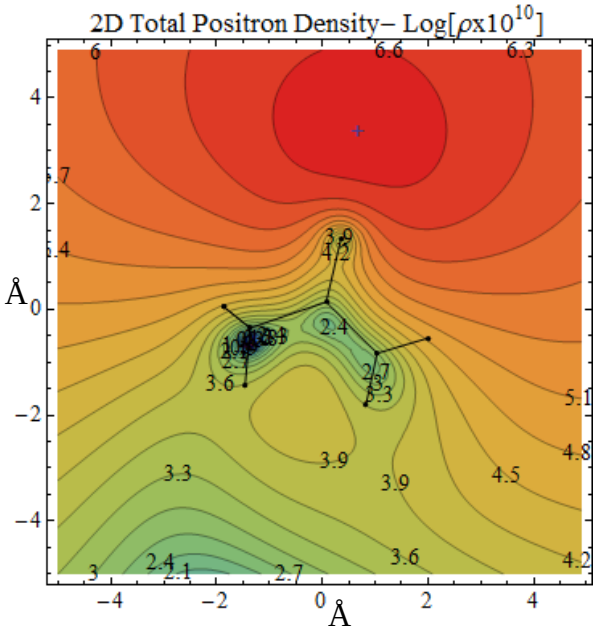

(b1)

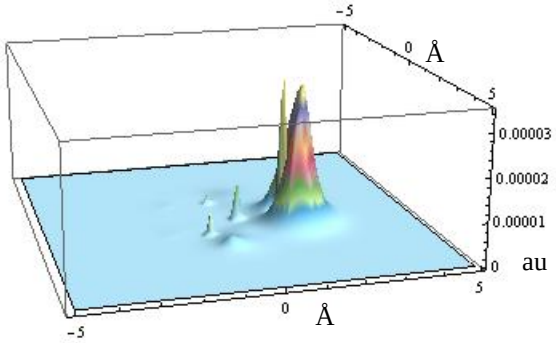

(b2)

Figure 4.5.5 Low Cost Calculation for Qualitatively Correct Contact Density (e^+(C) -2s, e^+(N) -2s and e^+(O)-13s9p)
$e^+CH_3COCH_3$ [E= -191.975887au] (a_1)Positron Density (a_2) Contact Density
$e^+CH_3CONH_2$ [E= -207.995816au] (b_1) Positron Density (b_2) Contact Density
$e^+NH_2CONH_2$ [E= -224.008584au] (c_1) Positron Density (c_2) Contact Density

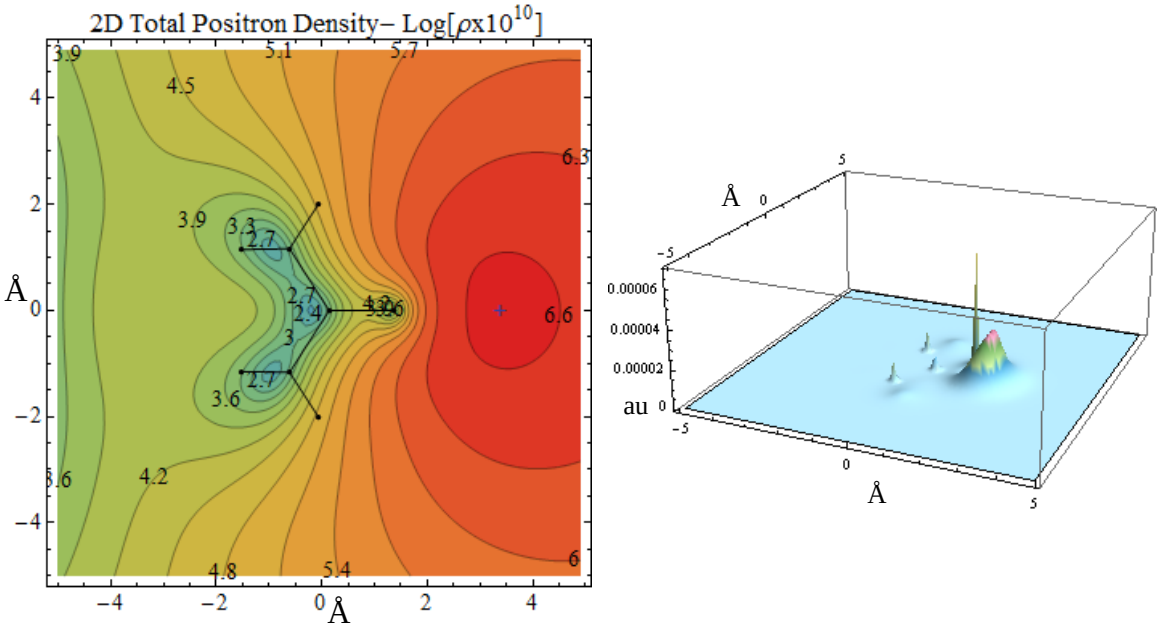

(c_1) (c_2)

Figure 4.5.5 Low Cost Calculation for Qualitatively Correct Contact Density (e^+(C) -2s, e^+(N) -2s and e^+(O)-13s9p)
$e^+CH_3COCH_3$ [E= -191.975887au] (a_1)Positron Density (a_2) Contact Density
$e^+CH_3CONH_2$ [E= -207.995816au] (b_1) Positron Density (b_2) Contact Density
$e^+NH_2CONH_2$ [E= -224.008584au] (c_1) Positron Density (c_2) Contact Density

n all cases, the smaller contracted 2s basis sets for the C and N sites are flexible enough to construct the dip of the e^+ density at the nucleus at relevant centers. Therefore, the calculated contact density is higher following the O site along the C=O bond axis, similar to the calculation done with all positronic basis centers with large basis sets (see Figure 4.4.1-3). When using the smaller contracted positronic basis sets for the C and N centers, as shown in above figures, there are seen small peaks around the C and N atoms sites. For the qualitative purposes, these small peaks can be ignored. Thus, one can do low-cost calculations using

these contacted positronic basis sets for C and N atom centers while having the 13s9p positronic basis set at O sites for the bigger molecules such as peptides, DNA and RNA.

4.6 "d" Type Gaussian Function Effects on the Contact Density

Other than the large 13s9p positronic basis sets, 13s9p3d positronic basis sets were also developed, which are appropriate for use with C, N, and O atom centers. Table 4.6.1 shows the ground state energy and the positron affinity of the moderate size e^+-molecule systems, which were calculated with 13s9p and 13s9p3d atom-centered positronic basis sets on heavy atoms and 4s3p positronic basis sets at the H atom sites.

Table 4.6.1 Ground State Energy:13s9p vs 13s9p3d

HF MP2 E (au)	4s3p/13s9p E(a.u) PA μH/meV	4s3p/13s9p3d E(a.u) PA μH/meV
CH_3COCH_3 -191.975691 -192.583177	-191.975934 243.50/6.63 -192.583561 383.56/10.44	-191.975935 244.62/6.66 -192.583567 390.25/10.62
Omit e^+(H)	-191.975931 240.39/6.54 -192.583541 364.14/9.91	-191.975933 242.84/6.61 -192.583560 382.85/10.42
CH_3CONH_2 -207.994794 -208.628430	-207.995939 1145.18/31.16 -208.630333 1902.66/51.77	-207.995941 1146.83/31.21 -208.630351 1920.67/52.26
Omit e^+(H)	-207.995929 1134.98/30.88 -208.630274 1843.16/50.15	-207.995936 1142.01/31.08 -208.630331 1901.00/51.73
NH_2CONH_2 -224.007736 -224.665870	-224.008713 977.27/26.59 -224.667519 1648.84/44.87	-224.008713 977.27/26.59 -224.667534 1664.12/45.28
Omit e^+(H)	-224.008703 967.37/26.32 -224.667471 1601.47/43.58	-224.008713 976.83/26.58 -224.667534 1663.91/45.28

Table 4.6.1 Ground State Energy:13s9p vs 13s9p3d

$HCOCH_3$ -152.926118 -153.388725	-152.926271 152.43/4.15 -153.388899 173.92/4.73	-152.926272 153.62/4.18 -153.388904 178.78/4.86
Omit e^+(H)	-152.9262697 151.31/4.12 -153.388892 166.10/4.52	-152.926271 152.82/4.16 -153.388901 175.81/4.78
$HCONH_2$ -168.946102 -169.435394	-168.947144 1041.63/28.34 -169.436903 1509.46/41.07	-168.947146 1043.23/28.39 -169.436930 1536.73/41.82
Omit e^+(H)	-168.9471390 1036.62/28.21 -169.436874 1480.22/40.28	-168.947143 1040.83/28.33 -169.436922 1527.87/41.58
H_2CO -113.873104 -114.192233	-113.873135 31.47/0.86 -114.192238 4.63/0.13	-113.873142 38.74/1.05 -114.192249 16.36/0.45
Omit e^+(H)	-113.873135 31.19/0.85 -114.192235 2.52/0.07	-113.873142 38.64/1.05 -114.192249 15.92/0.43

Adding d orbitals to the positron basis functions does not significantly improve the ground state energy/PA at the HF level, but improves it at the MP2 level, especially if there are N atom centers. The developed contracted basis, including d functions, show similar energy/PA values as obtained using 13s9p.

The positron density and the contact density distribution with respect to the 13s9p and 13s9p3d type positronic basis sets were also compared. The following figures show the contact density distribution of the e^+-molecule systems of the molecule in above table.

$e^+CH_3COCH_3$

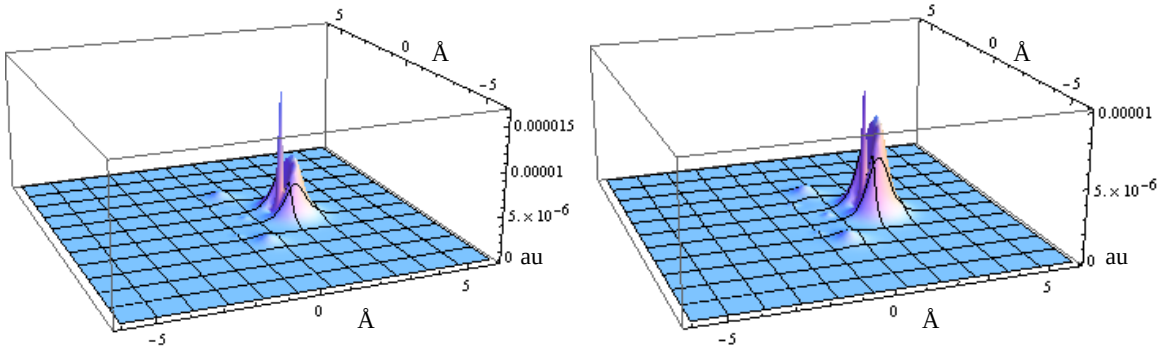

$e^+CH_3CONH_2$

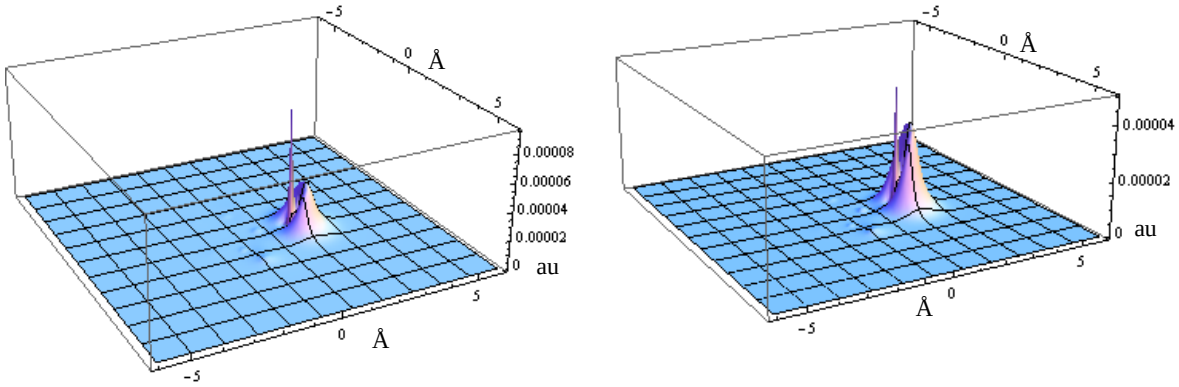

$e^+NH_2CONH_2$

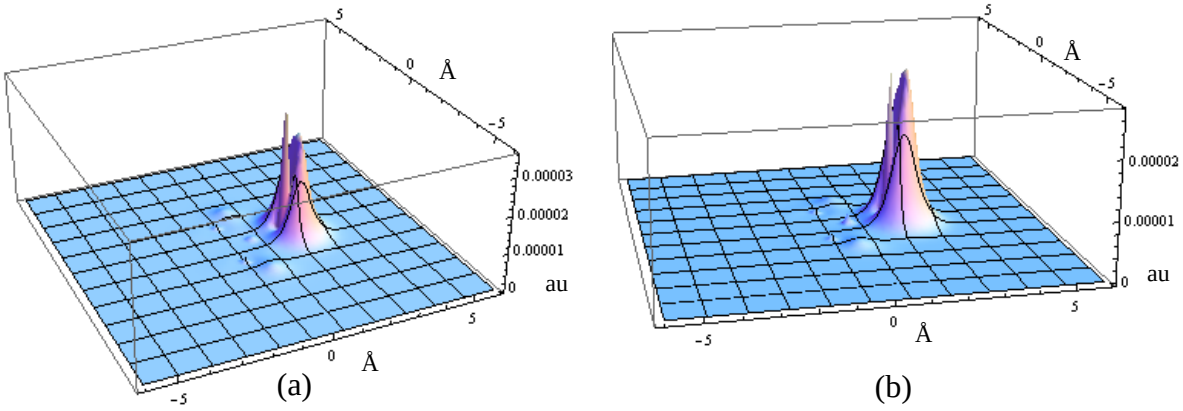

Figure 4.6.1 2D Center Layer Contact Density (a) 13s9p (b) 13s9p3d

e^+HCOCH_3

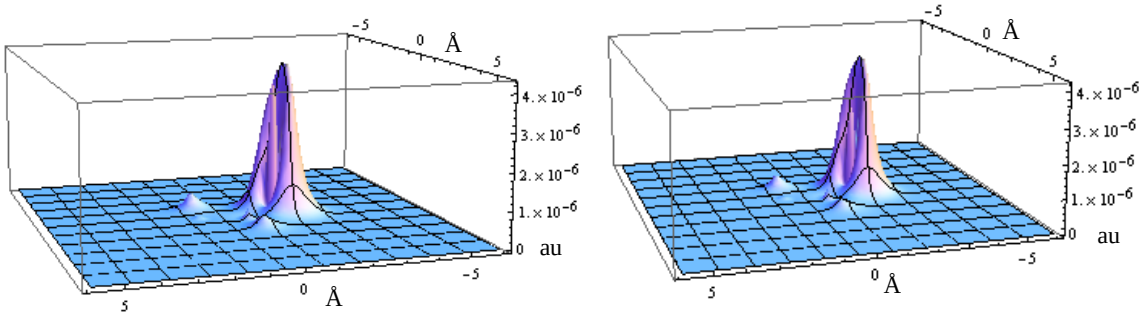

(a) (b)

e^+HCONH_2

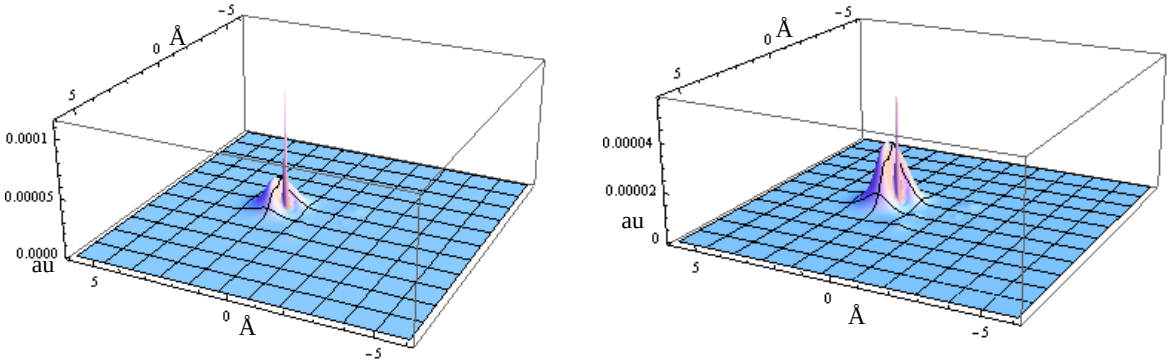

(a) (b)

e^+H_2CO

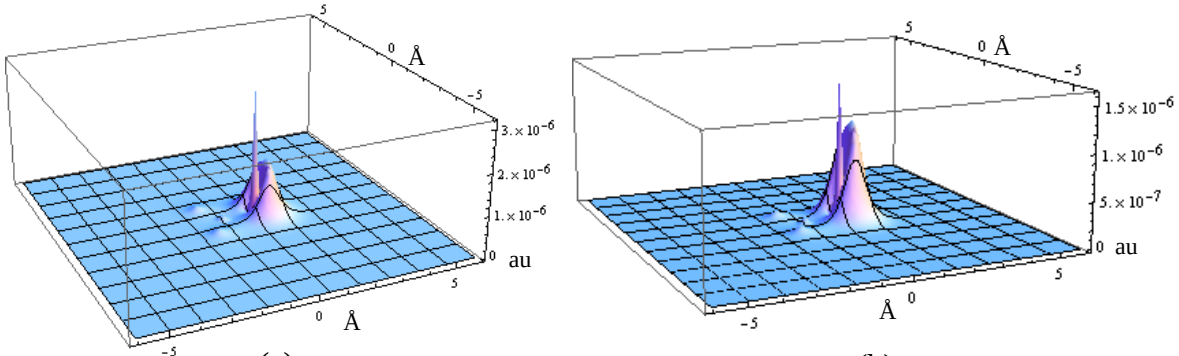

(a) (b)

Figure 4.6.1 2D Center Layer Contact Density (a) 13s9p (b) 13s9p3d

As shown in above figure the core contribution to the contact density, when using 13s9p3d type basis sets, less with respect to the 13s9p basis sets, while the valance peak (magnitude and width) remains the same. To understand the cause of the decreased contact density contribution in the core region (when adding the d functions) the positron density distribution was plotted along the C=O bond.

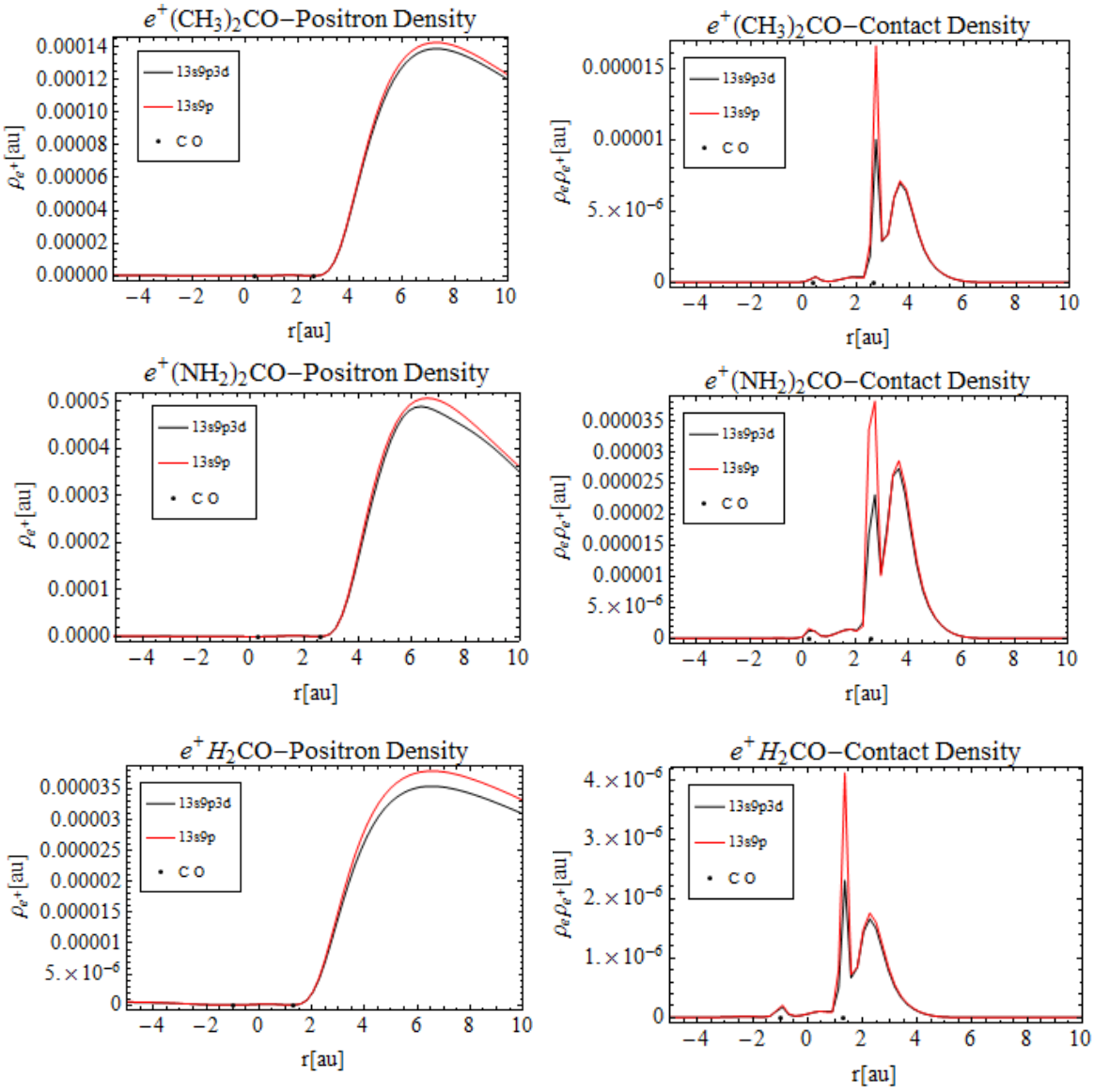

Figure 4.6.2 Positron and Contact Density -13s9p3d vs 13s9p

The Figure 4.6.2 shows the positron density and the contact density distribution of $e^+CH_3COCH_3$, $e^+NH_2CONH_2$ and e^+H_2CO, which were calculated with 13s9p and 13s9p3d atom-centered positronic basis sets. According to the calculations, the positron density calculated with the 13s9p3d basis set was reduced close to the nuclei with respect to the positron density calculated with the 13s9p basis sets. This reduction of the positron density in the core region of the O atom reduces the contact density while the valance region has similar behavior to the other calculations done only with 13s9p basis sets. According to the above results, the energy, positron affinity and the contact density were not significantly improved over the NEO-HF level,that is the calculations done by including the d functions to the positronic basis sets, have little effect on the results and causes only a slight improvement in the accuracy of the contact density when compared to the most accurate (ECG) calculations. One can calculate the qualitatively correct contact density using the smaller positronic basis sets for C and N atom sites and larger positronic basis sets for the most electronegative sites as discussed in section 4.5. In all the cases discussed above, the positron is more likely to annihilate with an electron at the most electronegative site, as both electron and positron wavefunction overlap maximally in that region.To understand which molecular orbital electron annihilates with the positron it is necessary to calculate the overlap of the positron wavefunction with each of the electronic molecular orbital (MO) wavefunction.

4.7 Molecular Orbital Annihilation Rate and Characteristics

The annihilation rate at each molecular orbital level was calculated in the NEO-HF level of theory by using a 1s-contracted positron basis set at the H centers and 13s9p uncontracted positron basis sets at all heavy atom centers. The calculated positron density of

above systems was higher on the side of the oxygen site along the bond axis opposite to the other atoms. According to the molecular orbital annihilation rate, the inner molecular orbital gave a higher contribution than the highest occupied molecular orbital except for the $e^+CH_3COCH_3$ and e^+CH_3COH systems. A population analysis for molecular orbitals was done to identify which type of Gaussian orbitals contribute most heavily to the MO annihilation rates. In all cases, middle C is labeled as the fragment 1 and O (connected to the middle C) is labeled as fragment 2.

Table 4.7.1 e^+H_2CO System (E_{NEO-HF} = -113.873135a.u , PA=0.86 meV)- Molecular Orbital Annihilation Rate

MO	Liberate Energy (Hartree)	Hartree Fock Annihilation Rate (1/ns)	Hartree Fock MO Population Analysis
6	0.21656	0.00013638	O-p=0.54, s=0.15, C-p=0.22, H-s=0.04 Fr2(O)=0.69, Fr1(C)=0.23, Fr3(H)=0.08
7	0.10492	0.00010110	O-p=0.66 C-p=0.32 Fr2(O)=0.67, Fr1(C)=0.33
8	0.0	0.00009696	O-p=0.63, C-p=0.08, d=0.03, H-s=0.13 Fr2(O)=0.63, Fr3(H)=0.27, Fr1(C)=0.10

Other MO annihilation rate < $6.6*10^{-5}$ (1/ns)

In the above e^+H_2CO case, the highest molecular orbital annihilation contribution is given by the MO6. According to the atomic contributions to Alpha molecular orbitals the highest contribution is form by the O atom. Even though the total contribution by O atom nearly equal in other MO 7, MO8, the individual s and p orbitals (of the O atom) contribution to particular molecular orbital are differ whereas for the MO6, 54% of p-orbital and 15% of s-orbital contribution has while the MO7 and MO8 mainly contributed from the p orbitals of the O atom. When the shapes of these MOs were considered there is a node on the top of the O atom in the MO6 which is not visible in the MO7 or MO8. According to the positron density

distribution, higher positron density can be seen following the O atom along the C=O bond axis. Therefore, higher overlap between the MO6 and the positron wavefunction is expected to give a higher annihilation rate.

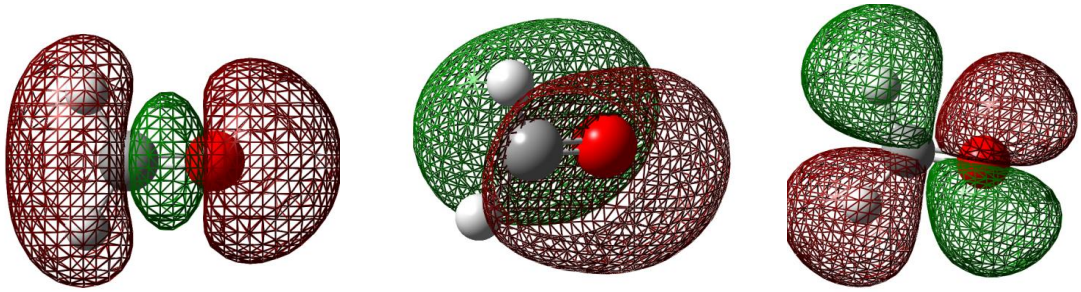

MO-6 MO-7 MO-8

Figure 4.7.1 H_2CO Molecular Orbital Shapes

In $e^+CH_3COCH_3$ system, the highest molecular orbital annihilation rate contribution is given by the highest occupied molecular orbital (MO16). In MO 8, and 12 there is a node on the top of the O atom along the C-O bond. But in those molecular orbitals, contribution from the p-orbital of the O atom is very small with respect to the MO 15 and MO16. The molecular shapes of the MO5 and MO9 have localized distributions behind the O atom along the bond axis than other MOs. Even though MO5 has the highest molecular orbital contribution from the O atom (75%), the p orbital of the O atom contributes only 6% to the total population of MO5. According to that, we can consider that MO10, MO15 and MO16 should give higher contributions to the annihilation rate. Even though, there is a node on the top of O atom in MO10, the p-orbital contribution is less than that of the MO15 and MO16. The orbital contribution by the O atom in the MO15 and MO16 is same.

Table 4.7.2 $e^{+}CH_3COCH_3$ System (E_{NEO-HF} = -191.975934 a.u , PA=6.62 meV)-Molecular Orbital Annihilation Rate

MO	Liberate Energy (Hartree)	HF Annihilation Rate (1/ns)	HF MO Population Analysis
5	0.99107	0.00028706	O-s=0.68, p=0.06, C1-s=0.15 , p=0.06 C(-CH_3)-s=0.02 Fr2(O)=0.75 Fr1(C)=0.22 Fr3,4(CH_3)=0.02
8	0.33131	0.00033516	C-s=0.23, O-p=0.19,s=0.11 C(-CH_3)-p=0.11, s=0.04, H-s=0.03 Fr2(O)=0.30, Fr1(C1)=0.24 Fr3(CH3)=0.23, Fr4(CH3)=0.23
9	0.23911	0.00019933	O-p=0.29, C1-p=0.24, C(-CH3)-p=0.15, s=0.01, H-s=0.04 Fr2(O)=0.29, Fr1(C1)=0.24, Fr3,4(CH3)=0.24
10	0.22786	0.00040236	O-p=0.27,s=0.09, C1-p=0.17, C(-CH3)-p=0.15, H-s=0.08 Fr2(O)=0.36, Fr3,4 (CH3)=0.24, Fr1(C1)= 0.17
12	0.15312	0.00023514	C(-CH3)-p=0.22, O-p=0.14,s=0.02, C1-p=0.05,s=0.01 Fr3,4(CH3)=0.38 Fr2(O)=0.17 Fr1(C1)=0.07
15	0.08302	0.00040562	O-p=0.57, C1-p=0.16, d=0.01 C(-CH3)-p=0.05, H-s=0.04 Fr2(O)=0.58, Fr1(C1)=0.17 Fr3,4(CH3)=0.13
16	0.0	0.00040684	O-p=0.58, C(-CH3)-p=0.14,s=0.02 C1-p=0.12,d=0.02 Fr2(O)=0.58, Fr3,4(CH3)=0.14 Fr1(C1)=0.14

Other MO annihilation rate < $1.3*10^{-4}$ (1/ns)

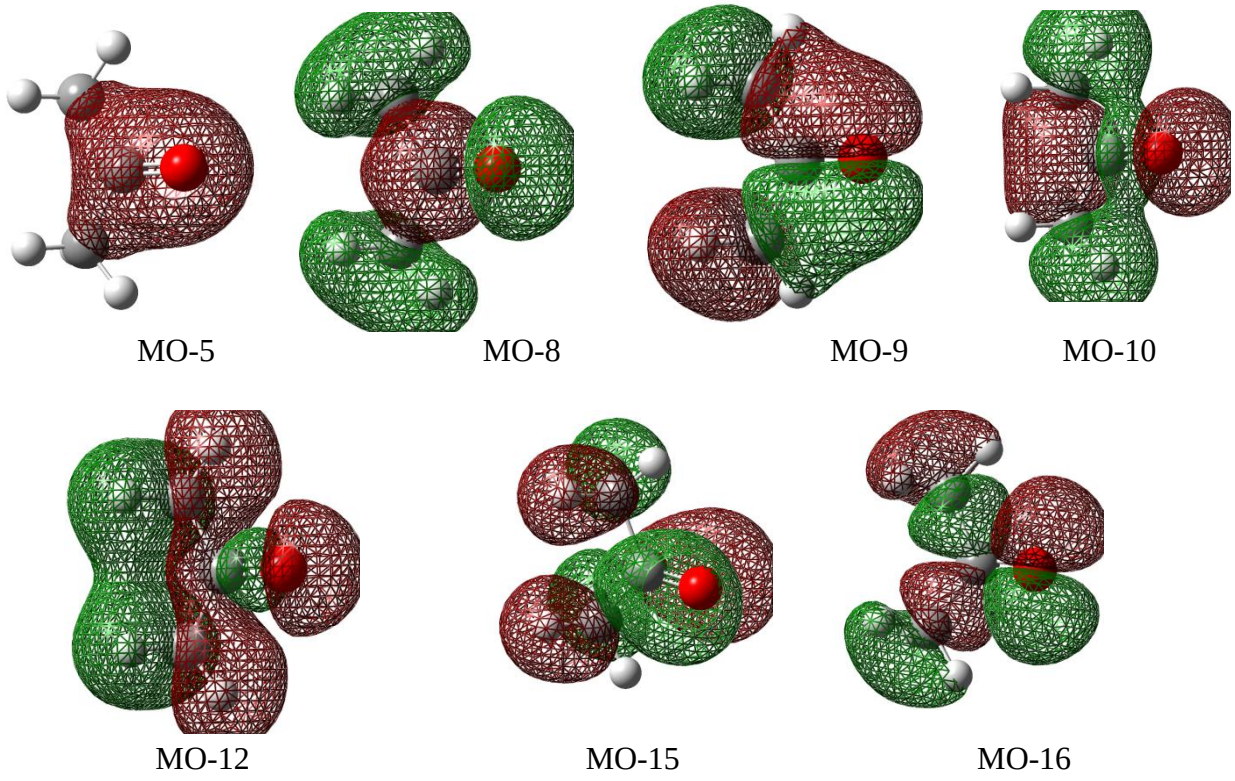

Figure 4.7.2 CH_3COCH_3 Molecular Orbital Shapes

Table 4.7.3 $e^+NH_2CONH_2$ System (E_{NEO-HF} = -224.008710 a.u , PA=26.5 meV) -Molecular Orbital Annihilation Rate

MO	Liberate Energy (Hartree)	HF Annihilation Rate (1/ns)	MO Population Analysis
12	0.19283	0.00262165	O-p=0.49,s=0.15, C-p=0.15 N-p=0.06, H-s=0.03 Fr2(O)=0.65, Fr1(c)=0.16 Fr3,4(NH2)=0.09
14	0.02662	0.00210478	O-p=0.79, N-p=0.06, C-p=0.04,d=0.02 H-s=0.01 Fr2(O)=0.79, Fr3,4(NH2)=0.08, Fr1(C)=0.06
16	0.0	0.00151084	O-p=0.53, N-p=0.22 C-d=0.02,p=0.02 Fr2(O)=0.53, Fr3,4(NH2)=0.22, Fr1(C)=0.03

Other MO annihilation rate < $9.2*10^{-4}$ (1/ns)

In this case, the highest contribution given to the annihilation rate is by MO12. According to the calculations, the highest O atom contribution is given in the MO14 (79%). The node on the top of the O atom along the C-O bond and the 15% s-orbital contribution of the O atom in the MO12 makes the annihilation rate higher than the MO14.

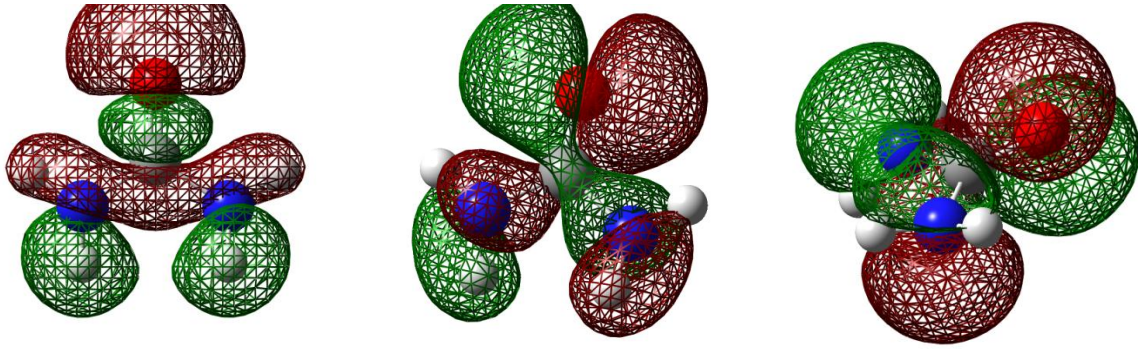

MO-12 MO-14 MO-16

Figure 4.7.3 NH_2CONH_2 Molecular Orbital Shapes

In the next system, MO15 gave the highest contribution to the annihilation rate in the $e^+CH_3CONH_2$ system, where the p-orbital contribution of the O atom is 71%. Even though the MO10 has a node on the top of the O atom similar to MO12, it not on the C-O axis where the e^+ density is higher behind the O atom along the same axis (e^+ density slightly off from the C-O axis to the NH_2 group). In MO12, the node on the O atom is aligned with the C-O bond with respect to the MO10 and the p-orbital and the s-orbital of the O atom contribute moderately to the alpha orbital. Due to a smaller p-orbital contribution of the O atom in MO16, the MO16 annihilation rate is less than other MOs. According to that, MO12 and MO15 gave higher contributions to the annihilation rate. Further, the highest annihilation rate observed is in MO15, due to the considerable contribution of the O atom.

Table 4.7.4 $e^{+}CH_3CONH_2$ System (E_{NEO-HF} = -207.995939a.u , PA=31.1 meV) -Molecular Orbital Annihilation Rate

MO	Liberate Energy (Hartree)	HF Annihilation Rate (1/ns)	HF MO Population Analysis
5	0.98009	0.00121175	O2-s=0.60, p=0.06, C1-s=0.22 , p=0.04 N3-s=0.06 Fr2(O)=0.67 Fr1(C)=0.26 Fr3(NH2)=0.07
10	0.25306	0.00178441	O-p=0.30,s=0.10 C1-p=0.17,s=0.04 C2-p=0.17,s=0.01, N-p=0.10 Fr2(O)=0.40, Fr4(CH3)=0.27, Fr1(C1)=0.21, Fr3(NH2)=0.12
12	0.17515	0.00219569	O-p=0.39, s=0.09, C1-p=0.20, C2-p=0.14, N-p=0.07 Fr2(O)=0.48, Fr1(C1)=0.20, Fr4(CH3)=0.19, Fr3(NH2)=0.13
15	0.00869	0.00227929	O-p=0.71, C2-p=0.12, N-p=0.06 C1-p=0.05,d=0.02 Fr2(O)=0.72, Fr4(CH3)=0.14 Fr1(C1)=0.08, Fr3(NH2)=0.06
16	0.0	0.00136361	N-p=0.59 O-p=0.38 C1-d=0.02 Fr3(NH2)=0.59 Fr2(O)=0.38 Fr1(C1)=0.02

Other MO annihilation rate < $8.8*10^{-4}$ (1/ns)

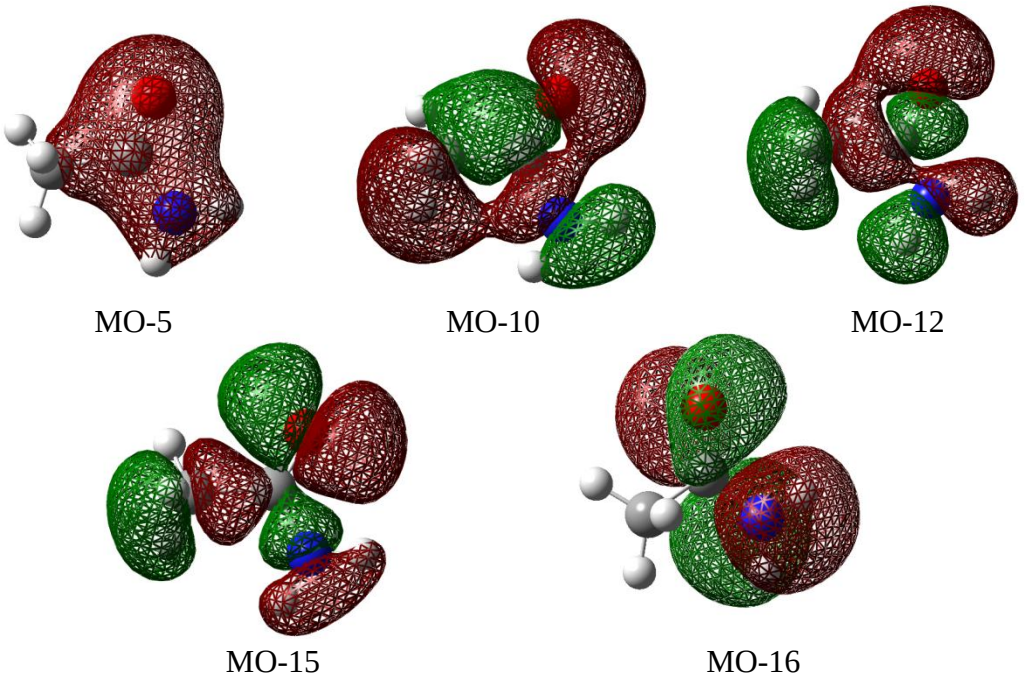

Figure 4.7.4 CH_3CONH_2 Molecular Orbital Shapes

Table 4.7.5 $e^{+}CH_3COH$ System (E_{NEO-HF} = -152.926271au , PA=4.14 meV) -Molecular Orbital Annihilation Rate

MO	Liberate Energy (Hartree)	HF Annihilation Rate (1/ns)	HF MO Population Analysis
4	0.98766	0.00018448	O-s=0.67,p=0.06, C1-s=0.17,p=0.07 Fr2(O)=0.74, Fr1(C)=0.26
6	0.38033	0.00015052	C1-s=0.25,p=0.14, H-s=0.19 O-p=0.11,s=0.08, C2-p=0.08,s=0.07 Fr1(C1)=0.57, Fr3(CH3)=0.24 Fr2(O)=0.19
7	0.25605	0.00025187	O-p=0.37,s=0.07, C1-p=0.25, C2-p=0.15, s=0.02, H-s=0.07 Fr2(O)=0.44, Fr1(C1)=0.32 Fr3(CH3)=0.24
8	0.20522	0.00026042	O-p=0.39, s=0.07, C1-p=0.24, C2-p=0.20, Fr2(O)=0.47, Fr3(CH3)=0.28, Fr1(C1)=0.25
11	0.08705	0.00025036	O-p=0.55, C1-p=0.18,d=0.01, C2-p=0.12, Fr2(O)=0.56, Fr3(CH3)=0.26 Fr1(C1)=0.19
12	0.0	0.00027184	O-p=0.60 C2-p=0.14 H-s=0.13 C1-p=0.08,-d=0.02, Fr2(O)=0.60, Fr1(C1)=0.23 Fr3(CH3)=0.17

Other MO annihilation rate < $1.0*10^{-4}$ (1/ns)

The highest molecular orbital annihilation rate is given by the MO12 in the $e^{+}CH_3COH$ system due to the larger p-orbital contribution of the O atom. Even though the highest O-atom contribution (74%) to the alpha molecule orbital is given in the MO4, the p-orbital contribution of the O atom is small. Due to that fact the molecular annihilation rate is less. The MO6 has a node on the top of the O atom along the C-O bond; but, the O-atom contribution is less in the MO6. Therefore, the molecular orbital annihilation is low. MO7 and MO8 have a node on top of O atom and the p-orbital population of the O atom is fairly high as well. MO11 also has fairly high p-orbital population from the O atom. Therefore MO 7, MO8, MO11 and MO12 show higher contributions to the total annihilation rate; however, the MO12 gave the highest contribution.

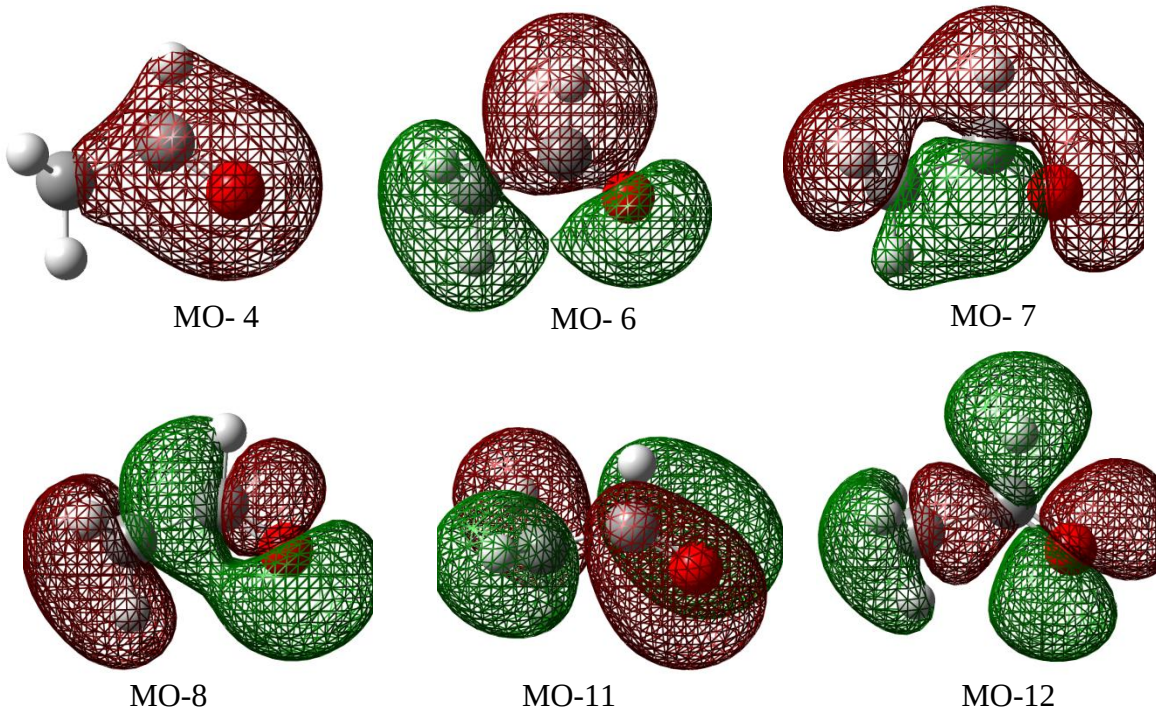

Figure 4.7.5 CH_3COH Molecular Orbital Shapes

Table 4.7.6 e^+NH_2COH System (E_{NEO-HF} = -168.947142 a.u , PA=28.3 meV) -Molecular Orbital Annihilation Rate

MO	Liberate Energy (Hartree)	HF Annihilation Rate (1/ns)	HF MO Population Analysis
4	0.98005	0.00104166	O-s=0.61, p=0.06, C-s=0.20,p=0.05 N-s=0.05 Fr2(O)=0.68, Fr1(C)=0.26 Fr3(NH2)=0.06
8	0.25872	0.00113717	N-p=0.29, O-p=0.22,s=0.06, C-p=0.20,s=0.03, H-s=0.11 Fr3(NH2)=0.41 Fr1(C)=0.31 Fr2(O)=0.28
9	0.19174	0.00213174	O-p=0.43,s=0.13,C-p=0.19 N-p=0.09 Fr2(O)=0.56 Fr1(C)=0.26 Fr3(NH2)=0.17
10	0.15594	0.00108709	O-p=0.36 C-p=0.32 N-p=0.30 Fr2(O)=0.37 Fr1(C)=0.32 Fr3(NH2)=0.31
11	0.01434	0.00195967	O-p=0.74, H-s=0.11 N-p=0.06,s=-0.02, C-p=0.04,d=0.03,s=0.02 Fr2(O)=0.75 Fr1(C)=0.20 Fr3(NH2)=0.05
12	0.0	0.00110185	N-p=0.59 O-p=0.38 C-d=0.02 Fr3(NH2)=0.60 Fr2(O)=0.38 Fr1(C)=0.02

Other MO annihilation rate < $5.3*10^{-4}$ (1/ns)

As in the above cases, MO4 has the highest O atom contribution to the alpha molecule in the $e^{+}NH_2COH$ system. Because the p-orbital contribution of the O atom is less, the calculation shows a low annihilation rate. MO 8 and MO12 have low O-atom contributions with respect to the N-atom contribution to the alpha molecule. In the MO10 all heavy atoms have nearly the same population; however, the shape of the MO10 is not wide enough to overlap with the e^{+} wave function in order to give a higher annihilation rate. The MO9 and MO11 have high p-orbital populations of the O atom to the overall population; however, in the MO9 has a node on the top of the O atom and there is a 13% s-orbital contribution of the O atom to the total population, which leads to the highest annihilation rate contribution.

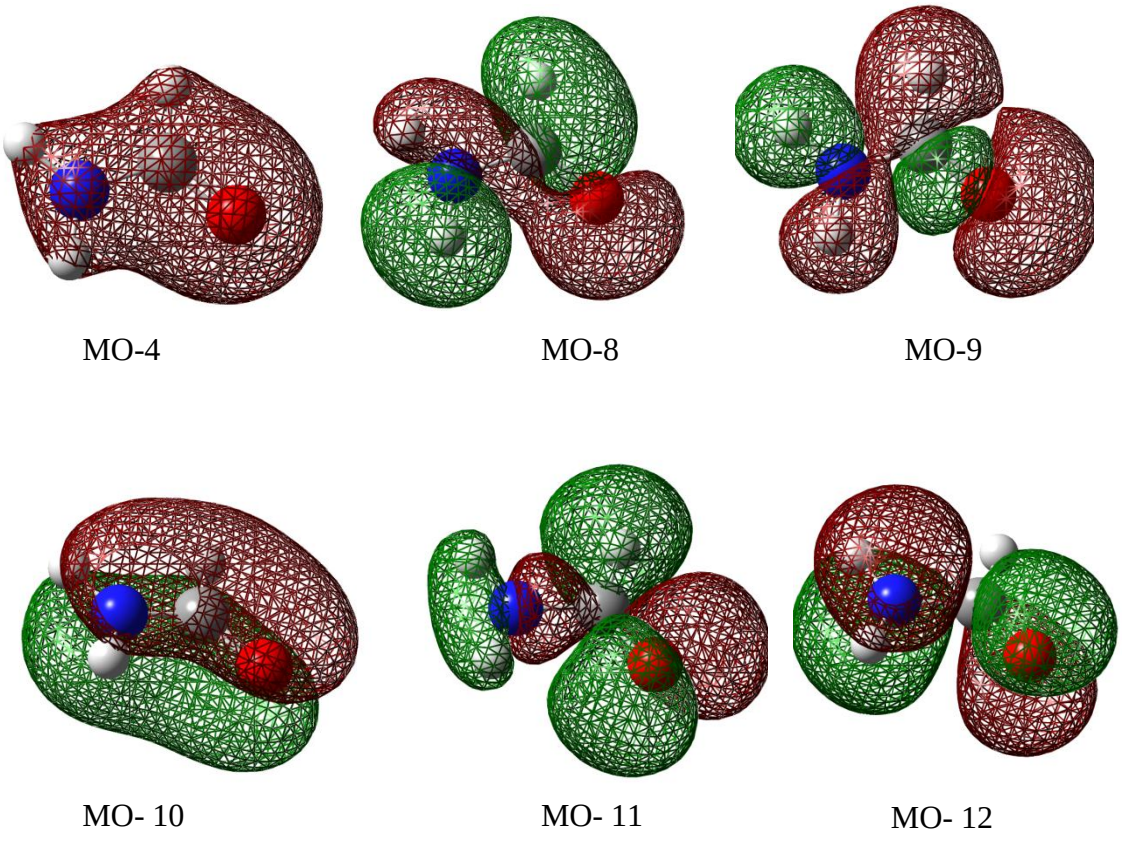

Figure 4.7.6 NH_2COH Molecular Orbital Shapes

In all of the above cases, the higher positron density and the higher contact density can be seen following the O atom along the bond axis. According to the above molecular orbital annihilation rates and the population analysis we can see that (i) the higher molecular orbital annihilation rates are associated with higher p-orbital population of the O atom. (ii) the MO annihilation rate increases if there is a node on the top of the O atom and if there is s-orbital contribution to the O atom as well. There is a higher probability that the positron will annihilate with one of the electrons in a particular molecular orbital having these characteristics. If the positron annihilates with an electron in an inner molecular orbital, one of the electrons in a higher energy states can jump to the vacant state by releasing energy. If the energy liberated is sufficient to break a particular bond in the molecule, fragment ions can be observed. Next, possible fragmentation pathways were studied when low energy e^+ impact with the CH_3COCH_3, CH_3CONH_2 and NH_2CONH_2 systems. Each fragment was optimized (freq-opt) in B3LYP model with the 6-31+G(d,p) electronic basis set and finally checked whether the optimized structure is stable or not (stable=opt). The energy required to conduct fragmentation (ΔE) is compared with the energy liberated during annihilation in order to assess if a particular pathway can lead to fragmentation.

4.8 Possible Fragmentation Pathways

The overlap between positron wave function and electronic molecular orbitals explains the annihilation rate of each molecular orbital. There is a higher probability that the positron will annihilate with one of the electrons in the highest overlapped molecular orbital creating a vacancy. Then one of the electrons in the highest occupied molecular orbital will transit to the vacancy, by liberating energy. If the liberated energy is sufficient to break a

particular bond, it will be a possible fragmentation pathway. In each of the pathways individual molecular energies and bond breaking energies (ΔE) are given in a.u. and calculated with the density functional theory (B3LYP-6-31+G(d,p)). The molecular weight of each component is given underneath in Daltons.

4.8.1 $e^+CH_3COCH_3$ – Possible Fragmentation Pathways

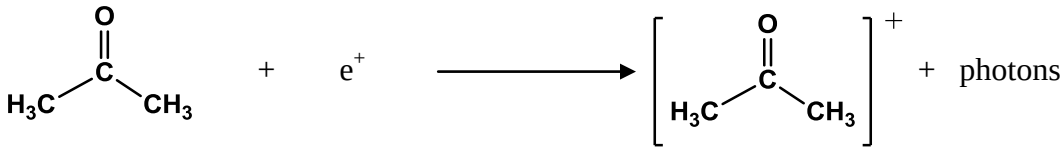

Path A

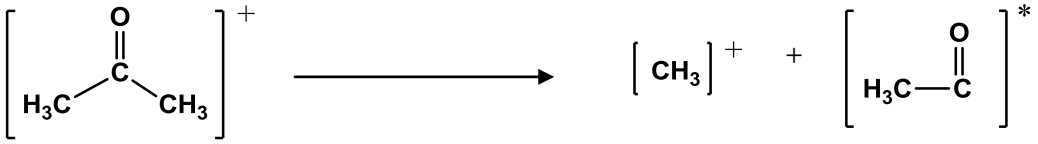

E^{B3}_i= -192.822424au E^{B3}= -39.484716au E^{B3}= -153.194510au

ΔE^{B3}=0.143198au (3.9eV)

MW 58Da 15Da 43Da

Path B

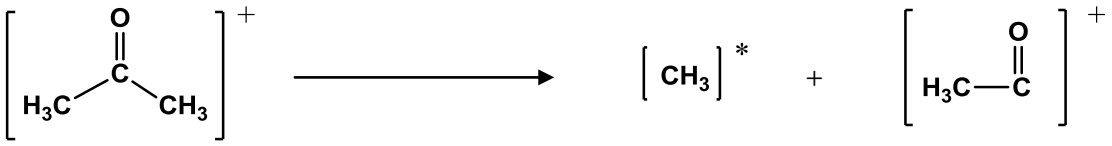

E^{B3}_i= -192.822424au E^{B3}=-39.847335au E^{B3}=-152.929757au

ΔE^{B3}=0.045332au (1.2eV)

MW 58Da 15Da 43Da

According to the Table 4.7.2, a higher contribution for molecular orbital annihilation was observed in MO 10, 15 and 16 in the case of $e^+CH_3COCH_3$. The molecular ion peak (58Da) is observed if the positron annihilates with the highest occupied molecular orbital (MO 16). If the positron annihilates with an inner molecular orbital such as MO10 or MO15, then 0.23a.u and 0.08a.u energy is liberated, respectively, when an electron jumps from the HOMO. A certain fragmentation pathway is possible if the energy liberated upon annihilation is higher than the bond breaking energy. Accordingly, Path A and B are possible if the positron annihilate with MO10; however, if the positron annihilate with MO15, only path B is possible. According to the bond dissociation energies, path B is energetically preferred, which should produce a prominent fragment at 43Da for the positive ion, unless the fragmentation pathway is determined by dynamics, rather than energetics.

4.8.2 $e^+NH_2CONH_2$ – Possible Fragmentation Pathways

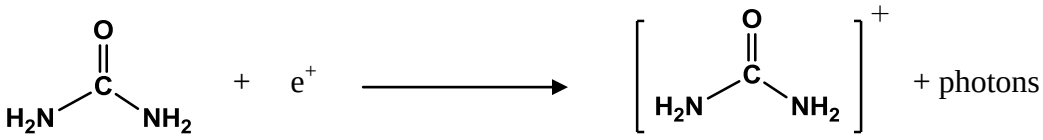

Path A

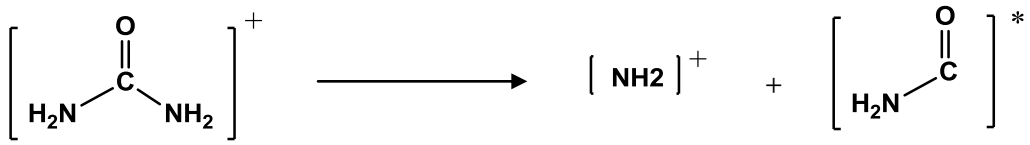

E^{B3}_i=-224.938884au unsatble E^{B3}=-169.252796au

Path B

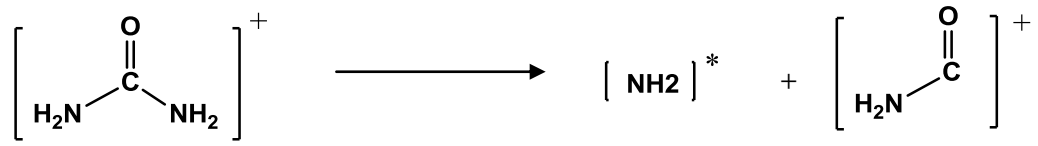

E^{B3}_{i}=-224.938884au E^{B3}=-55.885447au E^{B3}=-168.974766au

ΔE^{B3}=0.078671au (2.1eV)

MW 60Da 16Da 44Da

In $e^{+}NH_2CONH_2$ system, Table 4.7.3 indicates that the molecular orbital annihilation rate follows MO12 > MO14 > MO16. Therefore, MO12 has the highest probability to annihilate with a positron creating a vacancy. Energy liberated when this vacancy is filled by an electron jumping from the HOMO (MO 16) is 0.19283 au. This is greater than the bond dissociation energy in path B, leading to the formation of a positively charged fragment with 44 Da. However, path A is not possible due to the fact that $[NH_2]^{+}$ is unstable. Molecular ion peak at 60 Da will be observed if the positron annihilate with either MO16 or MO14 (if the fragmentation pathway is determined by energetic).

.

4.8.3 $e^{+}CH_3CONH_2$ – Possible Fragmentation Pathways

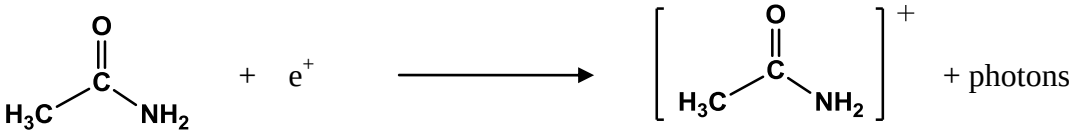

Path A

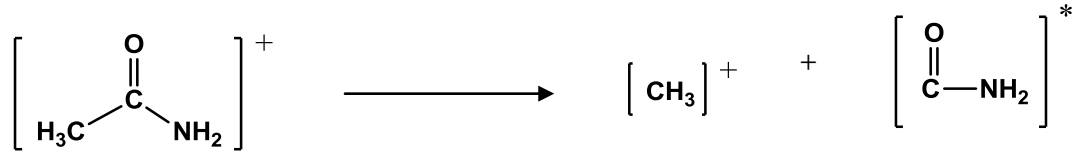

E^{B3}_{i}=-208.886315au E^{B3}=-39.484716au E^{B3}=-169.252796au

ΔE^{B3}=0.148803au (4.0eV)

MW 59Da 15Da 44Da

Path B

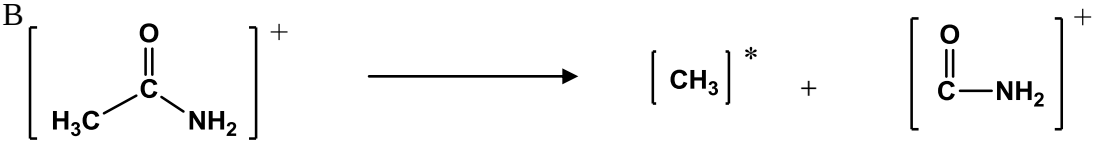

E^{B3}_{i}=-208.886315au E^{B3}=-39.847335au E^{B3}=-168.974766au

ΔE^{B3}=0.064215au (1.7eV)

MW 59Da 15Da 44Da

Path C

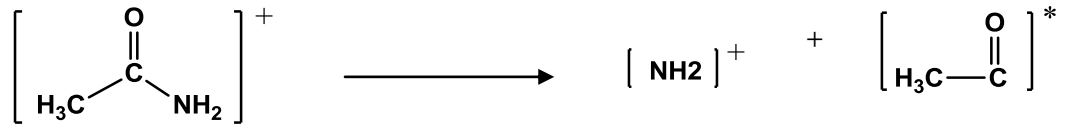

E^{B3}_{i}=-208.886315au Unstable E^{B3}=-153.194510au

Path D

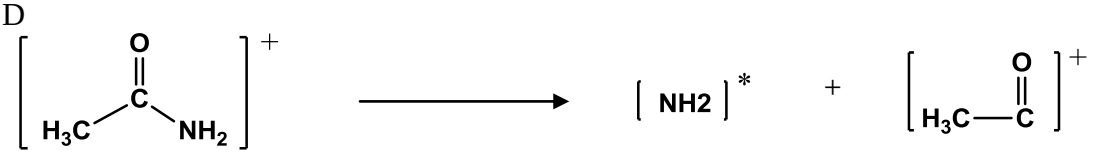

E^{B3}_{i}=-208.886315au E^{B3}=-55.885447au E^{B3}=-152.929757au

ΔE^{B3}=0.0711106au (1.9eV)

MW 59Da 16Da 43Da

According to the Table 4.7.4, the positron wave-function overlaps more heavily with the MO12 and 15 (nearly the same annihilation rates) than with the highest occupied molecular orbital (MO16) in $e^+CH_3CONH_2$ system. If the positron annihilates with one of the electrons in the MO15, the energy is released 0.00869 au. When an electron in the MO16 jumps to the vacancy in the MO15 the energy released is not sufficient to form fragments according to any of the pathways above; but, could yield a molecular ion at 59Da. However, if the positron annihilates with an electron in MO12, the amount of energy released upon annihilation is sufficient for fragmentation paths A, B, and D. Accordingly, the positive mode mass spectrum may contain peaks at 15Da for $[CH_3]^+$ from path A, 44Da for $[CONH_2]^+$ from path B, and 43Da for $[COCH_3]^+$ from path C in addition to the molecular ion peak at 59Da. However, the intensity of the observed peaks may depend on the bond dissociation energy involved with each pathway. The observed trend in bond dissociation energies follows as, path A: ΔE^{B3}=0.148803au (4.0eV), path B: ΔE^{B3}=0.064215au (1.7eV) and path C: ΔE^{B3}=0.0711106au (1.9eV). Therefore, the peak at 15Da should have a lower intensity than the 44Da and 43Da peaks, unless the natural preference for the lowest energy reaction products is reserved by unknown energy barriers and other kinetic factors during fragmentation. Further, fragmentation pathway B is energetically more favorable than D, hence the 44Da peak should be more dominant. This observation strongly agrees with the experimental positron ionization mass spectra of CH_3CONH_2, which indicates the presence of peaks at 44Da (highest intensity), 59Da and 15Da (lower intensity) [81].

4.9 Low-Energy Positron Interactions with Large Molecules

Our main focus here is to develop an efficient theoretical method which is reliable and computationally less expensive to study interactions of positrons with large biological molecules. Therefore, biomolecules such as amino acids, peptides, and nucleic acids were tested with the positronic basis sets developed in Chapter 3. According to the results in Section 4.5, large 13s9p uncontracted positronic basis sets (Appendix A) were used for most electronegative sites (eg. Oxygen) and smaller positronic basis sets (Table 4.5.2) were used for C and N centers and no positronic basis set were used for H atom centers.

4.9.1 e^+Gly-Ala System (E_{NEO-HF} = -528.711561au , PA= 50.36meV)

Amino acids are the building units of protein molecules which consist of an amine (-NH_2), carboxylic acid (-COOH), H and alkyl chain attached to the same carbon center. Two amino acids can be combined together by eliminating a water molecule (-OH from the carboxylic group and one of the H from the amine group) to yield a dipeptide and with further peptide formation results in proteins. Among 500 known amino acids only 20 amino acids are found in the human body. Therefore, it is important to study how positrons interact with the amino acids found in the human body.

As a starting point, the dipeptide formed between the smallest amino acids, glycine-alanine, is selected for this study of the interactions with a positron. This study targets on finding the most probable annihilation sites, the types of molecular orbitals that contribute heavily to the total annihilation rate, and finally the possible fragmentation pathways.

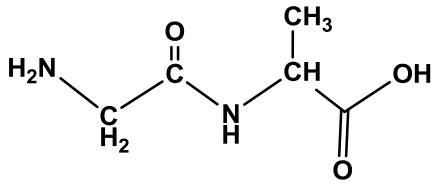

Figure 4.9.1.1 Chemical Structure of Gly-Ala

Figure 4.9.1.2 shows the 3D negative electrostatic potential, positron density and the contact density of e^{+}gly-ala system calculated using the 13s9p positron basis center on the O atom sites and the smaller contracted positronic basis centers (Table 4.5.2) for C and N atom sites.

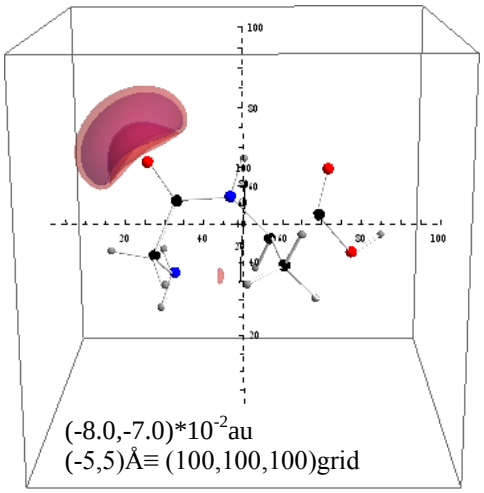

(a)

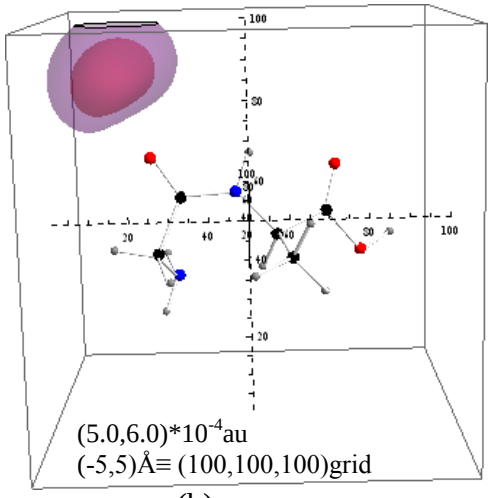

(b)

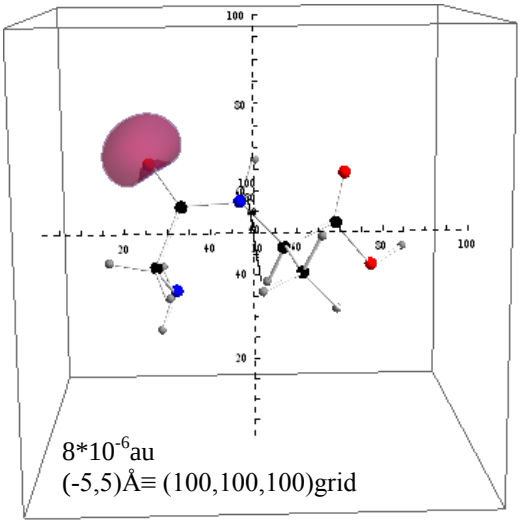

(c)

Figure 4.9.1.2 e^{+}Gly-Ala System

(a)Negative Electrostatic Potential

(b)Positron Density

(c)Contact Density

The 3D plot shown above consists of a 100x100x100 grid is representing the -5 Å to +5 Å for each axis. The calculations were conducted at NEO-HF level of theory with 6-31+G(d,p) electronic basis set. According to the Figure 4.9.1.2(a), negative electrostatic potential of the gly-ala system is concentrated around the O atom of the carbonyl group along the C=O bond axis (opposite to the Carbonyl group C) in the peptide bond and both positron density (Figure 4.9.1.2 b) and contact densities (Figure 4.9.1.2 c) are also highest in the same region. Therefore, the most probable annihilation site for gly-ala is O in the carbonyl group of the peptide bond.

Next, it is important to study the characteristics of molecular orbitals, which show a higher annihilation rate. In this case, population analysis was conducted for each molecular orbital considering atoms and fragments (Figure 4.9.1.3) as shown in Table 4.9.1.1 below.

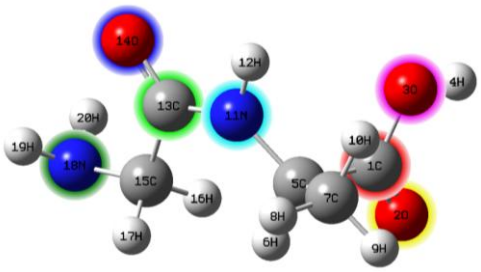

Figure 4.9.1.3 Gly-Ala Population Analysis

Fr1- atom 1-C, Fr2-atom13-C, Fr3-atom14-O, Fr4-atom2-O, Fr5-atom3-O, Fr6-atom11-N, Fr7-atom18-N and Fr8-rest of the atoms

Table 4.9.1.1 e^+Gly-Ala System – Molecular Orbital Annihilation Rate

MO	Liberated Energy (Hartree)	HF Annihilation Rate (1/ns)	MO Population Analysis
12	1.01066	0.00126270	O_{14}-s=0.58, p=0.06, C_{13}-s=0.22, p=0.04, N_{11}-s=0.07, p=0.02 Fr3=0.65 Fr2=0.26 Fr6=0.09
25	0.27504	0.00129288	O_3-p=0.22, C_1-p=0.15, O_2-p=0.13, C_5-p=0.09, C_7-p=0.08, O_{14}-p=0.05,s-0.02, N_{18}-p=0.05 N_{11}-p=0. Fr8=0.30 Fr5=0.22 Fr1=0.16 Fr4=0.14 Fr3=0.07 Fr7=0.05 Fr6=0.05 Fr2=0.01
37	0.04595	0.00238482	O_{14}-p=0.62, N_{18}-p=0.19 C_{15}-p=0.07 N_{11}-p=0.04 C_{13}-p=0.02 C_5-p=0.02 C_{13}-d=0.02 Fr3=0.62 Fr7=0.20 Fr8=0.11 Fr6=0.04 Fr2=0.03
39	-	0.00115730	N_{18}-p=0.53 O_{14}-p=0.12 N_{11}-p=0.09 C_{13}-p=0.07 C_{15}-p=0.05 N_{18}-s=0.03 H_{17}-s=0.02 C_{13}-s=0.02 Fr7=0.56 Fr8=0.13 Fr3=0.12 Fr2=0.09 Fr6=0.09

Other MO annihilation rate < $8.0*10^{-4}$ (1/ns)

In this molecule, the most probable annihilation site involves the carbonyl oxygen (O_{14}, fragment 3) as discussed above. Population analysis indicates a higher contribution from O_{14} in both MO 37 and MO12. However, the fact that MO37 shows the highest contribution to the annihilation rate is due to the higher p-orbital contribution in O_{14} when compared to MO12. This observation is clearly visible in the molecular orbitals shown in Figure 4.9.1.4 where higher s-character is visible for O_{14} in MO12 while p-character is dominant for MO37. Molecular orbitals 39 and 25 also show a decent annihilation rate. But the population analysis indicates maximum contribution from O_{14} atom, which is calculated to be the most probable annihilation site.

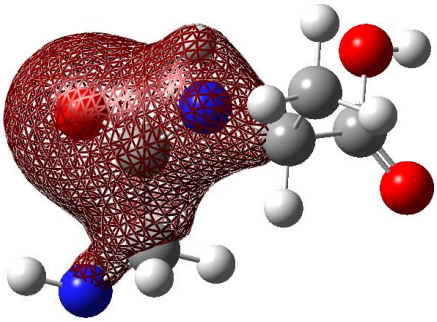

MO12

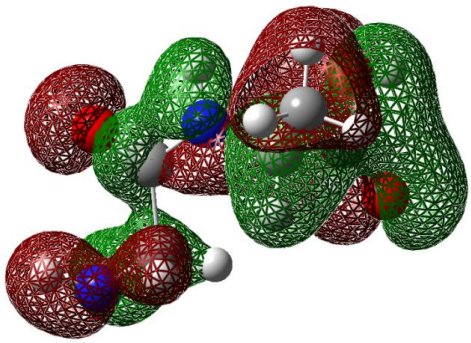

MO25

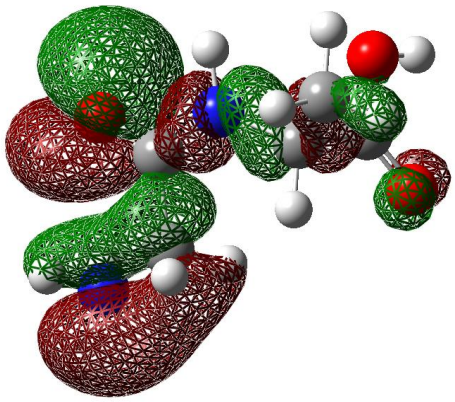

MO37

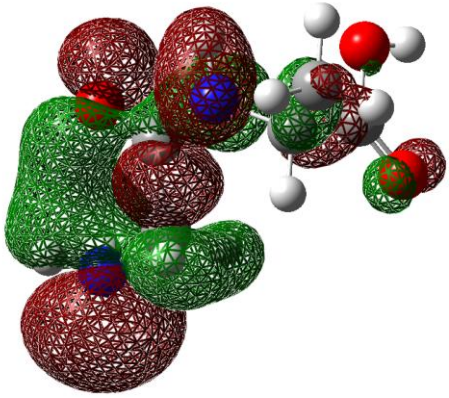

MO39

Figure 4.9.1.4 Gly-Ala Molecular Orbital Shapes

4.9.1.1 e^{+}Gly-Ala system- Possible Fragmentation Pathways

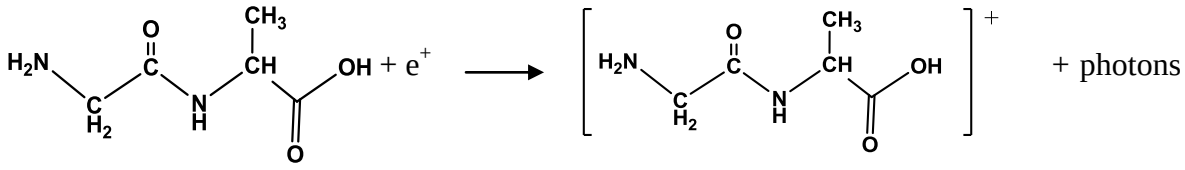

Path A

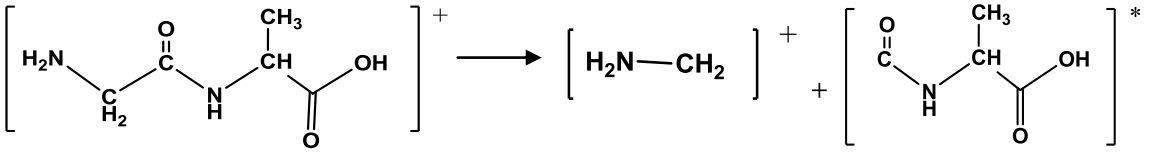

$E^{B3}{}_{i}$=-531.495434au E^{HF}=-94.984612au E^{HF}=-436.465279au

ΔE^{B3}=0.045543au (1.2eV)

MW 134Da 30Da 104Da

Path B

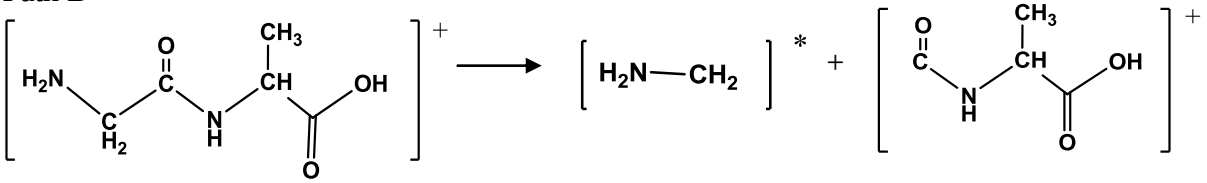

$E^{B3}{}_{i}$=-531.495434au E^{B3}=-95.215331au E^{B3}=-436.209391au

ΔE^{B3}=0.070713au (1.9eV)

MW 134Da 30Da 104Da

Path C

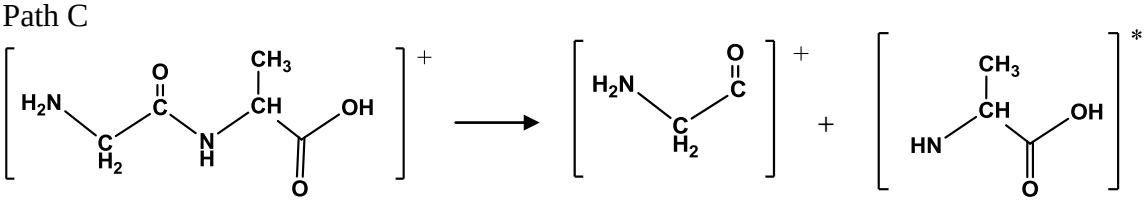

E^{B3}_{i}=-531.495434au E^{B3}=-208.308214au E^{B3}=-323.107032au

ΔE^{B3}=0.080187au (2.2eV)

MW 134Da 58Da 76Da

Path D

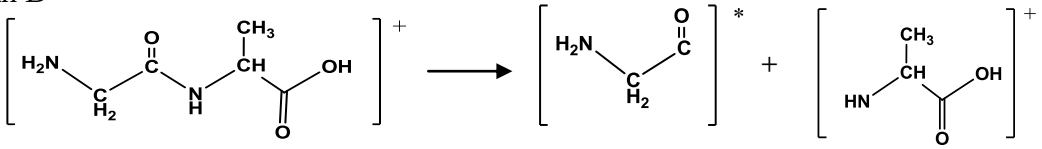

E^{B3}_{i}=-531.495434au E^{B3}=-208.542433au E^{B3}=-322.898397au

ΔE^{B3}=0.054604au (1.5eV)

MW 134Da 58Da 76Da

Path E

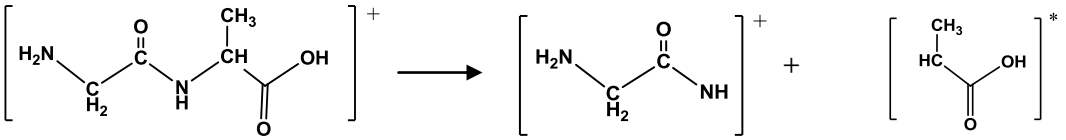

E^{B3}_{i}=-531.495434au E^{B3}=-263.699495au E^{B3}=-267.768382au

ΔE^{B3}=0.027557au (0.75eV)

MW 134Da 73Da 61Da

Path F

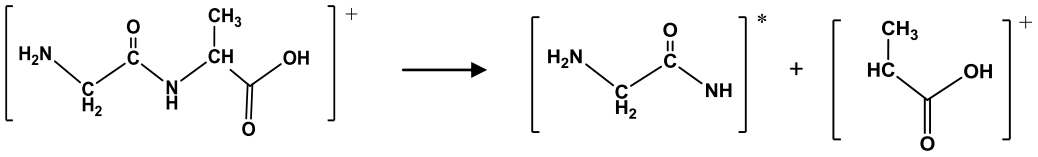

E^{B3}_{i}=-531.49543402au E^{B3}=-263.901537au E^{B3}=-267.451700au

ΔE^{B3}=0.142227au (3.9eV)

MW 134Da 73Da 61Da

A favorable fragmentation pathway is observed if the energy released during annihilation is higher than the bond dissociation energy. If the positron annihilates with the HOMO (MO39) orbital then the molecular ion peak is observed. If the positron annihilate with inner orbitals MO12 or MO25, the energy liberated is sufficient to conduct all pathways, A-F. However, if the positron annihilate with MO37, only pathways A and E are possible. We previously showed that the MO37 has the highest molecular orbital to overlap with a positron. Accordingly, the dominant peaks involving bond breaking along the backbone near the amide bond in this dipeptide, which may be observed in the positive mode mass spectrum, would be $[NH_2\text{-}CH_2]^+$ at 30Da from path A and $[NH_2\text{-}CH_2\text{-}CO\text{-}NH]^+$ at 73Da from path E.(x and z fragmentation).

4.9.2 e^+Gly-Lys system ($E_{NEO\text{-}HF}$ = -700.855766au, PA=67meV)

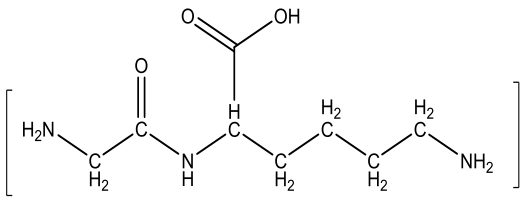

Figure 4.9.2.1 Chemical Structure of Gly-Lys

The dipeptide formed between glysine and lysine is shown above. The calculated (6-31+G(d,p)/HF) ground state energy of the gly-lys dipeptide is -700.853318 au and the positron affinity is 67meV.The interaction of positron with gly-lys dipeptide was studied in order to understand the most probable positron binding site, the molecular orbital with the highest annihilation rate, and possible fragmentation pathways. In order to identify the positron binding sites, the molecular electrostatic potential, positron density and contact density were calculated similar to the method followed for the gly-ala system and is illustrated in following Figure 4.9.2.2.

According to Figure 4.9.2.2(a), the negative electrostatic potential is localized in three different sites. The contour values indicate the deepest negative electrostatic potential well located at the carboxylic acid group and more specifically on the carbonyl oxygen atom. Population analysis results indicate a trend similar to above gly-ala system indicating higher p-character in the O_6 and O_{14} in the molecular orbital, which shows highest contribution to the annihilation rate. Hence it is the best position to trap a positron. This observation is further confirmed by the observed positron density and contact densities in Figure 4.9.2.2 b and c.

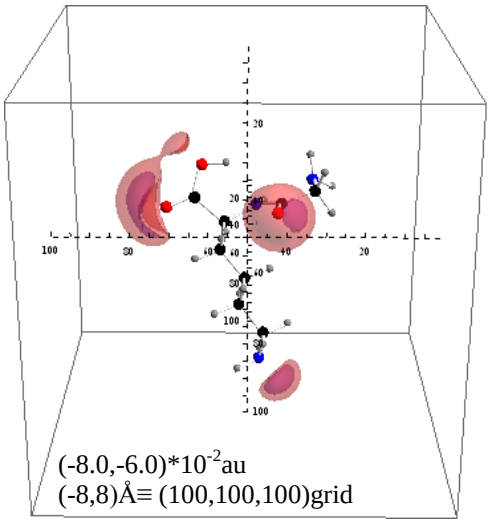

(a)

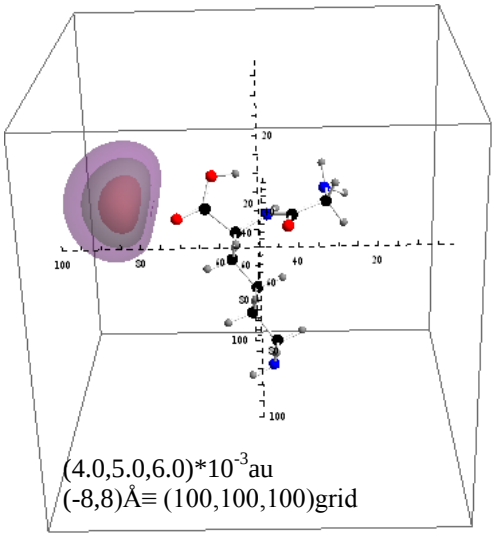

(b)

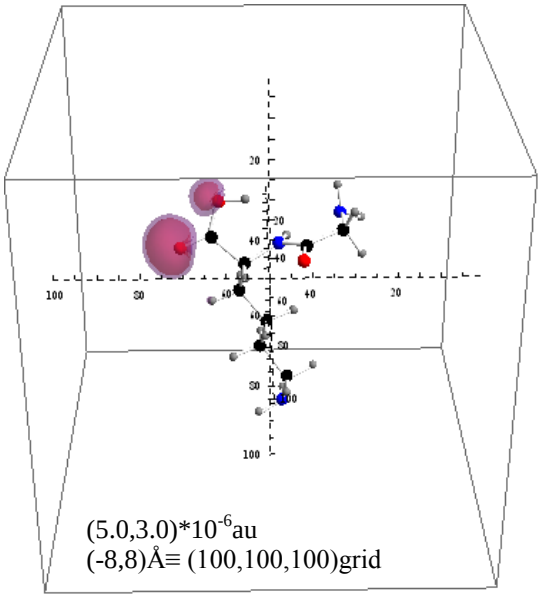

(c)

Figure 4.9.2.2 e^{+}Gly-Lys System

(a)Negative Electrostatic Potential

(b)Positron Density

(c)Contact Density

Table 4.9.2.1 e^{+}Gly-Lys System-Molecular Orbital Annihilation Rate

MO	Liberated Energy (Hartree)	HF Annihilation Rate (1/ns)	MO Population Analysis
17	0.98265	0.00118248	O_6-s=0.45, p=0.03 O_{14}-s=0.32, p=0.01 C_5-p=0.11,s=0.03 O14- Fr5=0.48 Fr8=0.33 Fr4=0.15 Fr9=0.02
34	0.2724	0.00218927	O_6-p=0.38, s=0.15 O_{14}-p=0.16, s=0.02 C_5-p=0.16, s=-0.01 C_7-p=0.03 N_1-p=0.01 N_8-p=0.01 Fr5=0.54 Fr8=0.18 Fr4=0.15 Fr9=0.09 Fr1=0.02 Fr6=0.01 Fr3=0.01
48	0.10478	0.00176761	C_{13}-p=0.22 C_{12}-p=0.20 C_{11}-p=0.10 C_7-p=0.07 Fr9=0.93 Fr4=0.02 Fr7=0.01
50	0.08575	0.00091927	O_6-p=0.39 O_{14}-p=0.29 O_2-p=0.06 C_5-p=0.04,s=-0.01,d=0.01 N_1-p=0.02 N_8-p=0.02 Fr5=0.39 Fr8=0.29 Fr9=0.19 Fr2=0.06 Fr4=0.04 Fr1=0.02 Fr6=0.01
55(HOMO)	-	0.00002180	N_9-p=0.66 C_{12}-p=0.10 C_{10}-p=0.04 Fr7=0.68 Fr9=0.28 Fr6=0.01

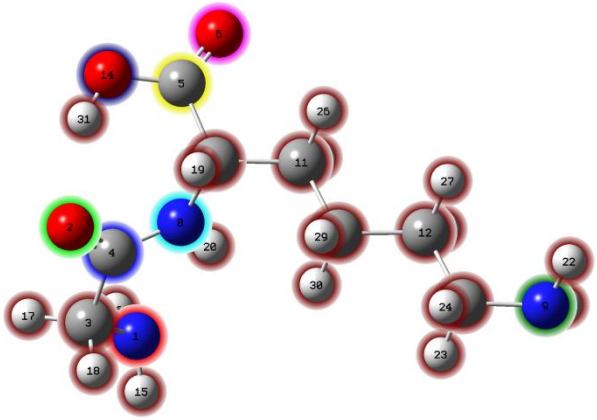

Figure 4.9.2.3 gly-lys Population Analysis

Fr1-N_1 Fr2-O_2 Fr3-C_4 Fr4-C_5 Fr5-O_6 Fr6-N_8

Fr7-N_9 Fr8-O_{14} Fr9-all other

4.9.2.1 e^+Gly-Lys System- Possible Fragmentation Pathways

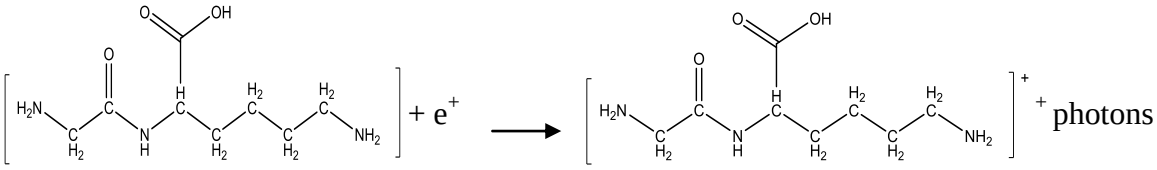

Path A

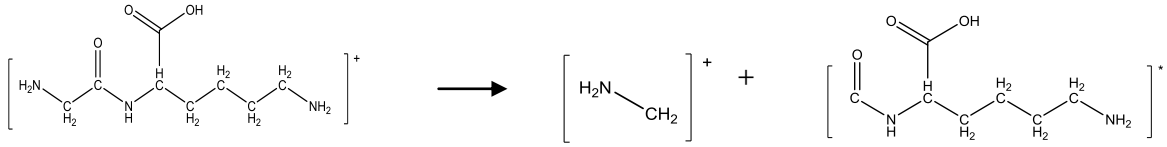

E^{B3}_i=-704.799466au E^{B3}=-94.984615au E^{B3}=-609.758925au

ΔE^{B3}=0.05592537au (1.5eV)

MW 203Da 30Da 173Da

Path B

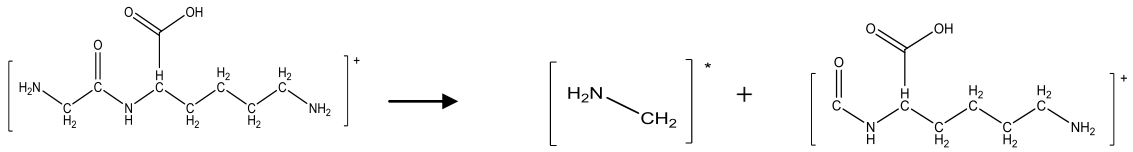

E^{B3}_i=-704.799466au E^{B3}=-95.215335au E^{B3}=-609.464789au

ΔE^{B3}=0.11934249au (3.2eV)

MW 203Da 30Da 173Da

Path C

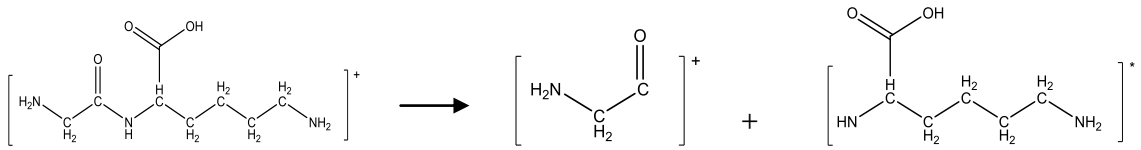

$E^{B3}{}_i$=-704.799466au E^{B3}=-208.308028au E^{B3}=-496.409274au

ΔE^{B3}=0.08216399au (2.2eV)

MW 203Da 58Da 145Da

Path D

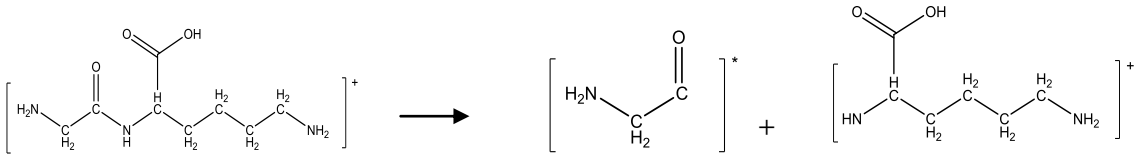

$E^{B3}{}_i$=-704.799466au E^{B3}=-208.542165au E^{B3}=-496.184212au

ΔE^{B3}=0.07308954au (2.0eV)

MW 203Da 58Da 145Da

Path E

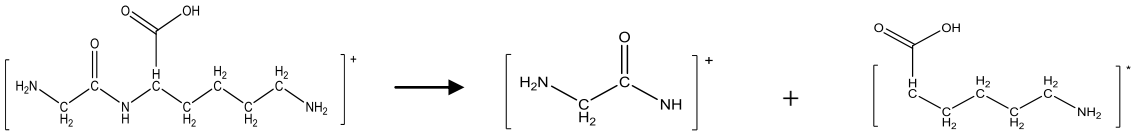

$E^{B3}{}_i$=-704.799466au E^{B3}=-263.699491au E^{B3}=-441.061249au

ΔE^{B3}=0.03872537au (1.1eV)

MW 203Da 73Da 130Da

Path F

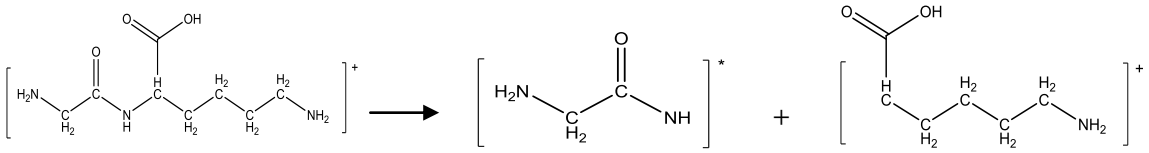

E^{B3}_i=-704.799466au E^{B3}=-263.905070au E^{B3}=-440.760905au

ΔE^{B3}=0.13349117au (1.1eV)

MW 203Da 73Da 130Da

Path G

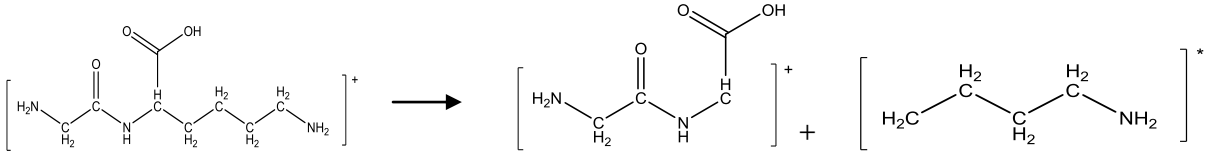

E^{B3}_i=-704.799466au E^{B3}=-491.563620au E^{B3}=-213.155418au

ΔE^{B3}=0.08042792au (2.2eV)

MW 203Da 131Da 72Da

Path H

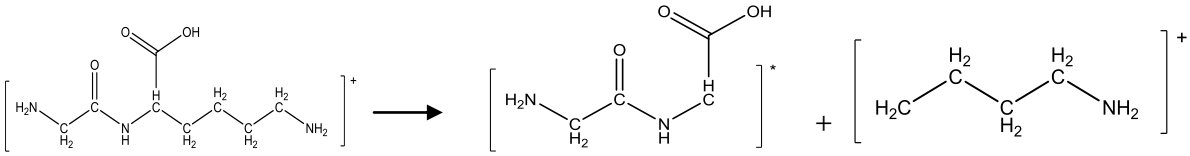

E^{B3}_i=-704.799466au E^{B3}=-491.839321au E^{B3}=-212.888128au

ΔE^{B3}=0.07212842au (2.0eV)

MW 203Da 131Da 72Da

The possible fragmentation pathways depend on the annihilation rate corresponding to each molecular orbital. If the positron annihilates with the HOMO (MO55) then the molecular

ion peak is observed. The preferred fragmentation pathways depend on the energy released during annihilation to overcome the bond dissociation energy. Therefore, if the positron annihilate with MO17 or MO34, then all the fragmentation pathways A-H are probable. However, if the positron annihilate with MO48 or MO50, all pathways except B and F are possible. Another factor that needs to be considered is the bond dissociation energies involved with each fragmentation pathway. The trend in bond dissociation energies follows the order, E < A < H < D < G < C < B < F. Since the interaction of positron with MO34, which shows the highest annihilation rate, can release energy sufficient for path E (i.e. energetically favorable pathway) the dominant peak would be $[NH_2\text{-}CH_2\text{-}CO\text{-}NH]^+$ at 73Da (if the fragmentation pathways is determined by energetically). We expect to see pathway E and not F; A and not B, because electrons are expected to be able to hop freely between fragments, so that the fragments can achieve the lowest energy distribution of charge. The energy differences for C/D and G/H may be close enough to be within error bars for calculation and if not, they may easily be within the kT_{eff} in the experimental situation.

4.9.3 e^+Uracil System ($E_{NEO\text{-}HF=}$-412.489489au, PA=11meV)

Nucleic acids are another class of biomolecules essential for life. Interaction of positrons with nucleic acids: uracil, thyamine, cyctocine, and guanine, were studied to find possible annihilation sites, molecular orbital contributions to the annihilation rate and the energy liberated during the annihilation process. The structure of the uracil is given in the Figure 4.9.3.1.

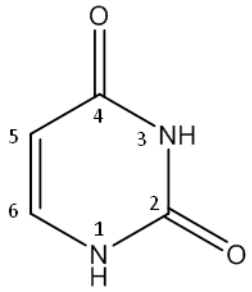

Figure 4.9.3.1 Chemical Structure of Uracil

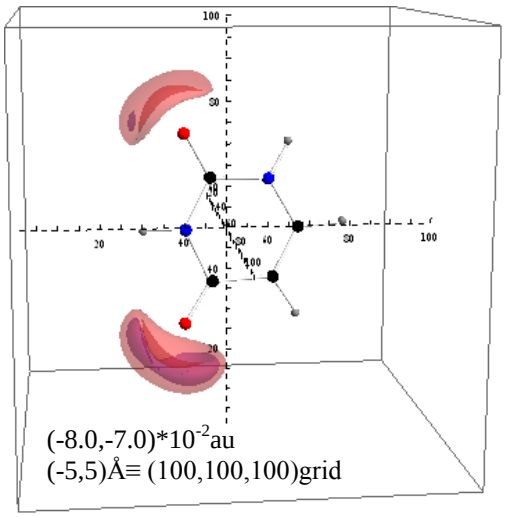

(a)

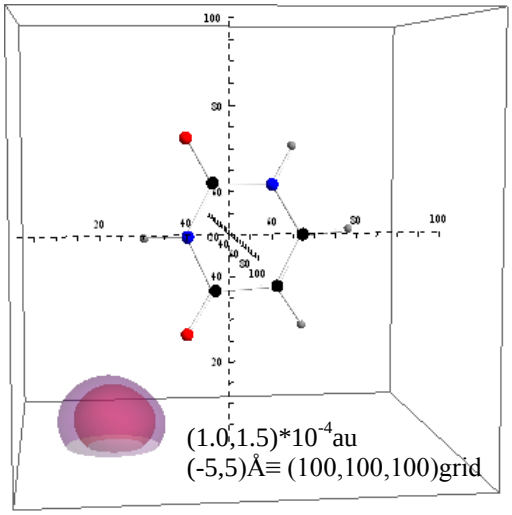

(b)

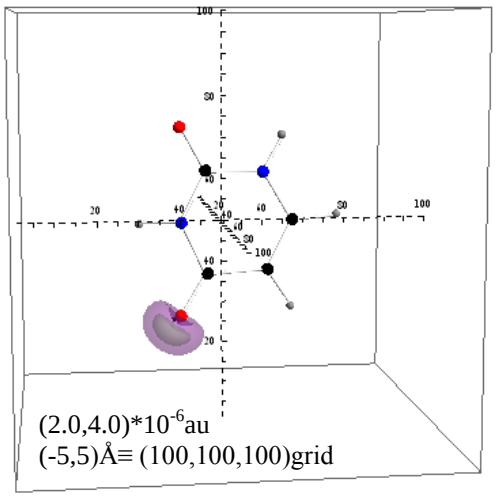

(c)

Figure 4.9.3.2 e^{+}Uracil System

(a) Negative Potential Well

(b) Positron Density

(c) Contact Density

As seen in Figure 4.9.3.2(a) a large negative electrostatic potential can be found in two locations near to the oxygen atoms. However, contour values suggests that the deepest potential well is located on the 4-oxygen hence being the most possible site for positron binding. The Figure 4.9.3.2(b) shows the higher positron density contours around the 4-oxygen atom (outside of the ring) verifying the above prediction. Therefore, the calculated contact density is also higher in the same region as shown in Figure 4.9.3.2(c). The molecular orbital annihilation rates were calculated and Table 4.9.3.1 shows the top five molecular annihilation contributions in the e^+uracil system.

Table 4.9.3.1 e^+Uracil System-Molecular Orbital Annihilation Rate

MO	Liberated Energy (Hartree)	HF Annihilation Rate (1/ns)
19	0.31183	0.00034058
22	0.25179	0.00029262
24	0.20908	0.00022637
27	0.07906	0.00033791
29(HOMO)	-	0.00008800

Experimental electron impact mass spectra and theoretical predictions often suggest that a ring cleavage occurs forming a neutral HNCO fragment for nucleic acid bases [82-84]. The remaining positive fragment will then appear as the molecular ion peak along with secondary fragments originated from it. In the case of uracil, the primary fragment $[NCHCH_2CO]^+$ (69Da) was observed and in addition, secondary fragments originated from the above positive fragment appear at 41Da for CH_2CNH^+, 42Da for CH_2CO^+, and 28Da for $HNCH^+$ [85,86]. Therefore, in developing possible fragmentation pathways for positron ionization mass spectra for nucleic acid bases, possible primary fragments that can be formed upon similar ring cleavages (according to literature of EI impact mass spectra) are considered.

As seen in Table 4.9.3.1, the molecular orbitals 19 and 27 heavily overlap with the positron wave function, even though the highest occupied molecular orbital is 29. According to the molecular annihilation rates, there is a higher probability for the positron to annihilate with one of the electrons in MO19 and MO27 (with equal probability). The possible fragmentation pathways of induced by high energy γ rays incident on uracil cations have been studied [86]. According to the literature, to form fragment ions of having mass of 69Da (breaking the bonds N1-C2 and N3-C4) involves a 1.9eV potential barrier. Other fragmentation pathways form fragment ions with masses of 42Da, 41Da and 28Da, all with energy barriers of 4.3 eV [86]. As shown in Table 4.9.3.1, the liberated energy (8.5eV) is sufficient to overcome these potential barriers if the bound positron annihilates with one of the electrons in the MO19. Therefore we can expect even at low incident energies, positrons can produce similar fragment ions as in other experimental methods.

4.9.4 e^+Guanine System ($E_{NEO\text{-}HF=}$-539.429544au, PA=203meV)

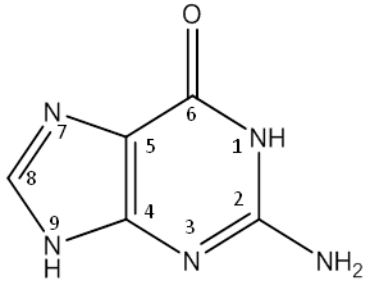

Figure 4.9.4.1 Chemical Structure of Guanine

The negative electrostatic potential, positron density and contact density were calculated for the e^+guanine system. According to Figure 4.9.4.2(a), a deep negative potential well can be seen around the 6-oxygen and 7-nitrogen atoms (opposite the other heavy atoms).

The calculated positron density distribution and contact density are located at the same region as shown in Figure 4.9.4.2(b) and (c). Therefore, the best site for positron binding will be located on either 6-oxygen or 7-nitrogen.

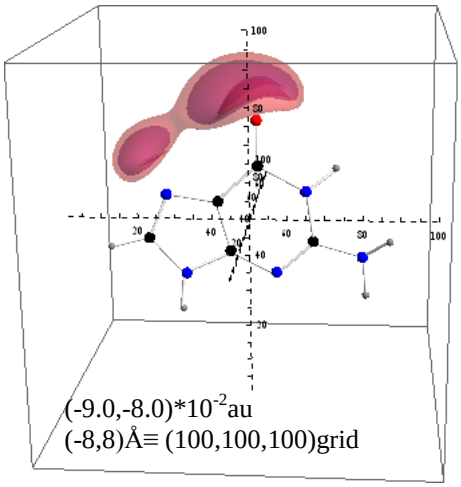

(a)

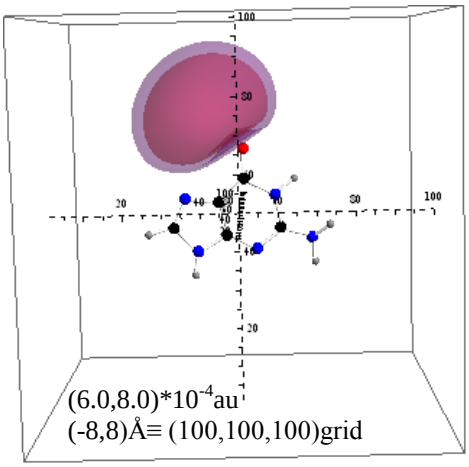

(b)

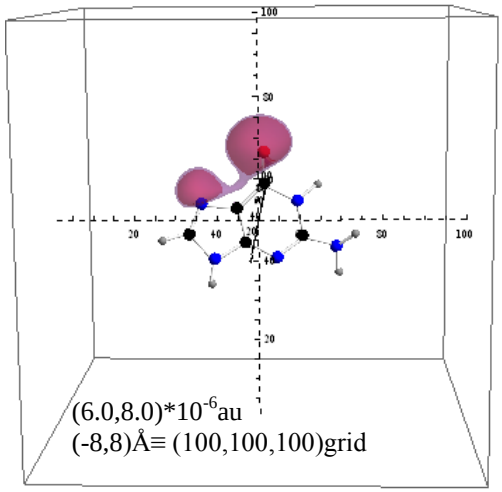

(c)

Figure 4.9.4.2 e^{+}Guanine System

(a) Negative Potential Well

(b) Positron Density

(c) Contact Density

Table 4.9.4.1 e^+Guanine System-Molecular Orbital Annihilation Rate

MO	Liberated Energy (Hartree)	HF Annihilation Rate (1/ns)
29	0.31597	0.00796700
34	0.15258	0.00739799
37	0.12443	0.00329536
39(HOMO)	-	0.00162059

The calculated molecular orbital annihilation rates of heavily overlaping positron and molecular orbitals are shown in Table 4.9.4.1. In this case the positron wave function overlaps more heavily with the inner molecular orbitals, MO29 and MO34 than with the HOMO (MO39). Possible fragmentation pathways are suggested according to the experimental mass spectra observed with CID [87] and EI methods [83]. In both experimental studies, positive fragment ions at 108Da were seen after cleaving HCNO neutral fragment from the parent molecule. Also the theoretical study for the formation of possible fragment ions of guanine radical cation [87] suggests that a stable fragment ion can be seen at 108 Da and 109Da due to HNCO and NH_2-C=N neutral fragment dissociation from the main ring by overcoming energy barriers of 3.17eV and 3.05eV, respectively. According to our calculations (Table 4.9.4.1), if the positron annihilates with one of the electrons in the MO29, the liberated energy is 0.31597au /8.6eV, which is sufficient to overcome those potential barriers and may form the fragment ions. Accordingly, the positron ionization mass spectrum will show the fragment peaks similar to the EI method [83] and CID method [87].

4.9.5 e^+Thymine System ($E_{NEO-HF=}$-451.531052au, PA=9meV)

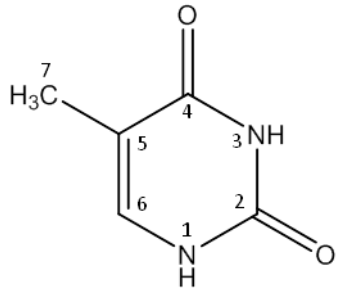

Figure 4.9.5.1 Chemical Structure of the Thymine

The chemical structure of the thymine molecule is shown in Figure 4.9.5.1. The low energy positron interaction with thymine molecule was studied to find possible binding sites and contribution of molecular orbitals to the annihilation rate. Figure 4.9.5.2(a) shows negative electrostatic potential around the 2-oxygen and 4-oxygen atoms (outside of the ring) along the bond axis in the thymine molecule. The calculated positron density is highest around the 4-oxygen atom and extend towards the 2-oxygen as shown in 4.9.5.2(b). The result of the contact density distribution shows higher overlap between the positron and the electron wave function near the both O atoms; hence, that will be likely e^+e^- annihilate site.

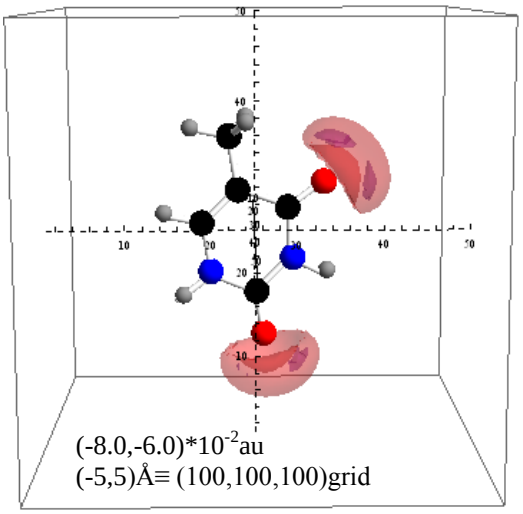

(a)

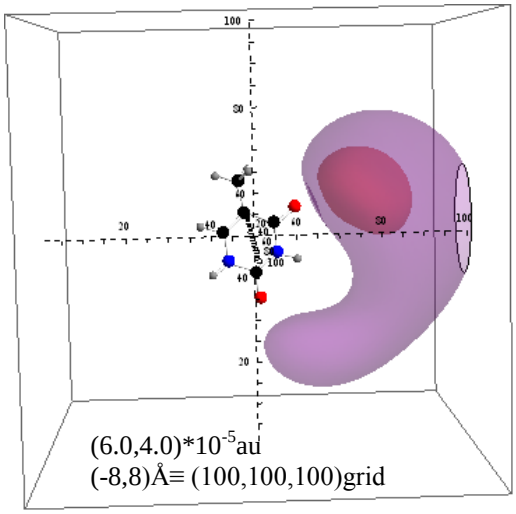

(b)

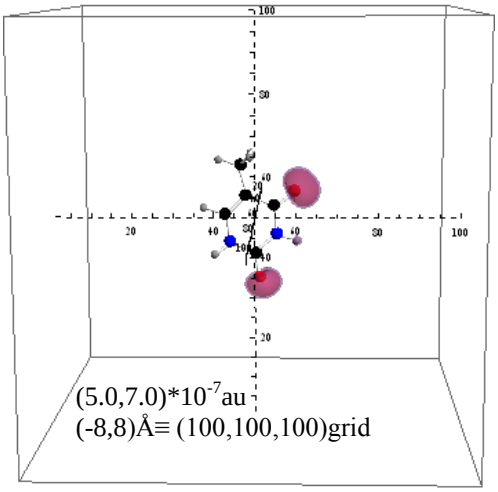

(c)

Figure 4.9.5.2 e^+thymine system

(a) Negative potential well

(b) Positron density

(c) Contact density

According to theoretical studies and experimental EI mass spectra of the thymine radical cation, primary fragments are formed by cleaving neutral [HNCO] fragment [82,84]. According to the literature, the dominant pathway to produce primary fragments involve bond breaking at N1-C2 and N3-C4 to produce $[HNCHC(CH_3)CO]^+$ (energy barrier ~ 2.0eV [84]) which undergo further fragmentation. However, the ring cleavage occurs via N1-C6 and C2-N3, and C2-N3 and C4-C5 lead to form four membered ring product [84].

Table 4.9.5.1 e^+Thymine System-Molecular Orbital Annihilation Rate

MO	Liberated Energy (Hartree)	HF Annihilation Rate (1/ns)
21	0.32414	0.00021649
23	0.28863	0.00019126
24	0.2673	0.00013531
30	0.1236	0.00015937
31	0.09136	0.00019623
32	0.07991	0.00014670
33(HOMO)	0	0.00005289

The molecular annihilation rates were calculated and shown in the Table 4.9.5.1 for the e^+thymine system. The probability for the positron to annihilate with the highest occupied molecular orbital, MO33, is very low due to the low orbital annihilation rate. The positron wavefunction heavily overlaps with the MO 21. Therefore, there is a higher probability that the low energy positron annihilates with one of the electrons in MO21 liberating 0.32414au/8.8eV energy, which is greater than the barrier potential (~2.0eV, Ref. [84]), and leads to the formation of $[HNCHC(CH_3)CO]^+$, which has a mass of 83Da.

4.9.6 e^+Cytosine System ($E_{NEO\text{-}HF=}$-392.648533au, PA=231meV)

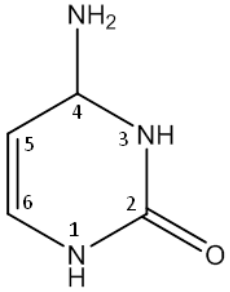

Figure 4.9.6.1 Chemical Structure of Cytosine

The chemical structure of cytosine is shown in the above Figure 4.9.6.1. The negative electrostatic potential, positron density and contact density were calculated for the e^+cytosine

system. According to the results, a deep negative potential well can be seen around the 2-oxygen atom and extend to the 3-nitrogen atom (outside of the ring) as shown in the Figure 4.9.6.2(a). The calculated positron density distribution is localized around the 2-oxygen atom along the bond axis (see Figure 4.9.6.2(b)) and Figure 4.9.6.2(c) shows a higher contact density contour around the same oxygen atom. Therefore the most probable location for e^+e^- annihilation is located near the 2-oxygen atom.

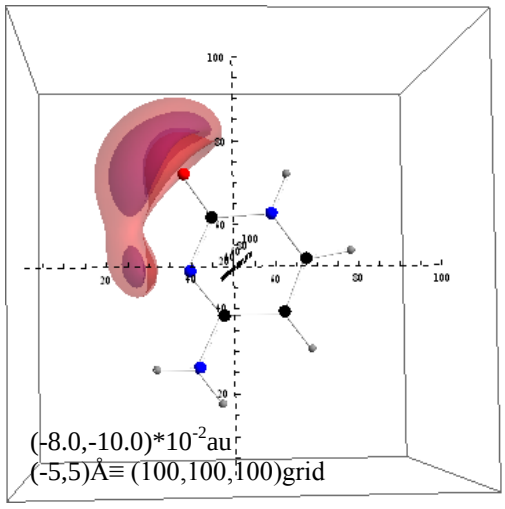

(a)

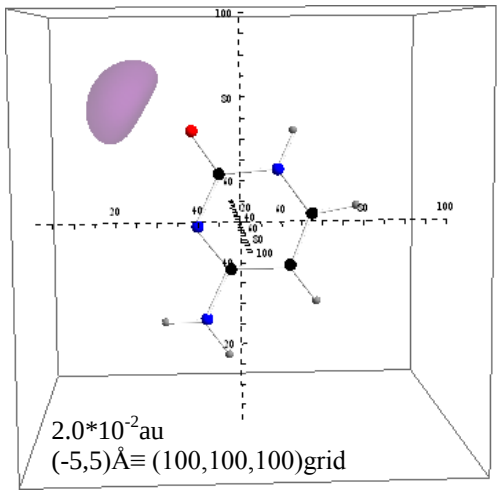

(b)

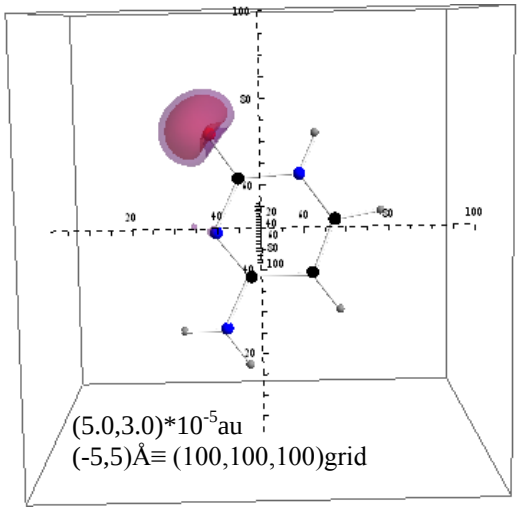

(c)

Figure 4.9.6.2 e^+Cytosine System

(a)Negative Potential Well

(b)Positron Density

(c)Contact Density

Table 4.9.6.1 e^+Cytosine system-Molecular Orbital Annihilation Rate

MO	Liberated Energy (Hartree)	HF Annihilation Rate (1/ns)
20	0.2879	0.00985760
25	0.1508	0.00514116
26	0.09772	0.01062256
27	0.07415	0.00582173
29(HOMO)	-	0.00259194

Experimental and theoretical studies were found in the literature for EI mass spectra for cytosine [82,84,88]. Similar to other pyrimidine bases, the preferred pathways involve formation of neutral [HNCO] fragments. Therefore, the fragmentation pathways proposed for the positron ionized mass spectra follows the same trend. The experimental EI mass spectra for the cytosine cation shows peaks at 111Da (molecular peak), followed by other fragments with peaks at 95 Da, 83 Da, 69 Da, 41 Da, and 28 Da [82]. Molecular orbital annihilation rates are shown in Table 4.9.6.1 for molecular orbitals with heavily overlapped wavefunction. The highest overlap is observed for MO26 due to the fact that it shows the highest annihilation rate. The amount of energy liberated when an electron jumps from HOMO to MO26 is 0.09772au/2.7eV. However, work done with CCSD(T)/aug-cc-pVTZ level of theory [88] showed that there is a 1.8eV energy barrier to produce the 68Da fragment ion. Since the amount of energy liberated when a positron annihilates with the MO26 is more than 1.8eV, fragment ion of having mass of 68Da is possible.

4.9.7 e^+(N-Acetyl-Phenylalanine-Ethyl Ester) System (E_{NEO-HF}=-781.317057au, PA=21meV)

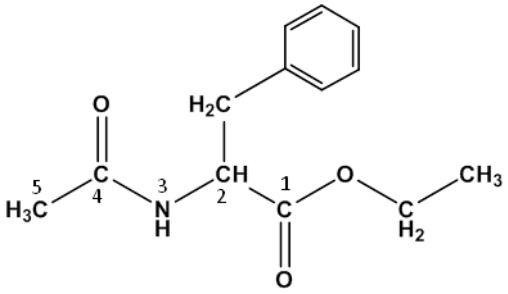

Figure 4.9.7.1 Chemical Structure of N-Acetyl-Phenylalanine-Ethyl Ester

The e^+(N-acetyl-phenylalanine-ethyl ester) system was studied in the NEO-HF level of theory. Since experimental positron induced mass spectra is available for this molecule, it serves as an excellent example to check the validity of our methods [81]. Calculations were performed using 13s9p uncontracted positronic basis sets for the O centers and 2s contracted positronic basis sets for the C and N atom centers. Basis set 6-31+(G(d,p) was used for the electrons. Interaction of the positron with N-acetyl-phenylalanine-ethyl ester was studied to identify the possible positron binding sites, molecular orbital contribution to the annihilation rate and possible fragmentation paths.

As shown in Figure 4.9.7.2(a) below, the negative electrostatic potential of the N-acetyl-phenylalanine-ethyl ester can be seen at the 4-oxygen of the N-acetyl group. The positron density and the e^-e^+ contact density can also be seen in the same region as the negative electrostatic potential well hence, serves as the best site for positron annihilation.

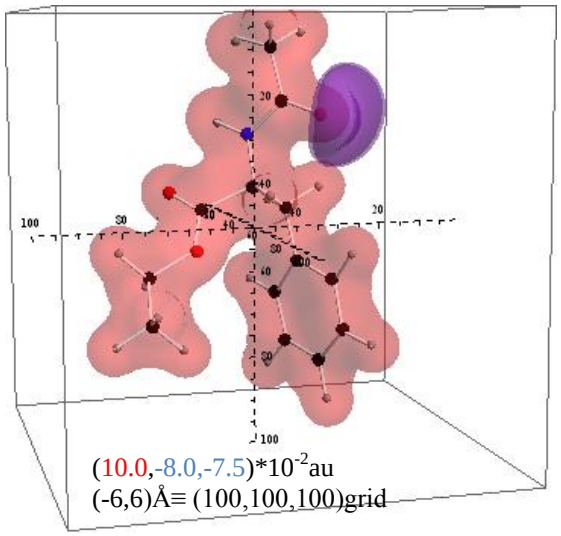

(a)

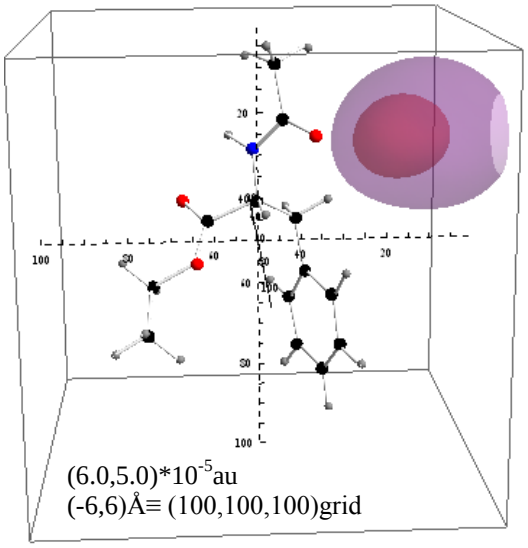

(b)

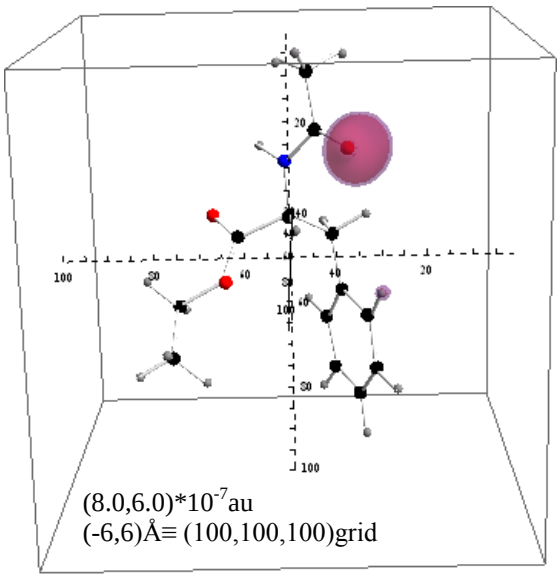

(c)

Figure 4.9.7.2 e^{+}N-Acetyl-Phenylalanine-Ethyl Ester

(a) Molecular Electrostatic Potential

(b) Positron Density

(c) Contact Density

Table 4.9.7.1 e^+(N-Acetyl-Phenylalanine-Ethyl Ester) System – Molecular Orbital Annihilation Rate

MO	Liberated Energy (Hartree)	HF Annihilation Rate (1/ns)
19	1.06719	0.00002161
38	0.33736	0.00002622
41	0.30191	0.00001126
43	0.27862	0.00001071
45	0.25862	0.00002950
47	0.24524	0.00001195
60	0.09456	0.00004638
61	0.06843	0.00002055
62	0.00856	0.00000527
63	-	0.00000417

Table 4.9.7.1 lists the top 10 molecular orbitals that make a significant contribution to the total annihilation rate. According to the calculations, the highest molecular orbital annihilation contribution is given in the MO60. This orbital has the highest probability that the positron will annihilate with one of the electrons. If one of the electrons in the highest occupied molecular orbital (HOMO) MO63 jumps to the vacancy at molecular orbital 60, then 0.09456au energy will be released. The second highest molecular annihilation contribution is given by the MO45, which has an energy gap of 0.25862 au to the HOMO. The possible fragmentation paths are studied and presented in the next section.

4.9.7.1 e^+(N-Acetyl-Phenylalanine-ethyl ester)-Possible Fragmentation Pathways

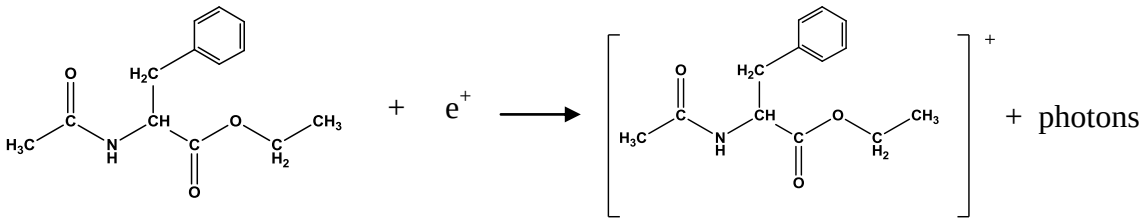

Path A

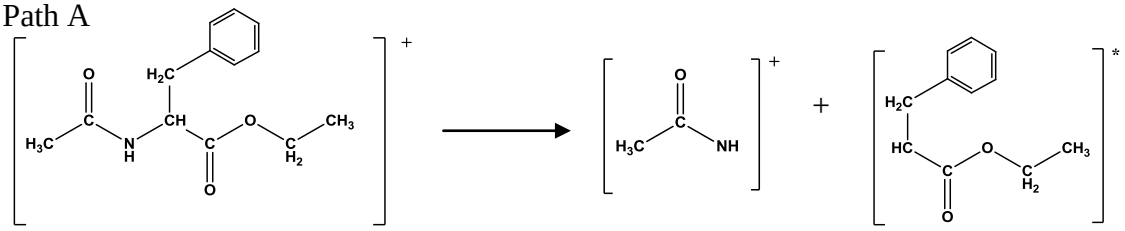

E^{B3}_i=-785.843296au E^{B3}=-208.187881au E^{B3}=-577.458638au

ΔE^{B3}=0.196777au (5.4eV)

MW 235Da 58Da 177Da

Path B

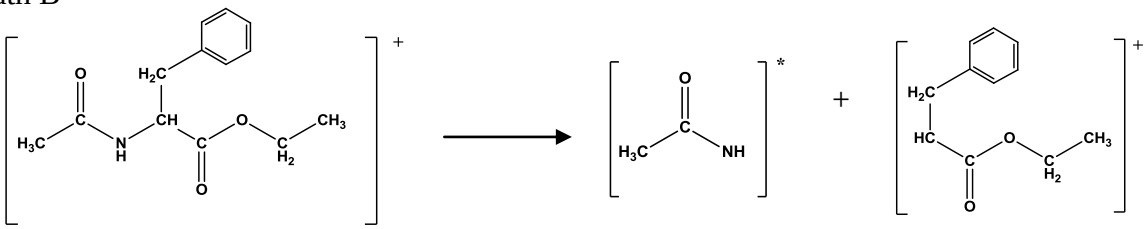

E^{B3}_i=-785.843296au E^{B3}=-208.551905au E^{B3}=-577.202379au

ΔE^{B3}=0.089018au (2.4eV)

MW 235Da 58Da 177Da

Path C

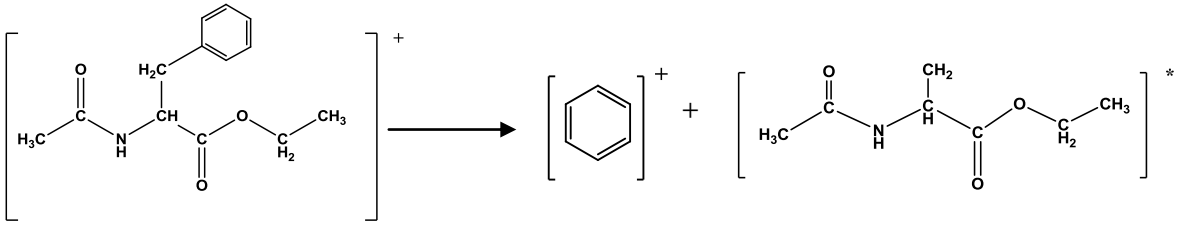

$E^{B3}{}_i$=-785.843296au E^{B3}=-231.274643au E^{B3}=-554.401885au

ΔE^{B3}=0.166768au (4.5eV)

MW 235Da 78Da 157Da

Path D

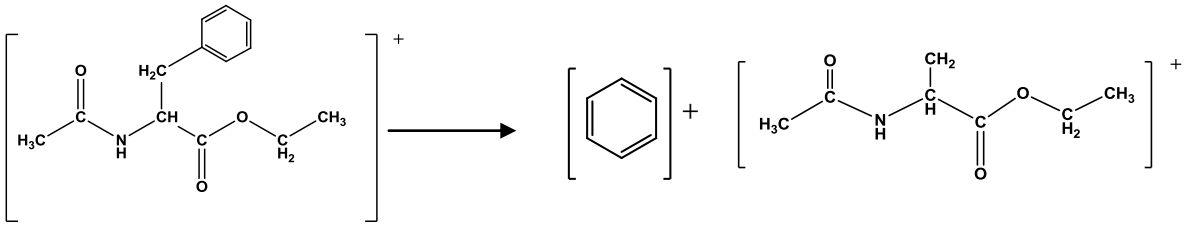

$E^{B3}{}_i$=-785.843296au E^{B3}=-231.579891au E^{B3}=-554.163405au

ΔE^{B3}=0.099999au (2.7eV)

MW 235Da 78Da 157Da

Path E

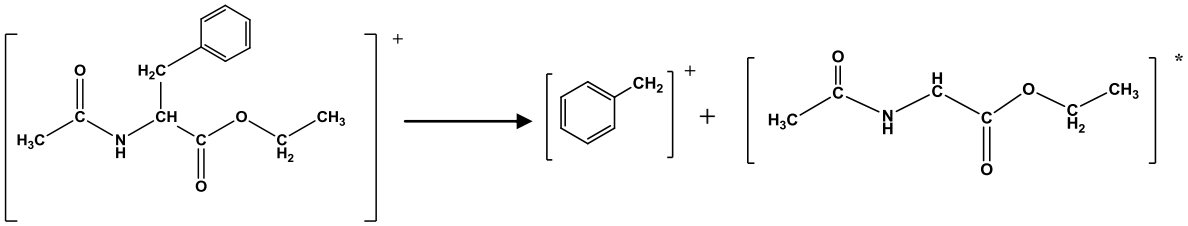

$E^{B3}{}_i$=-785.843296au E^{B3}=-270.677244au E^{B3}=-515.117260au

ΔE^{B3}=0.048793au (1.3eV)

MW 235Da 91Da 144Da

Path F

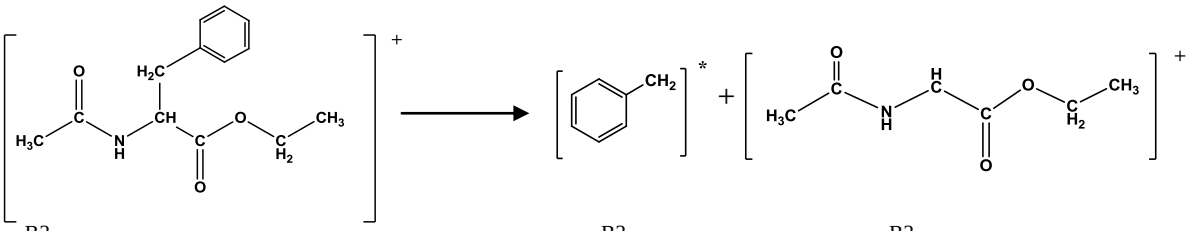

$E^{B3}{}_i$=-785.843296au E^{B3}=-270.937857au E^{B3}=-514.850380au

ΔE^{B3}=0.055059au (1.5eV)

MW 235Da 91Da 144Da

Path G

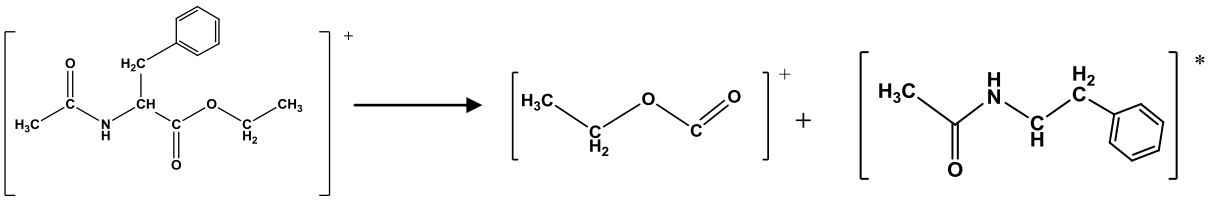

$E^{B3}{}_i$=-785.843296au E^{B3}=-267.472614au E^{B3}=-518.277246au

ΔE^{B3}=0.093436au (2.5eV)

MW 235Da 73Da 162Da

Path H

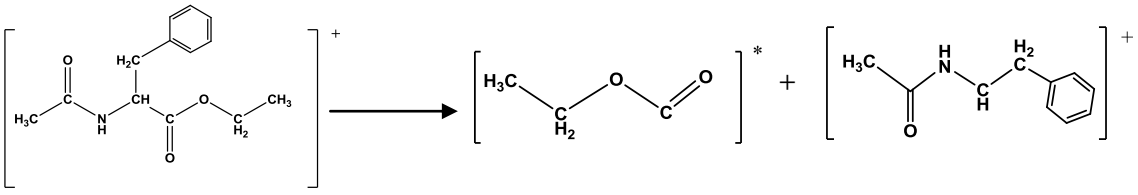

$E^{B3}{}_i$=-785.843296au E^{B3}=-267.736988au E^{B3}=-518.054824au

ΔE^{B3}=0.051484au (1.4eV)

MW 235Da 73Da 162Da

According to our calculations, if the positron annihilates with one of the electrons in the molecular orbital 60, the energy liberated is sufficient to produce fragments by following the pathways B, E, F, G, and H. Therefore, the positive mode positron-induced mass spectrum should have a peak at 177Da from path B, 91Da from path E, 144Da from path F, 73Da from path G, and 162Da from path H. In the experimental positron ionized mass spectra, a peak at 177Da is visible even at low positron energies (1.0-4.0eV) [81]. However, when the positron kinetic energy is increased to 8eV, other fragments ions are visible. Further analysis, involving the calculation of transition states and energy barriers, is underway, and will be published in the future in conjunction with the experimental results.

4.9.8 e^+Ethyl Sorbate System (E_{NEO-HF} =-459.673093au, PA=13meV)

It is important to compare the theoretically observed pattern of peaks in positron-induced mass spectra with experimental electron impact (EI) mass spectra. This will allow one to see if the fragmentation mechanism obtained from positron impact is similar to EI mass spectra. Therefore, e^+Ethyl sorbate system was studied in the NEO-HF model and compared to the experimental EI mass spectra obtained [89]. The following figure shows the chemical structure of the ethyl sorbate molecule.

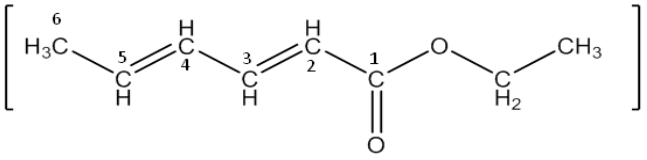

Figure 4.9.8.1 Chemical Structure of Ethyl Sorbate

The negative electrostatic potential, positron density and the contact density distribution are shown in following Figure 4.9.8.2 below. Negative electrostatic potential is localized on the carbonyl oxygen. Therefore, positron density is higher in the same region suggesting that the positron is trapped in the negative potential well similar to the previous cases. Further, the contact density distribution suggest that there is a higher probability of positron annihilation with one of the electrons at the carbonyl oxygen due to the higher overlap of electronic and positronic wavefunctions.

Table 4.9.8.1 e^+Ethyl Sorbate system-Molecular Orbital Annihilation Rate

MO	Liberated Energy (Hartree)	HF Annihilation Rate (1/ns)
12	1.03312	0.00043506
19	0.44797	0.00027335
23	0.34131	0.00094386
26	0.59061	0.00027442
32	0.18569	0.00030397
35	0.12562	0.00044014
36	0.11423	0.00083883
38(HOMO)	-	0.00011587

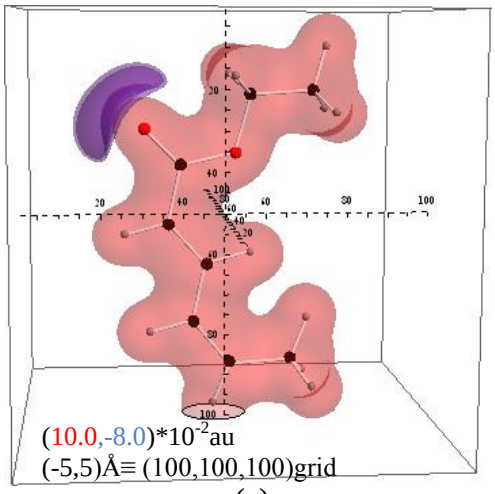

(a)

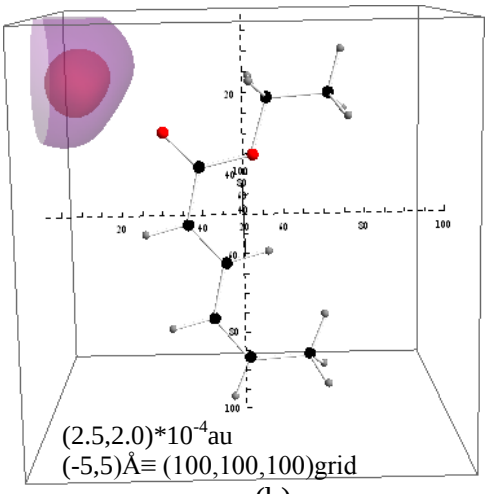

(b)

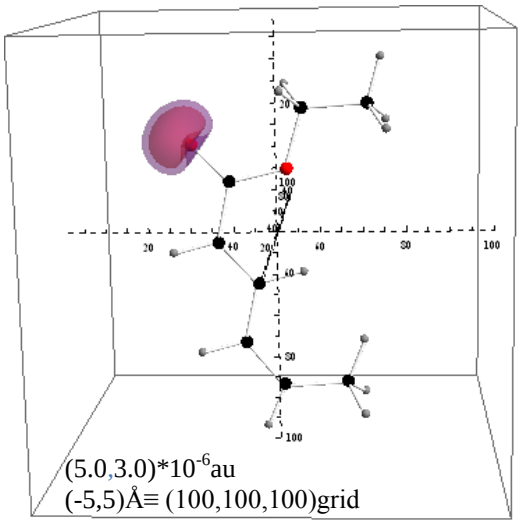

(c)

Figure 4.9.8.2 e^{+}Ethyl Sorbate System

(a) Molecular Electrostatic Potential

(b) Positron Density

(c) Contact Density

As seen in Table 4.9.8.1 the highest annihilation rate is observed when the positron interacts with the inner MO 23, hence it is most likely to be bonded with the positron. Energy is liberated during the annihilation process (when an electron jumps from the HOMO orbital to the MO23 (0.34131au.)). A fragmentation pathway is more probable when the energy liberated during annihilation overcomes the bond dissociation energy. The energy liberated when a positron annihilates with MO23 is sufficient to favor all pathways A-J as shown below. Therefore, theoretically predicted positive mode positron-induced mass spectra should

consists of fragment peaks at 41Da from path A, 99Da from path B, 67Da from path C, 73Da from path D, 95Da from path E, 111Da from path G, 29Da form path H, 125Da from path I and 15Da from path J, in addition to the molecular ion peak at 140Da. However, according to the trend in bond dissociation energies; E < I < C < G < D < H < A < B < J. The positive fragment ion from the energetically most favorable pathway E should yield the dominant peak at 95Da. This observed trend in the positron-induced mass spectrum strongly agrees with the experimentally observed electron impact mass spectrum [89]. Therefore, low energy positron mass spectra can be a potential tool for structure elucidation.

4.9.8.1 e^+Ethyl Sorbate System-Possible Fragmentation Pathways

Path A

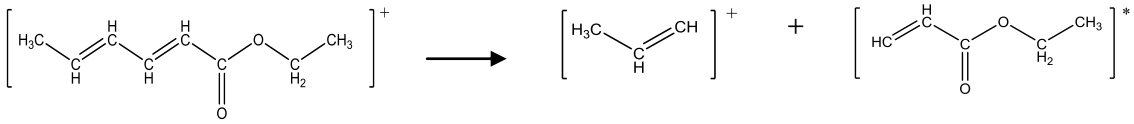

E^{B3}_i=-462.240470au E^{B3}=116.935436au E^{B3}=-345.125186au

ΔE^{B3}=0.179848au (4.9eV)

MW 140Da 41Da 99Da

Path B

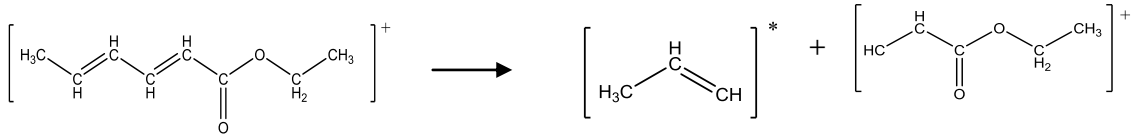

E^{B3}_i=-462.240470au E^{B3}=117.235617au E^{B3}=-344.815851au

ΔE^{B3}=0.189003au (5.1eV)

MW 140Da 41Da 99Da

Path C

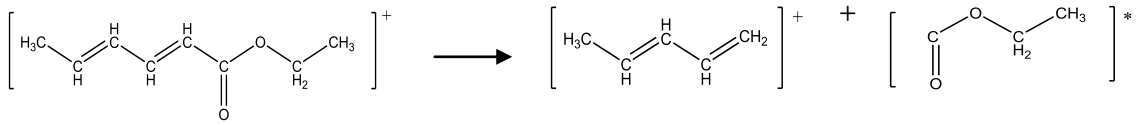

E^{B3}_i=-462.240470au E^{B3}=-194.409338au E^{B3}=-267.736988au

ΔE^{B3}=0.0941447au (2.6eV)

MW 140Da 67Da 73Da

Path D

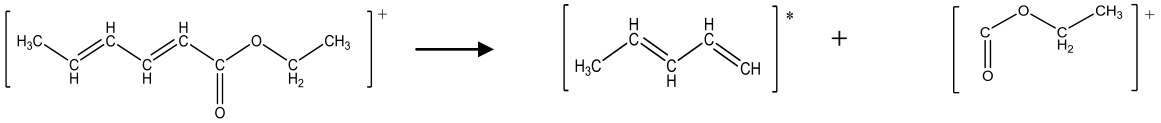

E^{B3}_i=-462.240470au E^{B3}=-194.643101au E^{B3}=-267.472614au

ΔE^{B3}=0.124754au (3.4eV)

MW 140Da 67Da 73Da

Path E

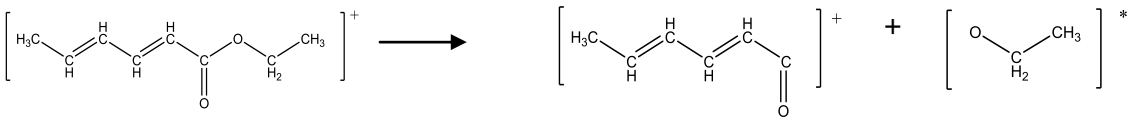

E^{B3}_i=-462.240470au E^{B3}=-307.786224au E^{B3}=-154.386792au

ΔE^{B3}=0.067454au (1.8eV)

MW 140Da 95Da 45Da

Path F

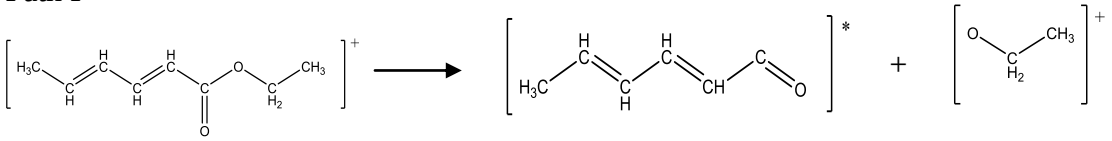

E^{B3}_i=-462.240470au E^{B3}=-308.013480au unstable

Path G

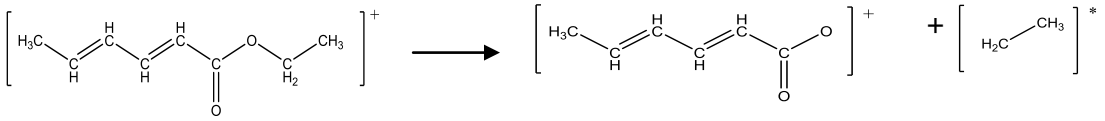

E^{B3}_i=-462.240470au E^{B3}=-382.955679au E^{B3}=-79.170104au

ΔE^{B3}=0.114687au (3.1eV)

MW 140Da 111Da 29Da

Path H

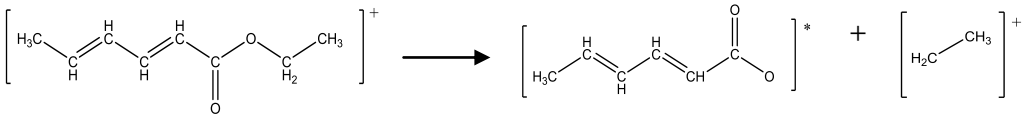

E^{B3}_i=-462.240470au E^{B3}=-383.244187au E^{B3}=-78.869235au

ΔE^{B3}=0.127049au (3.5eV)

MW 140Da 111Da 29Da

Path I

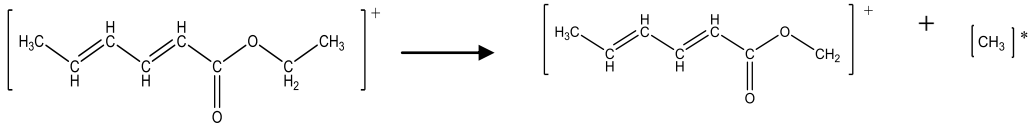

E^{B3}_i=-462.240470au E^{B3}=-422.316070au E^{B3}=-39.847334au

ΔE^{B3}=0.077065au (2.1eV)

MW 140Da 125Da 15Da

Path J

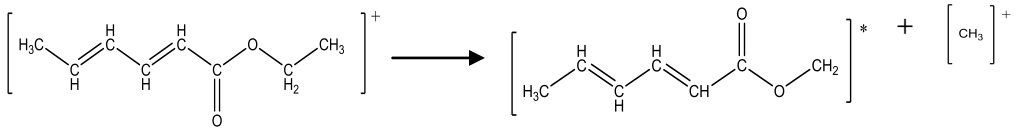

$E^{B3}{}_i$=-462.240470au E^{B3}=-422.558335au E^{B3}=-39.484716au

ΔE^{B3}=0.197418au (5.4eV)

MW 140Da 125Da 15Da

4.9.9 e^+Benzamide System ($E_{NEO-HF=}$-398.519009au, PA=12meV)

The electron impact mass spectrum of benzamide is compared with the theoretical positron-induced mass spectrum [89]. In this case, how the amide functional group interacts with the positron is studied, while in the previous cases it was the ester linkage. In order to understand the low energy positron-induced fragmentation, a similar calculation for the e^+benzamide system was carried out in the NEO-HF level of theory. Following Figure 4.9.9.1 shows the chemical structure of benzamide. The negative electrostatic potential of the molecule is localized on the carbonyl oxygen atom and no significant negative potential is observed near the amide nitrogen as illustrated in Figure 4.9.9.2(a). Accordingly, positron density and the contact density distribution of the e^+benzamide system are also found at the carbonyl oxygen atom. Therefore, the most probable annihilation site is the carbonyl oxygen.

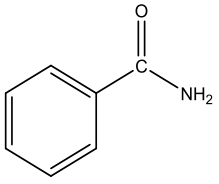

Figure 4.9.9.1 Chemical Structure of Benzamide

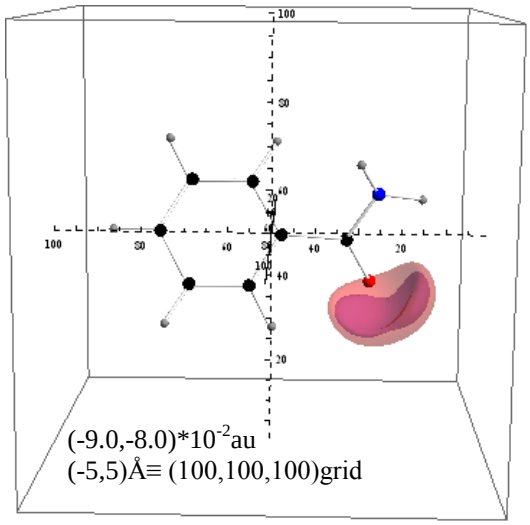

(a)

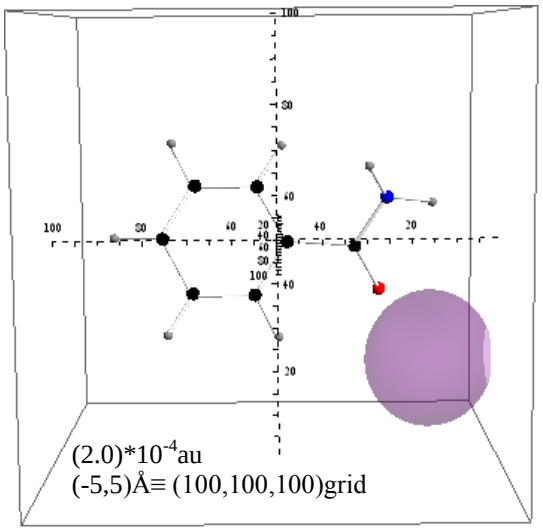

(b)

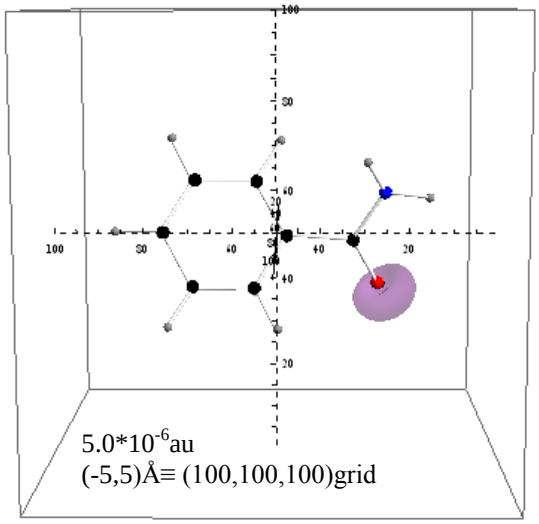

(c)

Figure 4.9.9.2 e^{+}Benzamide system

(a)Negative potential well

(b)Positron density

(c)Contact density

Our calculations show that a negative potential well can be seen around the O atom (C=O) along the bond axis (opposite to the carbonyl C). Similar to the previous e^{+}-molecule systems the higher positron density can be seen at the region of negative potential. Due to the higher electron density and the positron density near the O atom, the highest contact density can be seen around the O atom along the bond axis. When the positron annihilates with one of the electrons in that region a molecular ion of molecular weight 121Da can be seen in the

positron-induced mass spectrum. In order to study other possible fragmentation paths, molecular annihilation rates were calculated. The following table shows the molecular annihilation contribution of heavily overlap positron and molecular orbital wavefunctions.

Table 4.9.9.1 e^+Benzamide System-Molecular Orbital Annihilation Rate

MO	Liberated Energy (Hartree)	HF Annihilation Rate (1/ns)
20	0.32928	0.00045129
22	0.2777	0.00046898
23	0.25843	0.00047074
25	0.23384	0.00042152
29	0.08732	0.00084804
30	0.07103	0.00057120
32(HOMO)	0	0.00012808

There is a higher probability for the positron to annihilate with MO29 as shown in Table 4.9.9.1. In this case, when an electron from the HOMO jumps to the vacant site at MO29, 0.08732au of energy is released. Fragment ions of benzamide can be seen if the liberated energy is greater than the bond dissociation energies. According to the experimentally observed EI mass spectra, fragmentation can occur by breaking C-N bond in the amide group which yields a peak at 105Da $[C_6H_5CO]^+$ and C-C bond breaking to produce benzene fragment at 77Da $[C_6H_5]^+$ [89]. In this work, the theoretically calculated bond dissociation energies for above process are 0.074453au and 0.137079 au, respectively. If the positron annihilates with the MO29, which is the most probable orbital for positron annihilation, only the 105Da fragment ion is observed. However, if the positron annihilates with MO25, then both fragmentation pathways are possible.

CHAPTER 5

CONCLUSIONS AND FUTURE DIRECTIONS

I have developed and tested small/large and uncontracted/contracted Gaussian-type atom-centered positron basis sets for first-principles calculations which are appropriate for positrons bound to biological molecules containing O, N, C, and H. The results show that there is no need to scale the positron basis functions to take into account different effective charges on the atoms in different molecules, permitting these basis sets to be used in a general purpose quantum chemistry code like GAMESS.

Hartree-Fock calculations were found to give qualitatively reliable results for the relative contributions of different atoms to the contact density of a positron bound to a molecule with IE >> 6.8 eV. Many larger molecules of interest, including biological molecules such as amino acids, peptides, DNA and RNA bases were found to have IE's greater than 6.8 eV (9-11 eV). As these molecules have few strongly electronegative sites such as O and N, a positron should bind to them even at the HF level. As discussed, due to the weak e^+e^- correlation which occurs when IE >> 6.8 eV, the bound state can be correctly described as a positron-molecule (not as a positronium-molecule) bound state. Therefore qualitatively correct positron density and e^+e^- contact densities can be obtained for these biological molecules (and other molecules with IE >> 6.8 eV and regions of strongly different electronegativity) at the HF level.

In all my calculations, the positron density in the bound state is concentrated near the most electronegative site(s) in the molecule, such as O and N. An incoming positron with low energy may become trapped in the bound state, where it will be highly localized near the most electronegative site(s) in the molecule. Therefore, we expect that e^-e^+ annihilation will most

likely occur in this region at low incident energies leading to positron trapping in the bound state.

According to the results of the present work, using a single-center positron basis does not have the necessary flexibility to describe the contact density qualitatively correctly at the Hartree-Fock (HF) level, and more positron basis centers are needed for a qualitatively acceptable e^+e^- contact density. However, I can get qualitatively reliable values for the ground state energy, positron density, and contact density distributions for large positron-molecule systems by doing low-cost calculations, such as using the developed 13s9p positron basis sets for the most electro negative sites and smaller 2s contracted positron basis sets for the C and N atom centers (without e^+ basis centers at the H atoms).

According to the results obtained for positron bound to dipeptides, DNA and RNA bases, and similar moderate-size and large organic molecules, I find a higher contribution to the annihilation rate for electronic molecular orbitals with a higher occupation of p type orbitals on the site where the negative electrostatic potential and the e^+e^- contact density are both maximized (in all the cases this was an O atom site). A node near the same O atom along the C=O bond and higher s-orbital (in addition to p-orbital) occupation on the O atom are also capable of increasing the molecular orbital's contribution to the annihilation rate. The d-orbitals of heavy atoms showed minimal contribution to annihilation rates.

Also I find that the highest occupied molecular electronic orbital often does not make the highest contribution to e^+e^- annihilation rate, and the energy liberated by subsequent electronic relaxation is sufficient to break the backbone in several places in di-peptides and other organic molecules. The fragments obtained by theoretical calculations for acetamide and

N-acetyl-pheynylalanine-ethyl ester showed excellent agreement with the experimental positron mass spectra, thus validating this method of calculation.

In the future, this method can be used for other molecules when experimental positron mass spectra are available. Also, it is important to develop and test atom-centered basis sets for sulfur and phosphorus, as these elements are found in biomolecules as well.

In conjunction with experiments, further calculations using these basis sets and approximations can ultimately help us understand molecular fragmentation patterns induced by e^+e^- annihilation.

APPENDIX A

POSITRON BASIS SETS

As we discussed in section 3.2 we have developed different sizes of contracted and uncontracted positronic basis sets. Table A.1, A.2 and A.3 show the 13s9p, 13s9p3d and contracted positronic basis sets which are appropriate to use for e^+-molecule systems.

Table A.1 13s9p even-tempered uncontracted positronic basis sets

	e^+(O), a.u. Cs=2.3533615 Cp=2.8590844	**e^+(N), a.u.** Cs=2.4232008 Cp=2.9261163	**e^+(C), a.u.** Cs=2.5360684 Cp=2.4845328	**e^+(H), a.u.** Cs=2.5664117 Cp=2.6726866	**e^+(Li), a.u.** Cs=2.588323 Cp=2.901909	**e^+(Be), a.u.** Cs=2.234662 Cp=2.841344
1s	1.782284973	3.830782473	12.82044055	4.746615569	13.77439837	2.269803840
2s	0.757335803	1.580876967	5.055242422	1.849514429	5.321747096	1.015726328
3s	0.321810220	0.652392038	1.993338361	0.720661611	2.056060191	0.454532658
4s	0.136744912	0.269227384	0.785995505	0.280805140	0.794360091	0.203401183
5s	0.058106206	0.111104030	0.309926777	0.109415467	0.306901499	0.091021053
6s	0.024690726	0.045850111	0.122207578	0.042633637	0.118571578	0.040731484
7s	0.010491684	0.018921300	0.048187809	0.016612158	0.045810200	0.018227144
8s	0.004458169	0.007808391	0.019000989	0.006472912	0.017698798	0.008156559
9s	0.001894383	0.003222346	0.007492302	0.002522164	0.006837941	0.003650021
10s	0.000804969	0.001329789	0.002954298	0.000982759	0.002641842	0.001633366
11s	0.000342051	0.000548774	0.001164913	0.000382931	0.001020677	0.000730923
12s	0.000145346	0.000226466	0.000459338	0.000149209	0.000394339	0.000327084
13s	6.17609e-05	9.345756e-05	0.000181122	5.813906e-5	0.000152353	0.000146368
1p	1.384446478	1.533150727	1.204367861	1.130187473	1.179861733	0.840079626
2p	0.484227212	0.523954123	0.484746224	0.422865685	0.406581446	0.295662881
3p	0.169364433	0.179061274	0.195105589	0.158217457	0.140108343	0.104057444
4p	0.059237297	0.061194174	0.078528082	0.059197907	0.048281464	0.036622628
5p	0.020718974	0.020913104	0.031606781	0.022149214	0.016637837	0.012889196
6p	0.007246716	0.007147051	0.012721419	0.008287247	0.005733414	0.004536304
7p	0.002534628	0.002442504	0.005120246	0.003100718	0.001975739	0.001596535
8p	0.000886518	0.000834726	0.002060848	0.001160150	0.000680841	0.000561894
9p	0.000310070	0.000285267	0.000829471	0.000434076	0.000234618	0.000197756

Table A.2 13s9p3d even-tempered uncontracted positronic basis sets

	e^+(O), a.u. Cs=2.761013 Cp=3.263195 Cd=17.70825	**e^+(N), a.u.** Cs=2.751217 Cp=2.958834 Cd=8.613233	**e^+(C), a.u.** Cs=2.735229 Cp=2.519365 Cd=2.354433	**e^+(H), a.u.** Cs=3.076186 Cp=2.616741 Cd=2.876994	**e^+(Li), a.u.** Cs=2.63996 Cp=2.785693 Cd=9.689005	**e^+(Be), a.u.** Cs=2.278052 Cp=2.71762 Cd=8.27461
1s	8.951267417	8.201826502	9.975207887	19.92451459	15.85326464	4.224434711
2s	3.242023246	2.981162819	3.646937024	6.477017912	6.005115923	1.854406322
3s	1.174215252	1.083579585	1.333320549	2.105534910	2.274699759	0.8140314721
4s	0.4252842603	0.3938546090	0.4874621291	0.6844627135	0.861641816	0.3573365933
5s	0.1540319816	0.1431564928	0.1782162043	0.2225036517	0.326384445	0.1568605702
6s	0.0557882187	0.0520338748	0.0651558625	0.07233100365	0.123632354	0.0688573153
7s	0.0202057087	0.0189130376	0.0238209900	0.02351320550	0.046831150	0.0302263970
8s	0.0073182236	0.0068744254	0.0087089563	0.00764362175	0.017739342	0.0132685260
9s	0.0026505577	0.0024986850	0.0031839953	0.00248477195	0.006719550	0.0058245043
10s	0.0009599947	0.0009082107	0.0011640690	0.00080774426	0.002545322	0.0025567912
11s	0.0003476966	0.0003301123	0.0004255837	0.00026257975	0.000964152	0.0011223584
12s	0.0001259308	0.0001199877	0.0001555934	8.53588550e-05	0.000365214	0.0004926833
13s	4.5610375e-05	4.3612606e-05	5.6884986e-05	2.77482711e-05	0.000138341	0.0002162739
1p	3.100367483	1.767583665	1.463212435	0.8814851886	1.063560354	0.7253640938
2p	0.9501017230	0.5973920389	0.5807861790	0.3368636884	0.381793889	0.2669115080
3p	0.2911568674	0.2019011916	0.2305287856	0.1287340344	0.137055291	0.0982151635
4p	0.0892244686	0.0682367499	0.0915027301	0.04919631346	0.049199720	0.0361401365
5p	0.0273426688	0.0230620433	0.0363197576	0.01880060133	0.017661576	0.0132984503
6p	0.0083791089	0.0077943021	0.0144162342	0.00718473774	0.006340102	0.0048934176
7p	0.0025677620	0.0026342481	0.0057221695	0.00274568114	0.002275952	0.0018006260
8p	0.0007868857	0.0008902995	0.0022712744	0.00104927489	0.000817014	0.0006625745
9p	0.0002411396	0.0003008954	0.0009015265	0.00040098530	0.000293289	0.0002438069
1d	2.011662428	0.6801208027	0.1654817863	0.1968882512	0.557233392	0.4160414523
2d	0.1136003239	0.0789623156	0.0702852109	0.06843540181	0.057511931	0.0502792821
3d	0.0064151089	0.0091675585	0.0298522936	0.02378711879	0.005935793	0.0060763325

Table A.3 Contracted large positronic basis sets

e^+(O) 8s7p3d			e^+(N) 10s6p3d		
S	1		S	1	
1	30.35897358	1.000000000	1	13.30215354	1.000000000
S	1		S	1	
1	2.325763245	1.000000000	1	1.159104747	1.000000000
S	1		S	1	
1	0.1781738324	1.000000000	1	0.1010004740	1.000000000
S	1		S	1	
1	0.01364967592	1.000000000	1	0.008800840291	1.000000000
S	1		S	1	
1	0.001045684712	1.000000000	1	0.0007668755079	1.000000000
S	3		S	1	
1	0.1354757201	1.086875250	1	6.682294249e-05	1.000000000
2	0.01907732405	5.367747610	S	1	
3	0.002686417113	2.417776530	1	5.822725589e-06	1.000000000
S	3		S	2	
1	0.1117844439	-0.5666768510	1	0.4756961994	0.05220773490
2	0.03219752826	-2.235733710	2	0.01281444250	-0.1482444380
3	0.002671190478	-1.027799560	S	2	
S	2		1	0.2681755894	0.08640487120
1	0.05581541236	-0.7422534590	2	0.01725409046	-0.2991832480
2	0.002596231520	0.7042512040	S	2	
P	1		1	0.05278040745	-0.8069405330
1	9.632038234	1.000000000	2	0.006629877053	0.2291580040
P	1		P	1	
1	0.9565071034	1.000000000	1	0.7264322263	1.000000000
P	1		P	1	
1	0.09498569427	1.000000000	1	0.06331887454	1.000000000
P	1		P	1	
1	0.009432530175	1.000000000	1	0.005519138231	1.000000000
P	1		P	1	
1	0.0009366950064	1.000000000	1	0.0004810711978	1.000000000
P	2		P	3	
1	0.03514166946	0.1572159690	1	0.1486329667	-0.01922552690
2	0.007263034841	0.03501648510	2	0.03647120580	-0.08167734330
P	2		3	0.008949218213	0.01766302320
1	0.1020126769	0.03545022530	P	2	
2	0.01113937658	-0.04390496770	1	0.07632779278	0.03845564480
D	1		2	0.02626183657	-0.08501897960
1	1.517073706	1.000000000	D	1	
D	1		1	0.7251088177	1.000000000
1	0.2839920896	1.000000000	D	1	
D	1		1	0.1346563006	1.000000000
1	0.05316255012	1.000000000	D	1	
			1	0.02500634229	1.000000000

Table A.3 Contracted large positronic basis sets cont…

e^+(C)8s7p3d			e^+(H) 10s6s3d		
S	1		S	1	
1	20.99793623	1.000000000	1	85.70134030	1.000000000
S	1		S	1	
1	0.8368581147	1.000000000	1	15.03090731	1.000000000
S	1		S	1	
1	0.03335239695	1.000000000	1	2.636226854	1.000000000
S	1		S	1	
1	0.001329236537	1.000000000	1	0.4623601144	1.000000000
S	1		S	1	
1	5.297579583e-05	1.000000000	1	0.08109198760	1.000000000
S	3		S	1	
1	0.7724175618	-0.01779622330	1	0.01422248643	1.000000000
2	0.1263971975	-0.03224701020	S	1	
3	0.02068343902	0.04880021720	1	0.002494440281	1.000000000
S	3		S	2	
1	0.2852285608	0.1915021580	1	0.006037402232	-0.2248316210
2	0.08765540933	0.03368172720	2	0.001199696288	0.2859063260
3	0.008278471258	-0.05075701660	S	2	
S	2		1	0.04199314899	-0.09391609310
1	0.06388484782	-0.4787477490	2	0.002493855485	2.464088380
2	0.02333866434	-2.173203710	S	2	
P	1		1	0.002586940014	3.454247110
1	1.732260310	1.000000000	2	0.0008303921517	0.5057495900
P	1		P	1	
1	0.1736067099	1.000000000	1	1.092849480	1.000000000
P	1		P	1	
1	0.01739882254	1.000000000	1	0.3599857855	1.000000000
P	1		P	1	
1	0.001743705793	1.000000000	1	0.1185797021	1.000000000
P	1		P	1	
1	0.0001747537734	1.000000000	1	0.03906028051	1.000000000
P	2		P	3	
1	0.6203960502	0.009083205210	1	0.01422168199	0.2571992470
2	0.1571991062	0.06014685740	2	0.005196912073	0.3687640380
P	2		3	0.001899064760	0.2523363710
1	0.08168828044	-0.05344797730	P	2	
2	0.03240321987	-0.02508895350	1	0.008070217640	0.5152596200
D	1		2	0.003150955738	0.5413432040
1	0.1645496072	1.000000000	D	1	
D	1		1	0.2272238355	1.000000000
1	0.07084652040	1.000000000	D	1	
D	1		1	0.05826128364	1.000000000
1	0.03050283460	1.000000000	D	1	
			1	0.01493847317	1.000000000

Table A.3 Contracted large positronic basis sets cont…

e^+(Be) 9s7p3d			e^+(Li)9s7p3d		
S	1		S	1	
1	11.72073173	1.000000000	1	47.99008843	1.000000000
S	1		S	1	
1	2.436904365	1.000000000	1	12.59811763	1.000000000
S	1		S	1	
1	0.5066665648	1.000000000	1	3.307194738	1.000000000
S	1		S	1	
1	0.1053430785	1.000000000	1	0.8681881970	1.000000000
S	1		S	1	
1	0.02190230215	1.000000000	1	0.2279124168	1.000000000
S	1		S	1	
1	0.004553795525	1.000000000	1	0.05983042605	1.000000000
S	3		S	2	
1	0.01641888509	-0.5573530750	1	0.009790793989	-1.766357520
2	0.004619464269	0.3833706320	2	0.002361424800	-4.990325810
3	0.0003656684657	0.3130183050	S	3	
S	2		1	0.009144913637	-1.586032910
1	0.01317157735	26.58277320	2	0.002972054625	2.580751750
2	0.004716520601	-2.341211200	3	0.0009659040036	46.54978950
S	2		S	2	
1	0.01326852600	-3.622358200	1	0.002545322896	0.5440155860
2	0.005824504384	-4.743887950	2	0.0009641521415	4.355523490
P	1		P	1	
1	2.632453862	1.000000000	1	1.409064982	1.000000000
P	1		P	1	
1	0.2901669222	1.000000000	1	0.3417564894	1.000000000
P	1		P	1	
1	0.03198416653	1.000000000	1	0.08289007220	1.000000000
P	1		P	1	
1	0.003525511803	1.000000000	1	0.02010426804	1.000000000
P	1		P	1	
1	0.0003886058265	1.000000000	1	0.004876115835	1.000000000
P	2		P	2	
1	0.06195738487	0.05340656130	1	0.007397173252	0.4435731640
2	0.003480715329	0.08420927290	2	0.002180611136	-0.5015085510
P	2		P	2	
1	0.01429265912	-0.4374331900	1	0.006473697698	-0.1586247610
2	0.005649468923	-4.723620560	2	0.002316790772	0.1829573970
D	1		D	1	
1	0.3349370630	1.000000000	1	0.6629633087	1.000000000
D	1		D	1	
1	0.04391102577	1.000000000	1	0.05898329659	1.000000000
D	1		D	1	
1	0.005756837321	1.000000000	1	0.005247695055	1.000000000

Table A.4 Contracted positronic basis sets for C and N atom centers

e^+(C) 3s6p

```
S   3
  1      0.7724175618      -0.01779622330
  2      0.1263971975      -0.03224701020
  3      0.02068343902      0.04880021720
S   3
  1      0.2852285608       0.1915021580
  2      0.08765540933      0.03368172720
  3     0.008278471258     -0.05075701660
S   2
  1      0.06388484782      -0.4787477490
  2      0.02333866434      -2.173203710
P   1
  1       1.732260310        1.000000000
P   1
  1      0.1736067099        1.000000000
P   1
  1      0.01739882254       1.000000000
P   1
  1     0.001743705793       1.000000000
P   2
  1      0.6203960502       0.009083205210
  2      0.1571991062       0.06014685740
P   2
  1      0.08168828044      -0.05344797730
  2      0.03240321987      -0.02508895350
```

e^+(N) 3s5p

```
S   2
  1      0.4756961994       0.05220773490
  2      0.01281444250     -0.1482444380
S   2
  1      0.2681755894       0.08640487120
  2      0.01725409046     -0.2991832480
S   2
  1      0.05278040745     -0.8069405330
  2     0.006629877053      0.2291580040
P   1
  1      0.7264322263       1.000000000
P   1
  1      0.06331887454      1.000000000
P   1
  1     0.005519138231      1.000000000
P   3
  1      0.1486329667      -0.01922552690
  2      0.03647120580     -0.08167734330
  3     0.008949218213      0.01766302320
P   2
  1      0.07632779278      0.03845564480
  2      0.02626183657     -0.08501897960
```

Table A.5 Contracted positronic basis sets for H atom centers

```
S   4
  1       2.341422716       0.000286
  2       0.8396974068      0.000184
  3       0.3011381628      0.002345
  4       0.1079962762     -0.001438
```

BIBLIOGRAPHY

1. P. A. M Dirac. “The Quantum Theory of the Electron”. Proc. Royal Soc., **117,** 610-624 (1928).
2. P. A. M. Dirac. “A Theory of Electrons and Protons”. Proc. Royal Soc., **126,** 360–365 (1930).
3. P. A. M. Dirac. “On the Annihilation of Electrons and Protons”. Proceedings of the Cambridge Philosophical Society **26,** 361-375 (1930).
4. C. D. Anderson. “The Positive Electron”. Phys. Rev. **43,** 491-494 (1933).
5. C. D. Anderson. “Cosmic-Ray Positive and Negative Electrons”. Phys. Rev. **44,** 406-416 (1933).
6. M. Charlton, and J. W. Humberston. “Positron Physics (Cambridge Monographs on Atomic, Molecular and Chemical Physics)” ISBN 978-0521415507.
7. A. E. Ruark. “Positronium”. Phys. Rev. **68,** 278 (1945).
8. J. N. Sun, Y. F. Hu, W. E. Frieze, D. W. Gidley. “Characterizing Porosity in Nanoporous Thin Films Using Positronium Annihilation Lifetime Spectroscopy”. Radiation Phys. Chem. **68,** 345–349 (2003).
9. R. Krause-Rehberg, F. Borner, and F. Redmann. Positron Beam Studies of Defects in Semiconductors. Material Science Forum, **363-365,** 404–408 (2001).
10. A. P. Mills, Jr., D. B. Cassidy and R. G. Greaves “Prospects for Making a Bose-Einstein-Condensed Positronium Annihilation Gamma Ray Laser”. Materials Sci. Forum **445-446,** 424-429 (2004).
11. A. Passner, C. M. Sukro, M. Leventhal, and A. P. Mills. “Ion Production by Positron-Molecule Resonances”. Physical Rev. A **39,** 3706-3709 (1989).

12. Y. C. Jean, P.E. Mallon and D. M. Schrader. “Positron and Positronium Chemistry”. ISBN: 981-238-144-9
13. J. W. Shearer and M. Deutsch. “The Lifetime of Positronium in Matter” Phys. Rev. **76**, 462 (1949)
14. M. Deutsch “Evidence for the Formation of Positronium in Gases”. Phys. Rev. **82,** 455–456 (1951).
15. M. Deutsch “Three-Quantum Decay of Positronium”. Phys. Rev. **83,** 866–867 (1951).
16. A. Ore and J. L. Powell. “Three-Photon Annihilation of an Electron-Positron Pair”. Phys. Rev. **75,** 11 1696-1699 (1949).
17. D. A.L. Paul and L. Saint-Pierre. “Rapid Annihilation of Positrons in Polyatomic gases”. Phys. Rev. Lett. **11,** 493-496 (1963).
18. P. M. Smith and D. A. L. Paul. “Positron Annihilation in Methane Gas”. Can.J. Phys. **48,** 2984-2990 (1970).
19. W. E. Kauppila, T. S. Stein, J. H. Smart, M. S. Dababneh, Y. K. Ho, J. P. Downing, and V. Pol. “Measurements of Total Scattering Cross Sections for Intermediate-Energy Positrons and Electrons colliding with Helium, Neon, and Argon”. Phys. Rev. A **24,** 2 725-742 (1981).
20. K. R. Hoffman, M. S. Dababneh, Y.F. Hsieh, W. E. Kauppila, V. Pol, J. H. Smart, and T. S. Stein. “Total-Cross-Section Measurements for Positrons and Electrons Colliding with H_2, N_2, and CO_2”. Phys. Rev. A **25,** 3 1393-1403 (1982).
21. C. K. Kwan, W. E. Kauppila, R. A. Lukaszew, S. P. Parikh, T. S. Stein, Y. J. Wan, and M. S. Dababneh. “Total Cross-Section Measurements for Positrons and Electrons Scattered by Sodium and Potassium Atoms”. Phys. Rev. A **44,** 3 1620-1635 (1991).

22. Y.F. Hsieh, W. E. Kauppila, C. K. Kwan, Steven J. Smith, T. S. Stein, and M. N. Uddin. “Total-Cross-Section Measurements for Positron and Electron Scattering by O_2, CH_4, and SF_6”. Phy. Rev. A **38,** 3 1207-1216 (1988).

23. T. S. Stein, W. E. Kauppila, and L. O. Roellig. “Production of a Monochromatic, Low Energy Positron Beam Using the $^{11}B(p,n)^{11}C$ reaction”. Rev. Sci. Instrum. **45,** 7 951-953 (1974).

24. K. G. Lynn, B. Nielsen and J. H. Quateman. “Development and Use of a Thin-Film Transmission Positron Moderator”. Appl. Phys. Lett. **47,** 239-240 (1985).

25. C. M. Sukro, M. Leventhal, A. Passner. “Positron Plasma in the Laboratory”. Phys. Rev. Lett. **62,** 8 901-904 (1989).

26. R. G. Greaves, M. D. Tinkle, and C. M. Surko "Creation and Uses of Positron Plasmas", Phys. Plasmas **1**, 1439-1446. (1994).

27. R. G. Greaves and C. M. Surko. “An Electron-Positron Beam-Plasma Experiment”. Phys. Rev.**75**, 21,3846-3849 (1995).

28. R. G. Greaves and C. M. Surko. “Antimatter Plasmas and Antihydrogen”. Phys. Plasmas **4,** 1528-1543 (1997).

29. C. M. Surko, G. F. Gribakin and S. J. Buckman. “ Low-Energy Positron Interactions with Atoms and Molecules”. J. Phys. B: At. Mol. Opt. Phys. **38,** R57–R126 (2005).

30. C.M.Surko, A. Passner, M. Leventhal, and F. J. Wysocki. “Bound States of Positrons and Large Molecules”. Phys. Rev. Lettt. **61,** 16 1831-1834 (1988).

31. T. J. Murphy and C. M. Surko. “Annihilation of Positrons on Organic Molecules”. Phys. Rev. Lett. **67,** 21 2954-2957 (1991).

32. K. Iwata, R. G. Greaves, T. J. Murphy, M. D. Tinkle and C. M. Surko. “Measurements of Positron-Annihilation Rates on Molecules”. Phys. Rev. A **51,** 1 473-487 (1995).

33. K. Iwata, R. G. Greaves, and C. M. Surko. “γ-Ray Spectra from Positron Annihilation on Atoms and Molecules”. Phys. Rev. A **55,** 5 3586-3604 (1997).

34. K. Iwata, G. F. Gribakin, R. G. Greaves, C. Kurz and C. M. Surko. “Positron Annihilation on Large Molecules”. Phys. Rev. A **61,** 022719 1-17 (2000).

35. G. F. Gribakin. “Mechanisms of Positron Annihilation on Molecules”. Phys. Rev. A **61,** 022720 1-13 (2000).

36. L. D. Barnes, S. J. Gilbert, and C. M. Surko. “Energy-Resolved Positron Annihilation for Molecules”. Phys. Rev. A **67,** 032706 1-11 (2003).

37. J. R. Danielson, J. A. Young and C. M. Surko. “Dependence of Positron-Molecule Binding Energies on Molecular Properties”. J. Phys. B: At. Mol. Opt. Phys. **42,** 235203 1-9 (2009).

38. S. A. McLuckey, G. L. Glish, D. L. Donohue and L. D. Hullet Jr. “Positron Ionization Mass Spectrometry Ionization by Fast Positrons”. Inter. Jour. Mass Spec. and Ion Pro. **97,** 237-252 (1990).

39. Jun Xu, L. D. Hulett, Jr., T. A. Lewis, D. L. Donohue, S. A. McLuckey, and G. L. Glish. “Positron-Induced Dissociation of Organic Molecules”. Phys. Rev., **47,** 2 1023-1029 (1993).

40. L. D. Hullet Jr, D. L. Donohue, Jun Xu, T. A. Lewis, S. A. McLuckey and G. L. Glish.” Mass Spectrometry Studies of the Ionization of Organic Molecules by Low-Energy Positrons”. Chem. Phys. Lett. **216,** 1 236-240 (1993).

41. Jun Xu, L. D. Hulett, Jr., T. A. Lewis, D. L. Donohue, S. A. McLuckey, and O. H. Crawford. “Internal Energy Deposition into Molecules Upon Positron-Electron Annihilation”. Phys. Rev. A **49,** 5 R3151-R3154 (1994).

42. Jun Xu, L. D. Hulett, Jr., T. A. Lewis, and S. A. McLuckey. “Chemical Selectivity in the Dissociative Ionization of Organic Molecules by Low-Energy Positrons”. Phys. Rev. A **52,** 3 2088-2094 (1995).

43. Oakley H. Crawford. “Mechanism for Fragmentation of Molecules by Positron Annihilation”. Phys. Rev. A **49,** 5 R3147-R3150 (1994).

44. J. A Loo, H. R. Udseth, R. D. Smith. “Collisional Effects on the Charge Distribution of Ions from Large Molecules, Formed by Electrospray-Ionization Mass Spectrometry”. Rapid Commun. Mass Spectrom. **2,** 207-210 (1988).

45. M. D. Mabud, M. J. DeKrey, R. G. Cooks. “Surface-Induced Dissociation of Molecular Ions”. Int. J. Mass Spectrom. Ion Processes **69,** 277 285-294 (1986).

46. R. A. Zubarev, N. L. Kelleher, and F. W. McLafferty. “Electron Capture Dissociation of Multiply Charged Protein Cations. A Nonergodic Process”. J. Am. Chem. Soc. **120,** 3265-3266 (1998).

47. J. E. P. Syka, J. J. Coon, M. J. Schroeder, J. Shabanowitz, and D. Hunt. “Peptide and Protein Sequence Analysis by Electron Transfer Dissociation Mass Spectrometry”. PNAS **101,** 26 9528-9533 (2004).

48. A. G. Harrison, T. Yalcin. “Proton Mobility in Protonated Amino Acids and Peptides”. International Journal of Mass Spectrometry and Ion Processes **165/166,** 339-347 (1997).

49. J. Fenn, M. Mann, K. Meng, S. F. Wong, C. M. Whitehouse. “Electrospray Ionization for Mass Spectrometry of Large Biomolecules”. Science **246,** 65 64-71 (1989).

50. F. Hillenkamp, M. Karas, R. C. Beavis and B. T. Chait. “Matrix-Assisted Laser Desorption/Ionization Mass Spectrometry of Biopolymers”. Anal. Chem. **63,** 24 1193A-1203A (1991).

51. J. Throck Watson, Throck J. Watson and Watson. “Introduction to Mass Spectrometry”. ISBN 978-0397516889

52. K. Strasburger and H. Chojnacki. “Quantum Chemical Study of Simple Positronic systems using explicitly correlated Gaussian functions – PsH and $PsLi^{+}$”. J. Chem. Phys . **108,** 8 3218-3221 (1998).

53. K. Strasburger. “Binding Energy, Structure, and Annihilation Properties of the Positron-LiH Molecule Complex, Studied with Explicitly Correlated Gaussian Functions”. J. Chem. Phys. **111,** 23 10555-10558 (1999).

54. K. Strasburger . “Adiabatic Positron Affinity of LiH”. J. Chem. Phys. 114, 615 (2001)

55. D. Bressanini, M. Mella and G. Morosi. “Positron Chemistry by Quantum Monte Carlo. II. Ground-State of Positronpolar Molecule Complexes (LiH, BeO)”. J. Chem. Phys. **109,** 1716-1720 (1998).

56. D. Bressanini, M. Mella and G. Morosi. “Positron and Positronium Chemistry by Quantum Monte Carlo. III. Ground State of OHPs., CHPs., and NH_2Ps. Complexes” , J. Chem. Phys. **109,** 14 5931-5934 (1998).

57. M. Mella, G. Morosi and D. Bressanini. “Positron and Positronium Chemistry by Quantum Monte Carlo. IV. Can This Method Accurately Compute Observables Beyond Energy?”. J. Chem. Phys. **111,** 1 108-114 (1999).

58. M. Mella, G. Morosi, D. Bressanini, and S. Elli. “Positron and Positronium Chemistry by Quantum Monte Carlo. V. The Ground State Potential Energy Curve of e^+LiH”. J. Chem. Phys. **113,** 15 6154-6159 (2000).

59. C. Swalina, M. V. Pak, and Sharon Hammes-Schiffer. “Analysis of Electron-Positron wavefunctions in the Nuclear-Electronic Orbital Framework”. J. Chem. Phys. **136,** 164105 1-9 (2012).

60. K. Strasburger. “Positronic Formaldehyde—the Configuration Interaction Study”. Structural Chem. **15,** 415-420 (2004).

61. J. Mitroy, M. W. J. Bromley and G. G. Ryzhikh. “Positron and Positronium Binding to Atoms”. J. Phys. B: At. Mol. Opt. Phys. **35,** R81–R116 (2002).

62. M. W. J. Bromley and J. Mitroy. “ Configuration-Interaction Calculations of PsH and e^+Be”. Phys. Rev. A **65,** 012505 1-9 (2001).

63. M. Tachikawa, R. J. Buenker, and M. J. Kimura. “Bound States of Positron with Urea and Acetone Molecules Using Configuration Interaction ab Initio Molecular Orbital Approach”. J. Chem. Phys. **119,** 10 5005-5009 (2003).

64. M. Tachikawa. “The First-Principles Multi-Component Molecular Orbital Approach to Bound States of Positron with the 2-Deoxyglucose Molecule as a Reagent of Positron Emission Tomography”. J. Phys.: Condens. Matter **19,** 365235 1-7 (2007).

65. M. Tachikawa, Y. Kita1 and R. J. Buenker. “Bound States of Positron with Simple Carbonyl and Aldehyde Species with Configuration Interaction Multi-Component Molecular Orbital and Local Vibrational Approaches”. New J. Phys. **14,** 035004 1-10 (2012).

66. K. Koyanagi, Y. Kita, and M. Tachikawa. “Systematic Theoretical Investigation of a Positron Binding to Amino Acid Molecules Using the ab Initio Multi-Component Molecular Orbital Approach”. Eur. Phys. J. D **66**, 1-7 (2012).

67. R. J. Buenker, Heinz-Peter Liebermann, V. Melnikov, M. Tachikawa, Lukas .Pichl, and M. Kimura, “Positron Binding Energies for Alkali Hydrides”. J. Phys. Chem. A **109,** 26 5956-5964 (2005).

68. G. G. Ryzhikh, J. Mitroy, and K. Varga. “The Structure of Exotic Atoms Containing Positrons and Positronium”. J. Phys. B: At. Mol. Opt. Phys. **31,** 3965-3996 (1998).

69. J. Mitroy and G. G. Ryzhikh. “Improved Binding Energies for LiPs, e^+Be, NaPs and e^+Mg”. J. Phys. B: At. Mol. Opt. Phys. **34,** 2001-2007 (2001).

70. J. Mitroy, and G. G. Ryzhikh. “Positronium Binding to Potassium and Other Alkali Atoms”. J. Phys. B: At. Mol. Opt. Phys. **32,** 3839-3848 (1999).

71. K. Strasburger. “Quantum Chemical Study on Complexes of the LiH Molecule with e^+, Ps and Ps- Including Correlation Energy”. Chem. Phys. Let. **253,** 49-52 (1996).

72. S. P. Webb, T. Iordanov, and S. Hammes-Schiffer. “Multiconfigurational Nuclear-Electronic Orbital Approach: Incorporation of Nuclear Quantum Effects in Electronic Structure Calculations”. Jour. of Chem. Phys. **117,** 9 4106-4118 (2202).

73. P. E. Adamson, X. F. Duan, L. W. Burggraf, M. V. Pak, C. Swalina, and Sharon Hammes-Schiffer. “Modeling Positrons in Molecular Electronic Structure Calculations with the Nuclear-Electronic Orbital Method”. J. Phys. Chem. A **112**, 1346-1351 (2008).

74. D. B. Cook. “Handbook of Computational Quantum Chemistry”. ISBN 978-0-486-44307-2

75. C. J. Cramer. “Essentials of Computational Chemistry”. ISBN 978-0-470-09182-1

76. G. A. Petersson, S. Zhong, J. A. Montgomery and M. J. Frisch. “On the optimization of Gaussian basis sets”. Jour. Chem. Phys. **118** 3 1101-1109 (2003).

77. M.J.D. Powell. “UOBYQA: Unconstrained Optimization by Quadratic Approximation”. Math. Program., Ser. B **92,** 555–582 (2002).

78. C. M. Kao and P. E. Cade. “The Electronic/Positronic Structure of Positron/Pseudohalide systems:[OH^-;e^+],[SH^-:e^+,[CN^-;e^+], and [N_3^-;e^+]”. J.Chem. Phys. **80,** 7 3234-3245 (1984).

79. K. Strasburger. “Positronic Formaldehyde—the Configuration Interaction Study”. Struct. Chem. **15,** 5 415-420 (2004).

80. Masanori Tachikawa et al , “Bound States of Positron with Urea and Acetone Molecules Using Configuration Interaction ab Initio Molecular Orbital Approach”, J.Chem.Phys. **119,** 10 5005-5009 (2003).

81. R. G. Greaves. First Point Scientific, Inc., SBIR Report

82. J. M. Rice, G. Dudek, and M. Barber. “Mass Spectra of Nucleic Acid Derivatives. Pyrimidines”. J. Am. Chem. Soc. **87**, 20 4569-4576 (1965)

83. J. M. Rice and G. Dudek. “Mass Spectra of Nucleic Acid Derivatives. II. Guanine, Adenine, and Related Compounds". J. Am. Chem. Soc. **89,** 2719-2725 (1967).

84. R. Improta, G. Scalmani, V. Barone. “Radical Cations of DNA Bases: Some Insights on Structure and Fragmentation Patterns by Density Functional Methods”. Int. J. Mass Spectrom. **201,** 321–336 (2000).

85. C. Zhou, S.Matsika, M. Kotur, and T. C. Weinacht. “Fragmentation Pathways in the Uracil Radical Cation”. J. Phys. Chem. A **116,** 9217−9227 (2012)

86. L. S. Arani, P. Mignon, H. Abdoul-Carime, B. Farizon, M. Farizonb and H. Chermettea. “DFT Study of the Fragmentation Mechanism of Uracil RNA Base”. Phys. Chem. Chem. Phys. **14,** 9855–9870 (2012).

87. P. Cheng, Y. Li,b S. Li, M. Zhang and Z. Zhou. “Collision-Induced Dissociation (CID) of Guanine Radical Cation in the Gas Phase: an Experimental and Computational Study”. Phys. Chem. Chem. Phys. **12,** 4667–4677 (2010).

88. J. K. Wolken, C. Yao, F. Turecek , M. J. Polce, C. Wesdemiotis. “Cytosine Neutral Molecules and Cation–Radicals in the Gas-Phase Structures, Energetics, Ion Chemistry, and Neutralization–Reionization Mass Spectrometry”. Int. J. Mass Spectrom. **267,** 30–42 (2007).

89. Silverstein, Bassaler and Morrill. “Spectrometric Identification of Organic Compounds”. 7th edition, ISBN 978-0471393627

ABSTRACT

LOW ENERGY POSITRON INTERACTIONS WITH BIOLOGICAL MOLECULES

by

INDIKA L WANNIARACHCHI

August 2013

Advisor: Prof. Caroline Morgan

Major: Physics

Degree: Doctor of Philosophy

Calculations of the positron density distribution which can be used for positrons bound to midsize and larger molecules have been tested for smaller molecules and subsequently applied to investigate the most likely e^+e^- annihilation sites for positrons interacting with biological molecules containing C, H, O, and N. In order to allow consideration of positrons bound to extended molecules with regions of different character and no particular symmetry, atom-centered positron basis sets of Gaussian-type functions were developed for positrons bound to molecules containing O, N, C, H, Li, Na, and Be. Testing shows that there is no need to scale the positron basis functions to take into account different effective charges on the atoms in different molecules.

Even at the HF level of theory the calculated positron and the contact density of e^+LiH system is in qualitative agreement with the most accurate calculation was done in ECG method. Also it has been found that for larger biological molecules such as derivation of

formaldehyde can leave out positron basis sets centered on H atoms and still get qualitatively acceptable contact density distribution.

According to our results, the electronic and positronic wavefunctions have the most overlap in the regions of most negative electrostatic potential in the parent molecule, and we can expect that a positron bound to the molecule will be more likely to annihilate with one of the electrons in these regions. Also we find that the highest energy occupied electronic orbital often does not make the largest contribution to e^+e^- annihilation, and that the energy liberated by subsequent electronic relaxation is sufficient to break the backbone in several places in di-peptides and other organic molecules.

AUTOBIOGRAPHICAL STATEMENT

INDIKA L WANNIARACHCHI

EDUCATIONAL QUALIFICATIONS

- Ph.D. Candidate in Physics, Wayne State University, Detroit
- MS in Physics, Wayne State University, Detroit, 2011
- BS in Physics, University of Sri Jayawardanapura, Sri Lanka, 2005

PROFESSIONAL EXPERIENCE

- Graduate Teaching Assistant, Wayne State University, 2008 August to 2012 July
- Lecturer in Physics, Science and Technology, Uva Wellassa University, Sri Lanka, since 2006

AWARDS, AFFILIATIONS & ACTIVITIES

- Summer Dissertation Fellowship, Wayne State University, 2013
- Thomas C. Rumble Fellowship Award, Wayne State University, 2012-2013
- Daniel R. Gustafson Graduate Student Teaching Award, Wayne State University, 2012
- Member of the main organizing committee of the graduate research exhibition 2012, Department of Physics and Astronomy, Wayne State University
- Student committee member on 2012 CLAS Faculty Teaching Award Selection Committee
- Student member of American Physical Society

PUBLICATIONS AND PRESENTATIONS

Publications

- W. K. I. L. Wanniarachchi, C. G. Morgan, G. Kedziora, H. B. Schlegel, L. Burggraf, M. V. Pak, and S. Hammes-Schiffer. "Ab Initio Calculations for Positrons Interacting with Peptides and other Large Organic Molecules" (manuscript in preparation)
- W. K. I. L. Wanniarachchi, C. G. Morgan, H. B. Schlegel, L. Burggraf, and P. Adamson. " Theoretical Study of Positron Impact with Biological Molecules-Possible Fragmentation Paths" (manuscript in preparation)
- R.G.Greaves, W. K. I. L. Wanniarachchi, C. G. Morgan and H. B. Schlegel, "Positron Ionization Mass Spectrometry" (manuscript in preparation)

Oral Presentations

- APS Ohio Session October 2012 : "Low Energy Positron Interactions with Biological Molecules-Possible Fragmentation Paths" W. K. I. L. Wanniarachchi, C. G. Morgan, H. B. Schlegel, L. Burggraf, and P. Adamson.
- APS March meeting 2012 : "Low Energy Positron Interactions with Biological Molecules" W. K. I. L. Wanniarachchi, C. G. Morgan, G. Kedziora, H. B. Schlegel, L. Burggraf, M. V. Pak, and S. Hammes-Schiffer.